A New Flexible and Multi-purpose System for Printing 3D Microstructures with Heterogeneous Materials for Tissue Engineering

A Thesis

Submitted to the Faculty

of

Drexel University

by

Ho-Lung Li

In partial fulfillment of the

requirements for the degree

of

Doctor of Philosophy

March 2012

DEDICATIONS

To my family:

My parents and sisters

ACKNOWLEDGEMENTS

First and foremost, I would like to thank Dr. Jack G. Zhou, for his encouragement, helping me develop a keen perspective on research, and excellent guidance throughout my graduate studies, research, and thesis work. He always challenged me to do better, think further, and explore new possibilities with this work beyond the bench. I would also like to thank my co-advisor, Dr. Bor-Chin Chang, for his patience, excellent guidance, and constant support during my study at Drexel. His encouraging remarks inspired confidence in me during times when I faced setbacks.

I would also like to thank my thesis committee members Dr. David Wootton, Dr. Richard Chiou, and Dr. Matthew McCarthy for their participation, feedback, and insightful suggestions on this project, which have inspired me to explore this field more deeply.

I would like to thank my lab partners, Dr. Qingwei Zhang, Dr. Chris Geisler, Jephte, Haibo, Xiang, and Steven for many discussions on the research and making the lab environment so much fun. Thanks for all your help and encouragement. It was great sharing some of the same experiences with you.

I would also like to make a special acknowledgment to my dear colleague, Mishah Salman, for his generous support and helpful suggestions when I encountered difficulties in my research, and who often guided me on how to solve problems with different viewpoints and new perspectives.

My friends Ting, Lydia, Iris, Bin, Wei-Ting, Elli, Bobby, and Liang, who have shared so many special and memorable moments with me in Philly. I am forever grateful to all of you.

Finally, I greatly appreciate to be able to share this journey with Leko for her kindness, patience, and endless support in many ways. You really make my life more colorful.

Most of all, I am indebted to my family and Pei-Ying for their loving support and enduring encouragement throughout my doctorate studies. They have truly been a source of strength and inspiration for me.

TABLE OF CONTENTS

LIST OF FIGURES vii

LIST OF TABLES xi

ABSTRACT xii

CHAPTER 1 : INTRODUCTION 1

1.1 Tissue Engineering Technologies *1*

1.2 Microfabrication *6*

1.3 Solid Freeform Fabrication *8*

1.3.1 Conventional Fabrication Technologies 8

1.3.2 SFF manufacturing technology 11

1.3.2.1 Direct SFF Technology 12

1.3.2.1.1 Stereolithography Apparatus (SLA) 13

1.3.2.1.2 Selective Laser Sintering (SLS) 15

1.3.2.1.3 Fused Deposition Modeling (FDM) 16

1.3.2.1.4 Three-dimensional Plotting (3D-Plotting) 18

1.3.2.1.5 Three-dimensional Printing (3DP) 20

1.3.2.2 Indirect SFF Technology 23

1.4 Homogeneous and heterogeneous structures *24*

1.5 Research objectives *26*

1.6 Proposed APT based heterogeneous SFF system and its technical advantages *28*

1.7 Thesis Outline *31*

CHAPTER 2 : LITERATURE REVIEW 33

2.1. Introduction *33*

2.2 Contemporary 3D Bio-printing System *34*

2.2.1 NovoGen MMX bioprinter 34

2.2.2 Neatco bioprinter 37

2.2.3 Fab@Home Model 2 38

2.2.4 3D-Bioplotter 40

2.2.5 Rapid Prototype Robotic Dispensing System (RPBOD) 42

2.2.6 Computer Aided Biological Tool 44

2.3 Range of Materials *46*

2.3.1 Material processability 46

2.3.2 Mechanical strength of scaffolds 47

2.4 Scaffold Design *48*

2.4.1 Porous structure 48

2.4.2 Surface Topography 49

2.5 Bioactivity of the scaffold *50*

2.5.1 Cell seeding on 3D scaffolds 50

2.6 Extrusion study *52*

CHAPTER 3 : A NEW FLEXIBLE AND MULTI-PURPOSE SYSTEM DESIGN FOR 3 DIMENSIONAL HETEROGENEOUS PRINTING 55

3.1 System configuration *55*

3.1.1 Motion control unit 57

3.1.1.1 TMS320F2812 DSP microprocessor 57

3.1.1.2 MACH3 control software 60

3.1.1.2.1 Geckodrive motor controller 62

3.1.1.2.2 Whale3 DC servo drive 63

3.1.2 Model slicing unit 65

3.1.3 Microvalve unit 65
3.1.4 Electrical control unit 66
3.1.5 Temperature control unit 67
3.1.6 EFD multi-valve controller 69
3.2 Printing nozzle system 71
3.2.1 Piezoelectric nozzle 71
3.2.1.1 MJ-SF-01-50 71
3.2.1.2 MJ-ATP-01-80 74
3.2.2 Pneumatic microvalve 75
3.2.2.1 HP 7x pressure-driven valve 75
3.2.2.2 741MD-SS needle microvalve 76
3.3 Software Introduction 81
3.3.1 User friendly integrated software 81
3.3.2 Skeinforge 83
3.4 Scaffold and Structure Design for Our SFF Machine 85
CHAPTER 4 : HETEROGENEOUS ALGORITHM 87
4.1 Introduction 87
4.2 Description of heterogeneous structure by reasoning Boolean operations 89
4.3 Algorithm for heterogeneous object modeling and slicing 91
4.4 Heterogeneous algorithm and printing procedure 93
CHAPTER 5 : MATERIAL STUDY 102
5.1 Poly (ε-caprolactone) (PCL) 102
5.2 Alginate 104
5.3 PEG-PLGA-PEG (triblock) 106
5.3.1 Thermosensitive hydrogels 106

5.3.2 Photocrosslinkable hydrogels 108
5.3.3 Thermosensitive / Photocrosslinkable hydrogel 109
5.4 Sucrose *110*
5.5 Viscosity Measurement *112*
5.6 Flow Rate Measurement *113*
CHAPTER 6 : SYSTEM SETUP AND EXPERIMENTAL RESULTS 116
6.1 System Integration *116*
6.2 The Requirements for Scaffold Fabrication *118*
6.3 Dispensing Method *119*
6.4 Machine Calibration Procedures *121*
6.5 Experimental Results *124*
6.5.1 Homogeneous Material Printing 124
6.5.2 Heterogeneous Material Printing 135
CHAPTER 7 : CONCLUSIONS AND FUTURE WORK 140
7.1 Conclusions *140*
7.2 Contributions *143*
7.3 Future Work and Recommendations *144*
LIST OF REFERENCES 146
VITA 160

LIST OF FIGURES

Figure 1.1: PLLA/CHAp (carbonated hydroxyapatite) nanocomposite scaffolds 4

Figure 1.2: β-TCP/PLGA open porous copy of the root of a mandibular third incisor of a mini-pig. 4

Figure 1.3: Illustration of the fabrication process for polymer solar cells with spontaneous surface-directed phase separation. 8

Figure 1.4: SEM micrographs of PLGA/NHA (95/5) scaffold. Thermally induced phase separation technology. 9

Figure 1.5: SEM micrograph of PLGA/CaP (75/25) composite. 10

Figure 1.6: SEM micrograph of micro-porous chitosan produced by liquid nitrogen freeze drying process. 10

Figure 1.7: The illustration of the SLA technology 13

Figure 1.8: SEM micrographs of PPF scaffolds (Lee et al., 2007) 14

Figure 1.9: The illustration of the SLS technology 15

Figure 1.10: PCL scaffold fabricated by SLS (Williams et al., 2005). 16

Figure 1.11: An illustration of FDM system 17

Figure 1.12: Schematic of microsyringe method (Vozzi, et al., 2003) 19

Figure 1.13: (a) 2D PLGA scaffold, and (b) 3D PLGA scaffold (Vozzi et al., 2003) 20

Figure 1.14: The digital image of Z-printer 350 20

Figure 1.15: SEM micrograph of PLGA copolymer scaffold (Lam et al., 2002). 21

Figure 1.16: An example of heterogeneous structure with three different materials distribution. 26

Figure 2.1: NovoGen MMX Bioprinter (Jakab et al., 2008) 35

Figure 2.2: The vascular structure design and the fused constructs of different vessels diameters are fabricated by NovoGen MMX Bioprinter and the semi-solid cellular “bio-ink” material 36

Figure 2.3: Neatco-1 printing system (Mironov et al., 2009) 37

Figure 2.4: Neatco-2 printing system (Mironov et al., 2009) 38

Figure 2.5: Fabbers Model2 with two nozzles connection 38

Figure 2.6: Printing results with dual syringes by using Fabbers Model2 40

Figure 2.7: 3D-Bioplotter printing system 41

Figure 2.8: RPBOD printing machine set-ups via dual dispensing (Geng, et al., 2003)... 42

Figure 2.9: Chitosan scaffold built by RPBOD (Geng, et al., 2003)..... 43

Figure 2.10: 3D robotic industrial bioprinter -- Computer Aided Biological (CAB) tool (Mironov et al., 2009)..... 44

Figure 2.11: Three modes of biopolymer deposition (a) droplet mode (b) continuous mode (c) contact mode 54

Figure 3.1: Schematic of the 3D multi-nozzle printing system for freeform fabrication of tissue constructs.. 56

Figure 3.2: The Texas Instruments of eZDSP TMS320F2812 Microprocessor 58

Figure 3.3: The printing process by using eZDSP F2812 Microprocessor.. 59

Figure 3.4: The initial system set-up with one pressurized extruder..... 61

Figure 3.5: G320X DC servo drive with screw terminals and adjustable PID pots..... 62

Figure 3.6: Whale3 DC servo drive with integrated connection interface 63

Figure 3.7: The operation interface of MACH3 control software..... 67

Figure 3.8: digital temperature controllers (CNi8DH53 and CN8501TC-R1)..... 68

Figure 3.9: Connection diagram of the temperature controller 68

Figure 3.10: EFD VALVEMATE 8000 multi-valve controller 69

Figure 3.11: EFD BackPack actuator and solenoid driver 70

Figure 3.12: MicroFab MJ-SF-01-50 piezoelectric nozzle 72

Figure 3.13: Bipolar waveform is used for controlling the voltage time intervals..... 73

Figure 3.14: Microfab piezoelectric nozzle (MJ-ATP-01-80) 74

Figure 3.15: Microfab HP 7x Pressure-Driven Valve..... 76

Figure 3.16: Two custom made copper needle tips with inner diameter..... 78

Figure 3.17: Schematic of 741MD-SS needle microvalve..... 79

Figure 3.18: User friendly integrated software for pre-operation.. 82

Figure 3.19: Skeinforge operation interface.. 84

Figure 3.20: Slice simulation for one layer and for the whole structure 85

Figure 3.21 (a) Top view of the strut. (b) 3D design of a 20-layer scaffold. 86

Figure 4.1: All combinations of solid objects can be represented by implementing Boolean operation. (∩ : intersection; ∪ : union; -- : difference).. 91

Figure 4.2: (a) Model of a heterogeneous structure consisting of three objects (b) procedure to generate the database of a heterogeneous fabrication model in one layer ... 94

Figure 4.3: Combination procedure flow chart for one layer of heterogeneous models ... 98

Figure 4.4: Heterogeneous model structure slicing results with same slicing thickness.. 100

Figure 4.5: Procedure Flowchart Describing Layered Fabrication of a Heterogeneous Structure 101

Figure 5.1: Chemical Structure of PCL and glacial acetic acid 102

Figure 5.2: Chemical structure of alginate 104

Figure 5.3: Chemical Structure of PEG-PLGA-PEG 108

Figure 5.4: Chemical structure of Irgacure 2959..... 109

Figure 5.5: Chemical Structure of sucrose 110

Figure 5.6: Rheometer (Brookfield, DVII+Pro)..... 113

Figure 6.1: The 3D multi-nozzle heterogeneous printing system and machine integration.. 116

Figure 6.2: Flow chart of machine calibration procedures..... 122

Figure 6.3: 3D constructs printed from PCL in various conformations: a) 8mm cylinders; b) 10mm x 10mm struts; c) 30mm x 30mm strut with 15 layers; d) 30mm x 30mm strut with 20 layers 126

Figure 6.4: a) macroscopic view of 10mm x 10mm strut (S9); b) digital micrograph showing the detail of the line structure..... 131

Figure 6.5: a) macroscopic view of 10mm x 10mm strut (S10); b) digital micrograph showing the detail of the line structure..... 132

Figure 6.6: a) macroscopic view of 10mm x 10mm strut (S11); b) digital micrograph showing the detail of the line structure..... 133

Figure 6.7: a) macroscopic view of 30mm x 30mm strut (S20); b) digital micrograph showing the detail of the line structure..... 134

Figure 6.8: The strut was printed by two EFD dispensers using the heterogeneous printing algorithm.. 136

Figure 6.9: The mixed strut was printed by two EFD dispensers using the heterogeneous printing algorithm.. 138

LIST OF TABLES

Table 1.1 Comparison of different SFF manufacturing technologies……22

Table 1.2 Cell size and desired pore diameter of scaffolds for different TE applications ……30

Table 2.1 Comparison of commercial 3D bioprinting systems……46

Table 3.1 Characteristics and comparison of two solenoids……70

Table 3.2 Features comparison of four commercial printing nozzles……80

Table 4.1 Reasoning Boolean operations……90

Table 5.1: Viscosity of various sucrose mixtures……112

Table 6.1: System control parameters (set up with the spindle speed in the APT file kept constant at 500 rpm and the active frequency of MACH3 nozzles kept constant at 6Hz). ……125

Table 6.2: The key parameter settings for two EFD dispensers……135

Table 6.3: The key parameter settings for two EFD dispensers……137

ABSTRACT

A New Flexible and Multi-purpose System for Printing 3D Microstructures with Heterogeneous Materials for Tissue Engineering

Ho-Lung Li
Jack G. Zhou, Ph.D.

Tissue engineering is a regenerative medicine approach that combines the applications of engineering methods, material science, and biology research toward the development of biological substitutes that restore, maintain, or improve human tissue or organ function. It has appeared as a rapidly expanding field to address the organ shortage problem and comprises tissue regeneration and organ substitution. A variety of freeform fabrication methods for constructing tissue scaffolds have been developed due to the feasibility of producing scaffolds with customized external shape and predefined internal morphology, allowing accurate control of pore sizes and pore distribution.

A new type of solid freeform fabrication (SFF) machine combined with a novel heterogeneous algorithm based on Automatically Programmed Tools (APT) language has been developed to construct hydrogel scaffolds and porous structures. In this study, the system was connected into a PC to act as a high-performance servo controller for monitoring the control of a three axis x-y-z moving arm. The printing procedures were repeated layer-by-layer to form a 3D structure. Several biocompatible or thermosensitive materials such as PEG-PLGA-PEG triblock copolymer, poly (ε-

caprolactone) (PCL), and a composite of sucrose-based mixture have been printed by this new three-dimensional direct printing machine and the experimental results are discussed with respect to potential applications.

The SFF technique will allow us to easily control the porosity and the interconnectivity of the pores. However, some enhancements must be achieved in order to obtain optimal resolution of the fabricated 3D scaffolds. The modification of several dominant parameters of the deposition of the biopolymer such as the traveling speed, extrusion speed, flow rate, layer height, nozzle diameter, biopolymer concentration, viscosity and mechanical properties, as well as the design of the scaffold, will lead to the fabrication of optimized 3D scaffolds. Our self-designed biomaterial SFF system has notable advantages over other commercial SFF machines, including: 1. Changeable printing nozzles for materials with different viscosities and compositions. 2. Re-constructible system setup for different printing purposes. 3. Capability for heterogeneous printing. 4. User-friendly software development 5. Economical system design. The study of the hardware and software and their integration are described and its new heterogeneous printing algorithm is discussed for multiple purpose uses. The integrated software has been developed to link all components of the control system together and it is easy to adapt to different applications. In addition, PCL scaffolds, sucrose structures, and heterogeneous structures have been fabricated and tested with our SFF system. The optimization of dominant parameters for the fabrication of 3D scaffolds with desired pore sizes in the range of 100-500 μm was confirmed by light microscopy, and we have shown that our system is capable of fabricating

heterogeneous structures efficiently and economically. The system also demonstrated potential for modifications to be adapted for directly and accurately implanting cells for tissue regeneration based on the CAD system design.

CHAPTER 1 : INTRODUCTION

1.1 Tissue Engineering Technologies

Tissue loss and organ failure are the most detrimental and costly problems in contemporary medicine in the United States (Langer & Vacanti, 1993). Tissue substitutes for human bones, skin, and other organs are growing rapidly and playing an important role in replacing or repairing damaged, infected or tissue that has been rendered nonfunctional by trauma, pathological degradation, congenital deformation, or aging problems (Yang et al., 2004; Cuckler, 2004; Bock, Goode and Novartis, 2003). Annually, over 1 million patients need to undergo surgery for tissue transplantation or reconstruction (Kelly, 2000; Cutter and Babak, 2006). Since organ transplantation is totally restricted by the number of donors and limited by immunogenic issues, many patients die because there are no suitable organs that can be used. Recently, some mechanical devices have been developed to replace human bones for adults but not for juvenile patients. Even though a very few mechanical devices have been developed for adjusting the length for young people, it still takes too much risk for them to undergo a surgery every year.

In order to overcome these limitations, the field of tissue engineering has been expanding and developing since 1987. Tissue engineering is a new discipline which integrates biology, science, and engineering knowledge to develop technologies to restore, replace or enhance the function of human tissues and organs (NIH). The core

technologies of tissue engineering, incorporating cell culture, biomimetic scaffold structures and biochemically active agents, have allowed researchers to engineer and grow tissues and organs from a patient's own cells which can then be implanted back into the patient. Therefore, tissue engineering has a specific goal to create engineered tissues and organs and implant to repair and replacement of damaged or injured human organs for improving human life (Griffith and Naughton, 2002; Langer R, Vacanti, 1993).

A variety of methods have been employed to build human organs or tissues for replacement or repair purposes. Many developmental processes have already served as a reference and provided powerful insights into tissue engineering (Marga et al., 2007; Steer and Nigam, 2004). Nowadays one of the most widely adapted tissue engineering approaches involves building a synthetic porous scaffold that mimics aspects of the body's own extracellular matrix (ECM), onto which cells attach, migrate, proliferate and function (Freyman, Yannas and Gibson, 2001). The most commonly used method in tissue engineering is to obtain donor tissue from the patient, and then dissociate it into individual cells, which are allowed to proliferate in culture. The cells are then embedded in or coated on porous structures in a cell culture medium *in vitro* that serve as temporary "scaffolds" (Fedorovich et al., 2007; Tsang and Bhatia, 2004). The diseased or damaged tissue or organ is removed from the patient and the scaffold with attached cells is implanted. Over time, the synthetic scaffold degrades into the body and the cells produce their own natural ECM (Chapekar, 2000; Freyman et al., 2001).

The scaffold-based method is the most popular way to construct a tissue replacement structure. In this approach, scaffolds can provide a proper space for random seeding of cells and allow growth factors to be delivered into the scaffold to support the proliferation of cells. Scaffolds often have intricate internal architecture, porosity and connectivity in order to support their integration into the existing physiological environment and to provide the required structural integrity, transport capability, and microenvironment for cell and tissue growth (Mikos et al., 1994; Ratner et al, 1996; Jain, 2000). Thus, the micro-architecture of tissue scaffolds has a significant influence on cells in terms of migration, distribution, and proliferation (Maquet and Jerome, 1997; Wake, Patrick, and Mikos, 1994).

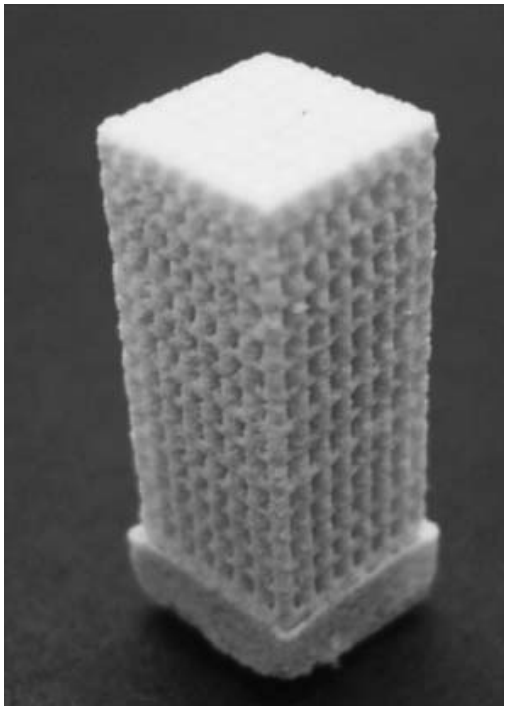

Figure 1.1: PLLA/CHAp (carbonated hydroxyapatite) nanocomposite scaffolds (Zhou et al., 2008)

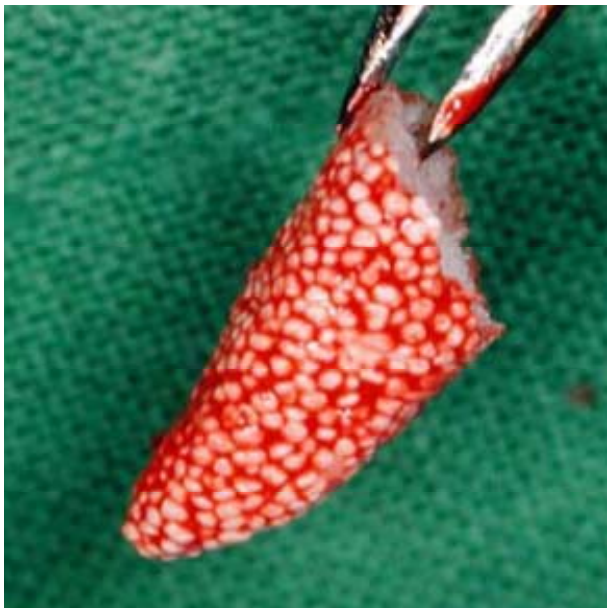

Figure 1.2: β-TCP/PLGA open porous copy of the root of a mandibular third incisor of a mini-pig. The open porosity of the scaffold allows the absorption of autologous blood. (Nair et al., 2004)

One of the challenges in tissue engineering is to provide adequate supplies of oxygen and nutrients to cells within the engineered tissue construct. Solid materials with built-in porosity, such as biodegradable poly-L-lactide (PLLA) (Ma et al., 2005; Ushida et al., 2002; Yang et al., 2004) or poly (lactic-co-glycolic acid) (PLGA) (Huang et al., 2004; Uematsu et al., 2005), have been assembled in three dimensions to provide a scaffold for the attachment of implanted cells and for perfusion. However, solid scaffold materials are often too rigid for application in soft tissues. A variety of natural materials or synthetic biopolymers can be selected to construct tissue scaffolds for specific applications (Langer & Vacanti, 1993). Numerous tissue scaffolds have been presented, of which biopolymer hydrogel-based scaffold materials, such as alginate, fibrin, gelatin, collagen and chitosan are highly appealing because of their property similarities to the macromolecular-based human tissues, and their biocompatibility, very low toxicity, relatively low cost, and availability. These polymers potentially have numerous applications in tissue engineering as delivery vehicles for cells and drugs, as wound dressings, dental impressions, and immobilization matrices (Lowman et al., 1999; Elissee et al., 1999; Mongia et al., 1996). However, most hydrogel scaffolds reported in the literature exhibit simple geometrical configurations, for example, injectable bulk gel, simple two-dimensional structure with lines and gel droplets (Drury and Mooney, 2003; Ma et al., 2003; Ma, 1995; Ma and Zhang, 1999). Although some of them might be suitable for studying cells' biological behavior in scaffold and hydrogel material formations, study on how to build scaffolds in a 3D structural configuration and the importance of these configurations for structure-cell-tissue formation have not been

well addressed (Draget and Smidsrod, 1991; Stevens et al., 2004; Vozzi et al., 2003). Particularly, the processing procedures for fabricating 3D hydrogel tissue scaffolds are still not sufficiently optimized.

1.2 Microfabrication

In order to mimic human organs and tissues, it is necessary to consider the spatial organization of tissue for cells in scaffolds. While approaching the design and fabrication of a viable tissue structure, we have to consider the cells and scaffolds to use according to the characteristics of the native tissue. Tissue consists of a dynamic 3D microenvironment with multiple cell types and their corresponding extracellular matrix (Zahair and Weaver, 2004). These interact with the cells of the tissue to control cytoskeletal organization and activate signaling cascades (Juliano, 2002). For tissue engineering applications, materials with cell-adhesive properties are patterned so that cells will adhere to the generated architecture. This patterning of cells has provided valuable information on fundamental cell biology and has also been used for some TE applications (McDevitt et al., 2002).

Two common methods used to build structures for microfabrication in tissue engineering are photolithography and soft lithography. For fabricating small-scale structures for biological applications, soft lithography has become more desirable than photolithography. Soft lithography technology is able to control the molecular structure of surfaces, patterning complex molecules, fabricating microchannels, and manipulating

cells (Whitesides et al., 2001). This technology uses stamps or molds to easily generate 10 to 100 μm size patterns on the surface, 50 to 500 μm sized culture chambers, and 10 to 100 μm sized capillaries for laminar flow of culture media (Mrksich et al., 1996; Xia et al., 1999).

Microcontact printing (μ-CP) is representative of the soft lithography technology that involves micromachining of an elastomeric polymer in order to stamp a pattern to which cells can easily adhere. It can simply generate features 1 μm in size or as small as 200 nm and provide valuable information on the effects of shape-based constraints on cells. An illustration of the fabrication process is shown in Figure 1.3. Although soft lithographic techniques have allowed the generation of hydrogel scaffolds containing a network of fluid channels, these structures are still restricted to two dimensions (Mrksich and Whitesides, 1996). The costs of complicated and often time-consuming manufacturing steps are also issues of concern.

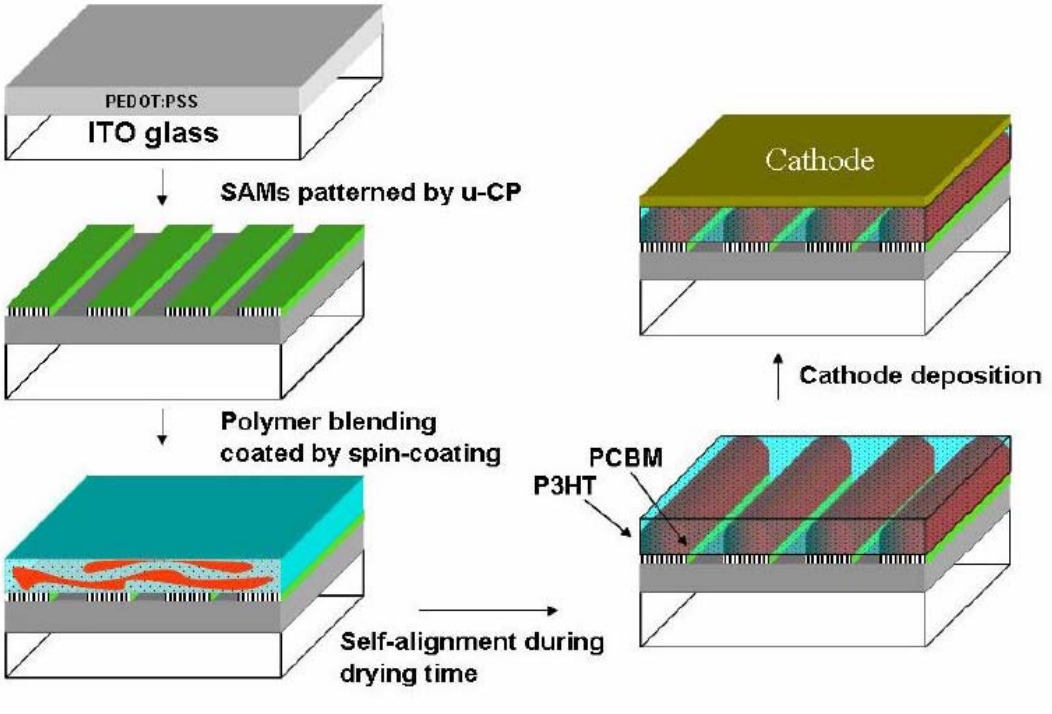

Figure 1.3: Illustration of the fabrication process for polymer solar cells with spontaneous surface-directed phase separation. PEDOT:PSS: Poly(3,4-ethylenedioxythiophene):poly(styrenesulfonate). ITO: Indium tin oxide. u-CP: Microcontact printing. PCBM: (6,6)-Phen yl-C_{61}-butyric acid methyl ester. P3HT: Poly(3-hexylthiophene). (Chen, 2008)

1.3 Solid Freeform Fabrication

1.3.1 Conventional Fabrication Technologies

In tissue engineering, numerous fabrication methods have been reported in the last decade. Some conventional chemical technologies, such as thermally induced phase separation technology (Figure 1.4) (Nam et al., 1999, Huang et al., 2008), particle

leaching process (Figure 1.5) (Kang, et al., 2006; Lickorisha et al., 2007), emulsion freeze drying (Figure 1.6) (Wang et al., 1995; Sultana and Wang, 2008) and gas forming method, have been widely used to form tissue scaffolds for different applications. However, these technologies still have some limitations in designing and fabricating highly reproducible scaffolds with complicated internal structures and porous interconnectivity, due to the lack of ability to control pore size and scaffold thickness, variation in solvent evaporation rates, and leaving behind residue of chemical materials or organic solvents. Therefore, rapid prototyping (RP), also called solid freeform fabrication (SFF), has been proposed and widely developed as a new technology to conquer these limitations in recent years.

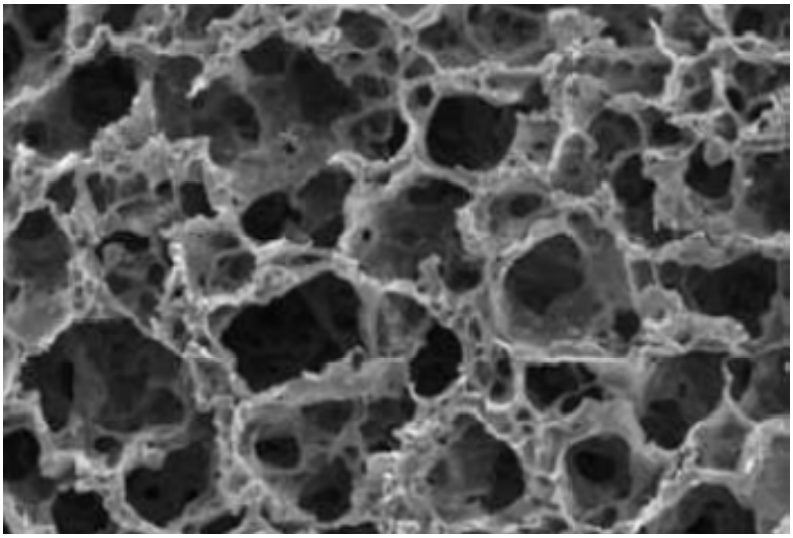

Figure 1.4: SEM micrographs of PLGA/NHA (95/5) scaffold. Thermally induced phase separation technology was used to generate highly interconnected macro-porous scaffolds from 100 to 150 μm for bone tissue engineering (Huang et al., 2008).

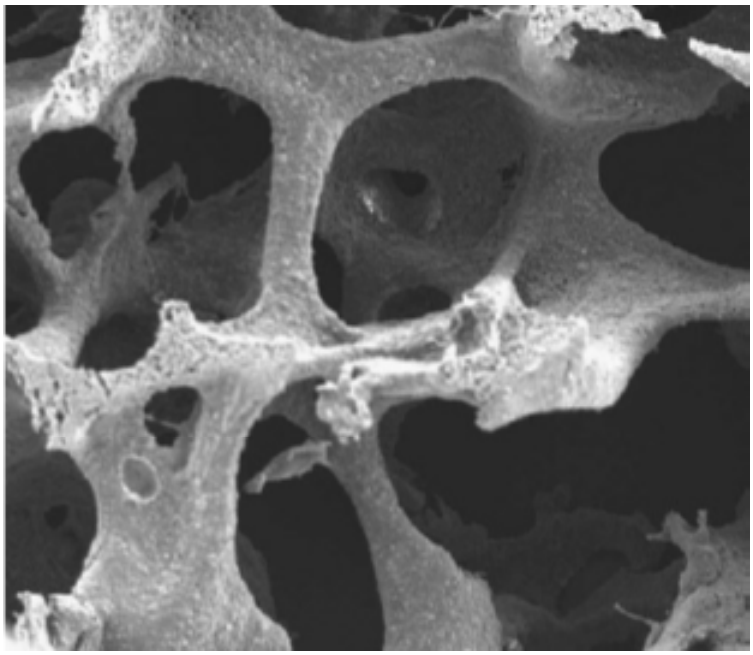

Figure 1.5: SEM micrograph of PLGA/CaP (75/25) composite. The scaffold was fabricated by a particulate-leaching method and had a nominal macro-pore size in the range of 800-1800µm with porosity between 81–91%. (Lickorisha et al., 2007)

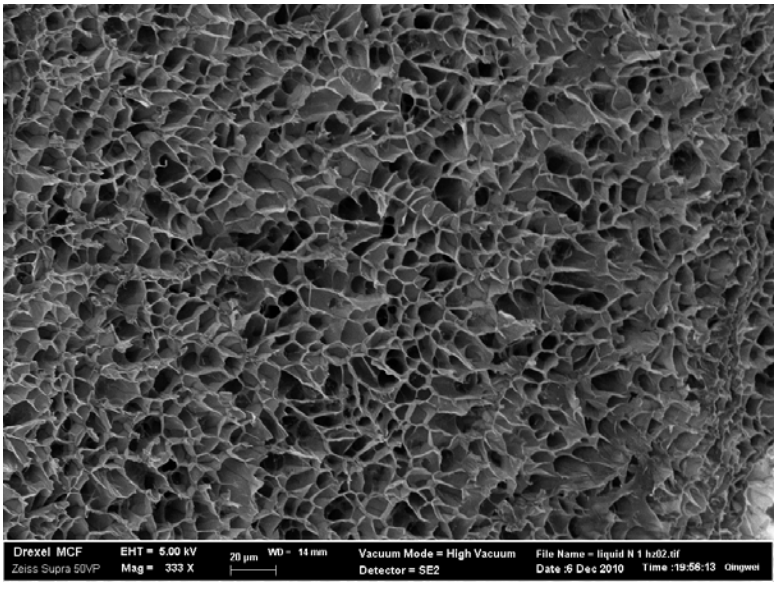

Figure 1.6: SEM micrograph of micro-porous chitosan produced by liquid nitrogen freeze drying process that generated highly porous and interconnected porous structures with pore sizes ranging from 10 to 50µm (Qingwei Zhang).

1.3.2 SFF manufacturing technology

SFF manufacturing technology, also called rapid prototyping (RP) and layered manufacturing, has shown rapid growth for decades. It is capable of producing complex freeform parts directly from a computer aided design (CAD) model of an object without part-specific tooling or fixture. The CAD model can be designed using a large range of powerful CAD software or obtained through reverse engineering to reconstruct three-dimensional models. The CAD model is then transferred into sliced layers and a series of scanning lines, tool paths or dots for SFF manufacture machine instruction; based on this, numerical control codes are generated to control the machine in rebuilding the part (Jacob., 1992).

Solid freeform fabrication (SFF) technology such as selective laser sintering (SLS), stereolithography (SLA), layered manufacturing (LM), three-dimensional plotting (3D-Plotting) and three-dimensional printing (3DP) have been widely developed in recent years. SFF is a computerized fabrication technique that can rapidly produce highly complex three-dimensional objects using data from CAD systems and medical imaging equipment. This is achieved in a layer-by-layer process whereby CAD designs are sliced into two-dimensional layers, where the prototyping material is deposited to build the final structure. SFF technology possesses several unique advantages that make it a powerful manufacturing tool for 3D scaffolds. First, the three-dimensional CAD model of the tissue can be reconstructed precisely by reverse engineering software based on the

data from a CT or MRI system. The SFF machine can subsequently make the scaffold with any complex geometry with high accuracy (Cinibulk., 2008). This will significantly eliminate the problems caused by the mismatch between implant and remaining host tissue. Second, SFF technology makes parts in an additive fashion through a layer-by-layer process. In each layer, materials can be added line-by-line, or even dot-by-dot, so the internal structure of the porous scaffold can be controlled directly and precisely to meet any special requirements. Third, a wide range of biomaterials is available to make scaffolds using SFF technology. Fourth, SFF technology can be combined with other manufacturing technologies, such as powder metallurgy processes, casting processes or plastic injection modeling that make the technology flexible. Finally, heterogeneous structures can be achieved by implementing multiple printing nozzles and special algorithms in the system. Recently, SFF has been widely used in direct fabrication of porous scaffolds for skeletal part replacement (Porter N.L. 2001).

1.3.2.1 Direct SFF Technology

A variety of direct SFF technologies have been employed to construct tissue structures or scaffolds for bone replacement (Sodian, 2000; Lange and Bhavnani, 1994; Porter et al., 2001). The most common methods are s*tereolithography apparatus, selective laser sintering process, fused deposition modeling, and 3D Printing process.*

1.3.2.1.1 Stereolithography Apparatus (SLA)

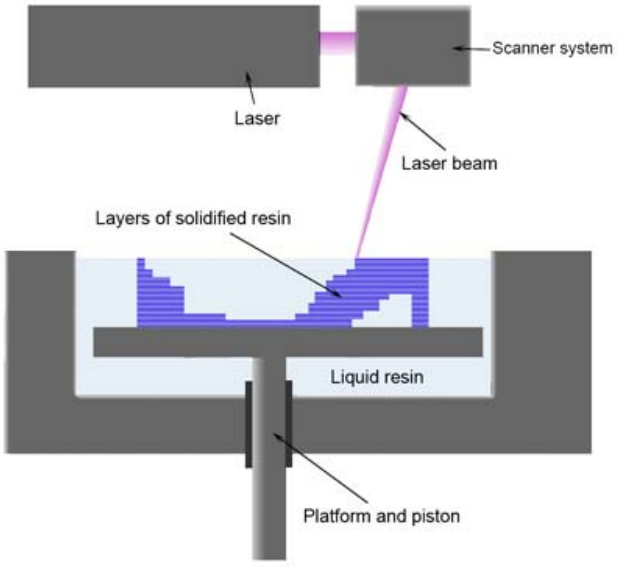

Figure 1.7: The illustration of the SLA technology

"http://commons.wikimedia.org/wiki/Commons:GNU_Free_Documentation_License_1.2" \o "Commons:GNU Free Documentation License 1.2"
(http://en.wikipedia.org/wiki/Stererolithographic_apparatus)

The s*tereolithography apparatus* (SLA) is one of the most common types of SFF technology (Figure 1.7). This method mainly uses a laser beam which shines on the surface of a vat of liquid photopolymer. When the laser beam touches the liquid, the polymer material solidifies rapidly. The laser beam moves the entire geometry of each layer until each layer is completely traced and totally solidified. The substrate is then lowered down to a specified distance and the same procedures are repeated. A support material is also used to sustain the model when the fabrication has undercuts or

overhangs. When all layers are completely built, each layer adheres to adjacent ones. The support material and remaining excess photopolymer then need to be removed from the model by drying and wiping off. After a UV curing method has been applied to stabilize the model, a complete solid 3D model is created.

Although SLA has been considered the most accurate technology to build a structure, the time-consuming UV curing method and the cost of the photopolymer pose significant problems for users. Figure 1.8 shows a scaffold structure where poly (propylene fumarate) (PPF) was used as the material, diethyl fumarate (DEF) was used as the solvent, and bisacrylphosphrine oxide (BAPO) was used as the photo-initiator. Pore size up to 1000µm with good interconnectivity was obtained using SLA method (Lee et al., 2007).

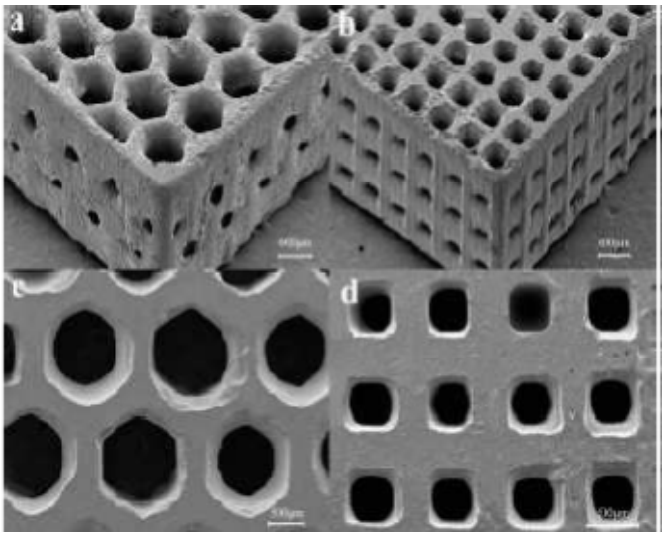

Figure 1.8: SEM micrographs of PPF scaffolds (Lee et al., 2007)

1.3.2.1.2 Selective Laser Sintering (SLS)

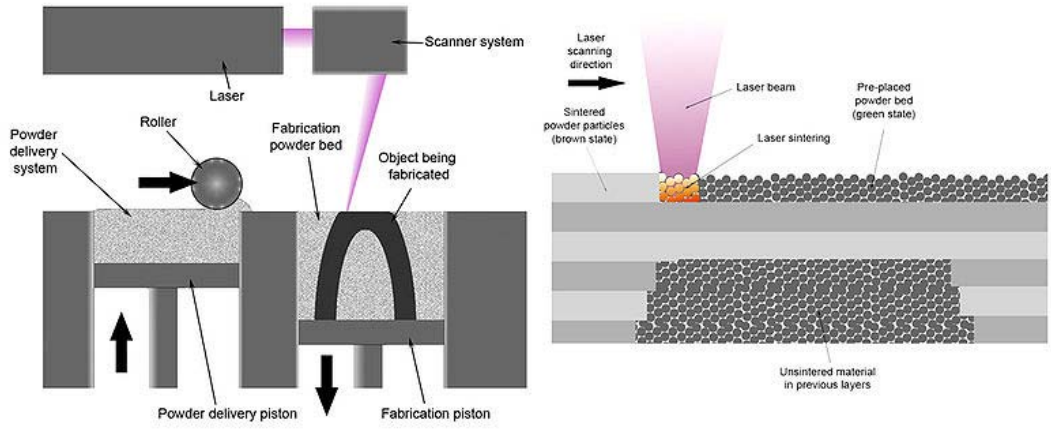

Figure 1.9: The illustration of the SLS technology

"http://commons.wikimedia.org/wiki/Commons:GNU_Free_Documentation_License_1.2" \o "Commons:GNU Free Documentation License 1.2" (http://en.wikipedia.org/wiki/File:Selective_laser_melting_system_schematic.jpg)

Selective laser sintering (SLS) technology (Figure 1.9), developed at the University of Texas at Austin in the mid-1980s, is a layer additive production process that creates 3D models usually by using high power carbon dioxide laser to melt or sinter, and fuse selective powder molecules based on CAD files. The laser selectively fuses powdered material by scanning cross-sections generated from a model on the surface of a powder bed. After each cross-section is scanned, the powder bed is lowered by one layer thickness, a new layer of material is built on top, and the process is repeated until the part is completed. Unlike the other SFF technologies, the greatest advantage of the SLS method is that it does not need support structures, as the part being constructed is

always surrounded by unsintered powder. The disadvantage is that the potential accuracy of models is limited to size of powder particles, and parts have rough, grainy and porous surface finish. As shown in Figure 1.10 below, porous polycaprolactone (PCL) scaffolds were computationally designed and then fabricated via SLS technique. Pores ranged from 1.75–2.5 mm in diameter, producing scaffolds with designed volumetric porosity ranging from 63 to 79% (Williams et al., 2005).

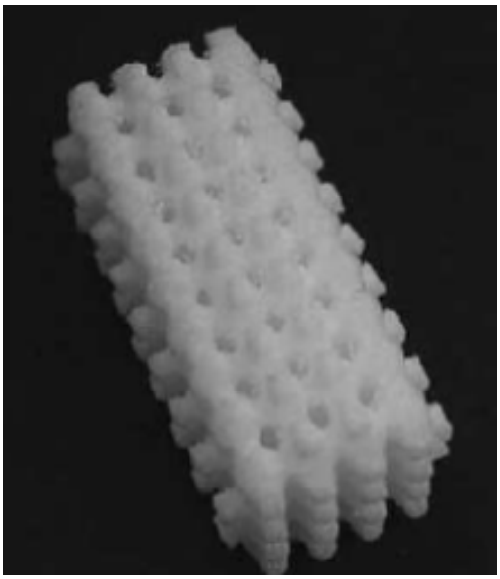

Figure 1.10: PCL scaffold fabricated by SLS (Williams et al., 2005).

1.3.2.1.3 Fused Deposition Modeling (FDM)

F*used deposition modeling* (FDM), commercialized from Stratasys inc. in the 1990s, involves a process where a plastic filament about 1.58mm in diameter is

unwound from a coil and passes through a nozzle (Figure 1.11). The nozzle tip is heated up to melt the plastic filament as it is about to be printed out. A moving arm or table is able to move in the x, y, and z axes in order to deposit the plastic filament on the substrate and form a 3D structure according to a pre-specified pattern. This method still needs support structures to maintain a 3D model when overcuts or overhangs are present. Compared to the other technologies, this method provides an easy way and a low cost method to construct 3D structures without applying a post-curing step. On the other hand, the printing accuracy cannot reach a sufficiently high resolution for microstructure purposes, as it is limited by a millimeter scale nozzle.

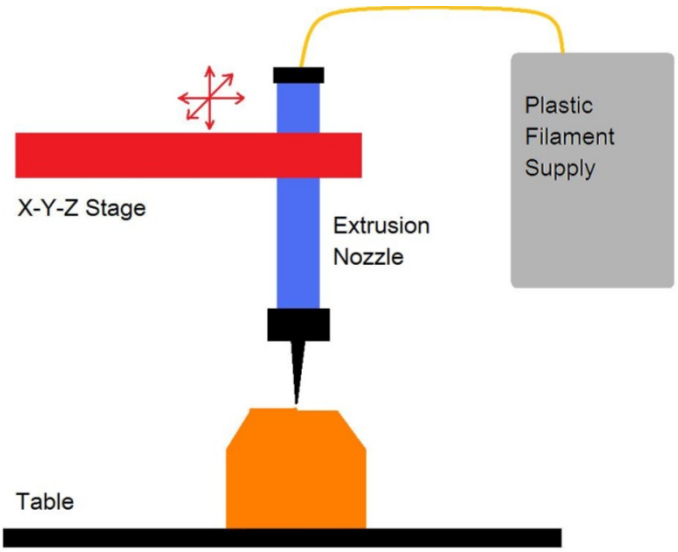

Figure 1.11: An illustration of FDM system

1.3.2.1.4 Three-dimensional Plotting (3D-Plotting)

In this system, a dispenser head is controlled by a 3-axis platform, typically a CNC machine or robot. The process generates an object by building micro strands or dots in a layered fashion. Depending on the type of dispenser head, a variety of materials can be used to build scaffolds.

The advantage of the system is its versatility with a wide range of material and the absence of hot processes, often adverse for biological materials. This method is generally low cost with minimal specialized equipment required. A simple adaptation of dispenser heads will allow a wide variety of thermoplastic polymers as well as practically any pastes and solutions.

Landers et al. presented a new technique that can make use of a wide variety of polymer hot melts as well as pastes, solutions and dispersions of polymers and reactive oligomers (Landers et al. 2002). However, resolution is the primary limiting factor, determined by the size of dispensing tip. Vozzi et al. achieved resolution as low as 10µm through the use of microsyringes and electronically regulated air pressure valves (Vozzi et al., 2001). Vozzi et al. proposed a microsyringe-based 3D scaffolds fabrication technique that employs a highly accurate three-dimensional micropositioning system with a pressure-controlled syringe to deposit biopolymer structures with a lateral

resolution of 50µm (Figure 1.12) (Vozzi et al., 2003). The pressure-activated microsyringe is equipped with a fine-bore exit needle, through which tiny amounts of polymer come out when pressure is applied to the syringe. A wide variety of 2D and 3D patterns can be fabricated. Poly-lactic-glycolide (PLGA), polycaprolactone (PCL) and blend of PLLA and PCL were used in their research. Experiments indicated the simplicity and possibility of scaffold fabrication with various biopolymers. Figure 1.13(a) and (b) show a single layer and multi-layer structure respectively with 20% PLGA solution.

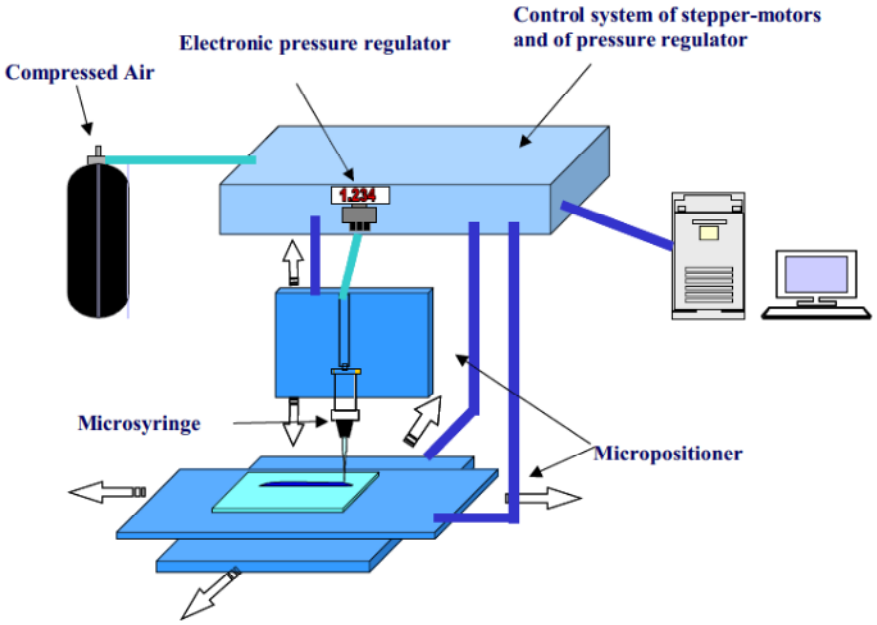

Figure 1.12: Schematic of microsyringe method (Vozzi, et al., 2003)

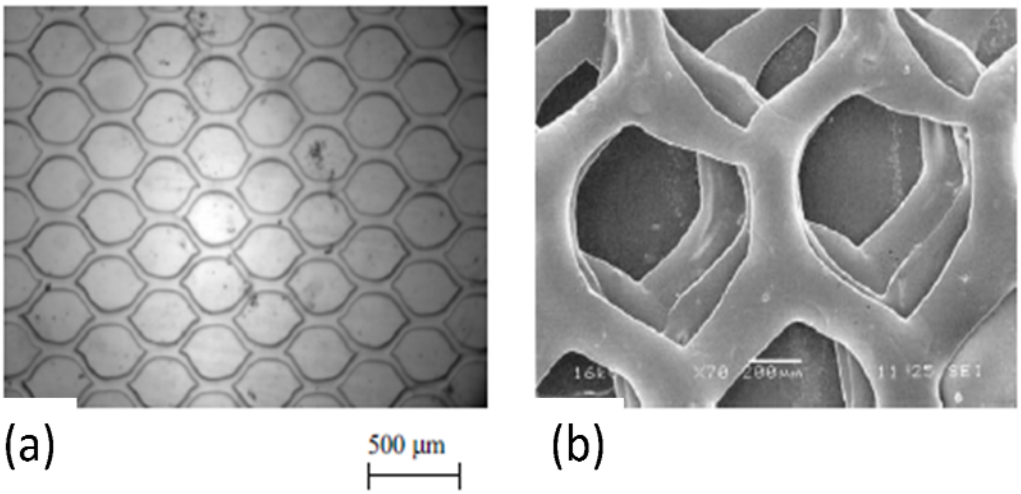

Figure 1.13: (a) 2D PLGA scaffold, and (b) 3D PLGA scaffold (Vozzi et al., 2003)

1.3.2.1.5 Three-dimensional Printing (3DP)

Figure 1.14: The digital image of Z-printer 350

(http://www.zcorp.com/en/Products/3D-Printers/ZPrinter-350/spage.aspx)

The *three-dimensional printing* (3DP) process is a relatively new RP technology, developed at MIT. This method mainly uses an ink-jet head to print out liquid adhesive onto a bed of powder to build a structure by a layer-by-layer manner. After each layer is fully completed, the bed is moved up and the remaining powder needs to be cleaned away. Since this is a powder-based fabrication technique, the part still needs to use solidified material, such as wax liquid, to maintain the shape of the model. The major advantages of this technology are rapid printing and low cost of powder material; however, the printing resolution, surface finish and material selectivity are major disadvantages. Figure 1.14 shows a 3DP machine called Z-printer 350 developed by Z Corporation Inc. This 3D printing method makes it possible to fabricate cylindrical scaffolds of copolymers polylactide–coglycolide (PLGA, 85:15) in a suitable solvent like dichloromethane. As shown in Figure 1.15, interconnected porous channels are about 800µm in diameter and micro-porosities of 45–150µm can be achieved (Lam et al., 2002). Table 1.1 summaries the advantages and disadvantages of different direct SFF technologies.

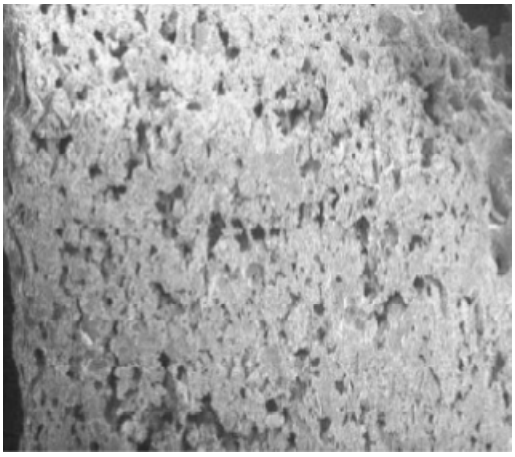

Figure 1.15: SEM micrograph of PLGA copolymer scaffold (Lam et al., 2002).

Table 1.1 Comparison of different SFF manufacturing technologies

RP Technique	Materials	Advantages	Disadvantages
SLA	Photopolymer resins	Relative easy to remove support materials, Relative easy to achieve small features	Limited by the development of photopolymerizable and biocompatible, biodegradable liquid polymer material
SLS	Metals, ceramics, bulk polymers compounds	High accuracy, Good mechanical strength, Broad range of bulk materials	Materials trapped in small inner holes is difficult to be removed, biodegradable materials maybe degrade in the chamber
FDM	Some thermoplastic polymers/ceramics	Low costs	Elevated temperatures Small range of bulk materials Medium accuracy
3DP	Ink + powder of bulk polymers, ceramics	No inherent toxic components Fast processing Low costs	Weak bonding between powder particles Bad accuracy-rough surface
3D Plotting	Swollen polymers (hydrogels) thermoplastic polymers reactive resins, ceramics	Broad range of materials Broad range of conditions Incorporation of cells proteins and fillers	Slow processing Low accuracy Time consuming adjustment to new materials

1.3.2.2 Indirect SFF Technology

SFF technology also includes an indirect manufacturing method which has been used for bone fabrication by a few research groups (Taboas et al., 2003; Limpanuphap and Derby, 2002; Chu et al., 2002). Taboas and colleagues proposed a method to build a polylactic acid (PLA) scaffold by implementing a ceramic/cement mold which was built by Solidscape system. PLA in chloroform with NaCl or PLA melt grains were cast into the ceramic mold. Following evaporation of the solvent and cooling of the PLA melt, the PLA scaffold was formed by removal of the mold via acid.

Limpanuphap and Derby fabricated tricalcium phosphate (TCP) scaffolds by first building a mold using Solidscape DPP system. The scaffolds were made by selective dissolution of the mold in acetone. Then a heating treatment was applied to remove the acrylic binder, followed by sintering. Chu et al. have developed an indirect fabrication method to produce hydroxyapatite (HA) based porous scaffolds. First, a suspension of HA in acrylate was prepared and the HA slurry was then poured into a mold fabricated using stereolithography. The injected mold was thermally cured and burned in order to remove the mold material. However, sintering the whole scaffold under high temperature causes the distortion and shrinkage of the scaffolds and other unexpected fabrication problems.

Although most of these techniques have achieved the goal of building a porous scaffold for bone reconstruction, many drawbacks and difficulties still exist. For instance, these indirect fabrication processes mentioned above are very complicated and not suitable for mass production. Most of the organic solvents used for mold removal are relatively toxic and removal of the mold involves high temperature sintering, which renders it impossible to simultaneously culture cells or introduce temperature-sensitive bioactive components in the scaffold during the fabrication process of an integrated structure. Thus, a biocompatible scaffold material, non-toxic mold material and solvent, and the ability to eliminate sintering from the process are requirements for using the indirect SFF method in tissue engineering.

1.4 Homogeneous and heterogeneous structures

Conventional solid modeling concepts have focused on developing models of physical objects to capture their geometry. These approaches have been well developed, due to the fact that most physical models found in engineering applications are homogeneous. Homogeneous modeling is a fundamental step towards the design and analysis of structural optimization (Bendsoe and Kikuchi, 1988; Cherkaev, 1994). This modeling method allows the description of heterogeneous structure by constitutively correspondent. On the other words, the concept of material feature is defined as the specified material distribution of a certain sub-region within a solid. Recently, more and more research has focused on the effect of heterogeneous modeling

based on material features. A simple idea of the heterogeneous modeling with three different materials has been shown in Figure 1.16. For example, in tissue engineering, human bones could be considered as heterogeneous objects. The rapid development of biological technologies demands the manufacturing of heterogeneous objects, in order to build the physical models of tissues for applications in reconstructive surgeons and tissue implementation (Sun and Lal, 2002).

In particular, rapid prototyping or layered manufacturing (LM) technologies have shown great potential for fabricating high resolution synthetic models in many areas, including surgery, architecture, engineering, and art. In order to mimic an object found in nature, composition control is crucial for improving a variety of properties, such as thermo conduction, surface tension, elasticity, conductivity, strength, fatigue performance, stress distribution, and reducing the weight of the structure in each element (an approach widely implemented in the automobile and aerospace industries without decreasing the strength of the composite). Furthermore, by conducting finite element analysis (FEA), the overall behavior of the entire heterogeneous structure can be predicted and analyzed. As we know, heterogeneous models are rarely present in man-made productions, but commonly exist in nature. Since RP technology and its algorithms have rapidly developed in the last decade, constructing heterogeneous structures has become achievable by applying RP technologies. It is also possible to embed components, such as sensors, actuators, and microprocessors, to create complete assemblies (Rajagopalan et al., 2001). To overcome certain limitations in current heterogeneous modeling methods, such as material identification and

distribution in CAD systems, a novel RP processing algorithm for SFF of heterogeneous structures that is based on an automatically programmed tools (APT) file is discussed in Chapter 4 of this thesis.

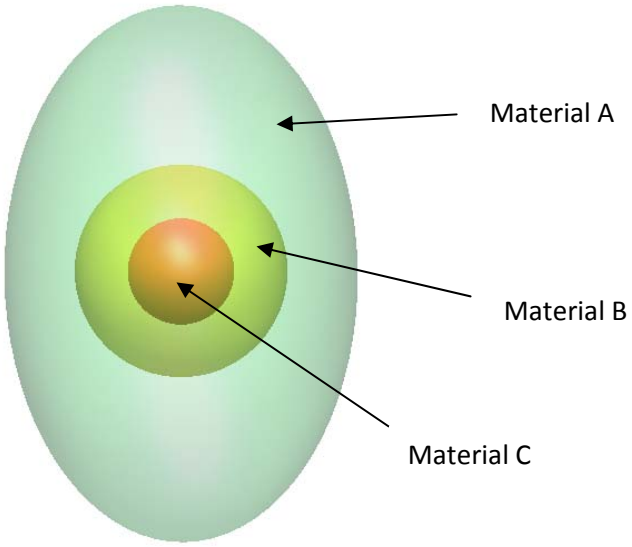

Figure 1.16: An example of heterogeneous structure with three different materials distribution.

1.5 Research objectives

The objective of this research is to develop a multi-functional, multi-nozzle, and multi-material SFF system based on an advanced computational heterogeneous algorithm for fabricating 3Dimensional tissue structures. Our long term goal is to design and fabricate native-like functional human tissues and organs suitable for regeneration, repair and replacement of damaged or injured human organs. In this study, many

different types of materials including natural materials and synthetic biopolymers are described in Chapter 5 and used to construct 3D structures for tissue scaffolding purposes.

Toward this long-term goal, the work in this thesis addresses three specific aims:

1. Develop a new multi-functional 3D printing system with high resolution for fabrication of biocompatible tissue substitute structures.

2. Develop a novel RP processing algorithm for SFF of heterogeneous printing in the system.

3. Analyze and select specific parameters of this multi-functional 3D printing system for printing 3D structures using a range of model biomaterials.

The proposed research and activities will help to develop knowledge and lead to novel solutions in determining optimal design for bioactive scaffolds in tissue engineering applications. In this research, a new multi-functional 3D printing system has been designed and a novel RP processing heterogeneous algorithm has also been developed and applied to creating biocompatible structures. The properties of natural materials and synthetic biopolymer materials were studied to select a suitable printing nozzle. The parameters that need to be optimized for different materials in order to

print 3D structures using this multi-functional 3D printing system are presented and discussed. Different kinds of CAD models, such as cylinders and struts, are presented for homogeneous and heterogeneous structure printing and then compared to experimental results.

1.6 Proposed APT based heterogeneous SFF system and its technical advantages

In general, many processes have been developed in the area of biomanufacturing for the development of tissue engineered systems by adopting different printing methods, algorithms, materials, and mechanisms for regeneration of different tissues. These structures are dramatically distinct in resolution, smoothness, and material strength. In order to fit the requirements of the tissue scaffold design, it is necessary to develop a novel SFF system for multiple application purposes. The machine should be able to fit the special requirements for tissue construction as follows:

(1) Various biomaterials:

Since different human tissues or organs need to be reconstructed by using different biomaterials, the SFF system should have the flexibility to change different printing nozzles and different size of printing tips, an adjustable pressure system, and heating or cooling mechanisms to melt or freeze the biomaterials.

(2) High resolution:

It is well known that scaffolds play a critical role in tissue engineering. The primary regenerative tissue engineering approach involves the transplantation of cells onto scaffolds. Scaffolds mimic the function of the natural extracellular matrices for cell attachment, proliferation, and differentiation (Kandel et al., 2007). In order to regenerate body tissues by seeding cells into porous matrices, the SFF machine should be able to reach high resolution for axes moving and material deposition. Scaffold design may allow for cell growth and tissue remodeling through a combination of structure and chemical signaling. In comparison to cell culture on 2D plates, culturing cells in 3D scaffolds results in a microenvironment more closely resembling that found *in vivo*, such that the seeded cells respond to mechanical and biological cues from the 3D space to promote cell adhesion, proliferation and differentiation (Xie et al., 2006). Therefore, the resolution of the scaffold pore size for implanting cells is taking an important role in scaffold-based tissue construction. The preferred scaffold pore sizes for different cell types are summarized in Table 1.2 (Leong et al., 2008).

Table 1.2 Cell size and desired pore diameter of scaffolds for different TE applications

Tissue type	Cell size (μm)	Preferred pore diameter (μm)
Vascular	60-200	5 (for neovascularisation)
Liver (Hepatocyte)	20-40	20
Skin (Fibroblast)	20-50	90-360
Bone	20-30	100-350

(3) Heterogeneous printing:

Recently, SFF has received great interest for fabrication of complex-shaped implants and heterogeneous structures. To mimic human organs, such as bone, a multi-material printing process needs to be implemented for freeform fabrication of tissue structures. The machine should have a multi-nozzle system which can rotate or exchange nozzles automatically and sequentially through its heterogeneous algorithm to fulfill the multi-material printing purpose. The heterogeneous algorithm should combine with special modeling schemes which allow designers to design not only the geometry, but also the material distribution of the objects. For that reason, a well defined heterogeneous algorithm must be developed and is critical for success in heterogeneous printing.

Based on the above requirements, a unique SFF system has been developed in order to fulfill these requirements. Printing with different types of biomaterials has been achieved by adopting flexible nozzle selection design with a temperature control system

and other mechanisms. The high resolution can be attained by upgrading hardware and using a high accuracy motor controller. A novel computational algorithm for characterization of heterogeneous tissue scaffolds and composite structures is also applied to accomplish 3D heterogeneous tissue fabrication. To summarize, our self-designed multi-function SFF system has notable advantages over other commercial SFF machines with all of these features integrated together.

1.7 Thesis Outline

The outline of the thesis is organized as follows:

The first chapter is a general introduction of tissue engineering and commonly used SFF printing systems. The existing problems with current tissue manufacturing techniques are presented and discussed in detail. The proposed research is also introduced.

The second chapter presents an overall review of the existing available technologies for 3D tissue printing, including systems, printing methods, studies on different printing nozzle designs, and relevant methods for heterogeneous printing. The advantages and limitations of our novel SFF printing system are compared with those of other commercial SFF machines. The third chapter introduces the system configuration, which includes the design of the heterogeneous SFF system, the type of nozzle used, the motion control system, and the principle of the integrated software. In particular, the

nozzles' operating parameters and their deposition performance are also presented. The fourth chapter introduces a novel RP processing algorithm for SFF with heterogeneous printing, and of the structure formation methods and techniques for fabricating 3D structures. In the fifth chapter we describe the results from our study of the properties of many different types of materials including natural materials and synthetic biopolymers. The drop formation of each material is discussed for modeling 3D structures. The sixth chapter details the results of printing by using the heterogeneous algorithm and the 3D tissue printing system we developed. In this chapter, sucrose and PCL are the materials we selected to form different types of structures.

Finally, the conclusions and recommendations for future work of this thesis research are detailed in the seventh chapter.

CHAPTER 2 : LITERATURE REVIEW

2.1. Introduction

Various methods for manufacturing 3D structured scaffolds have been developed, including microfabrication, fiber bonding, solvent casting or salt leaching, phase separation, high-pressure gas expansion, and emulsion freeze-drying. However, these conventional fabrication methods do not allow for precise control of porous structure and can only be used with limited types of materials. To conquer these limitations, new fabrication methods have been developed. In recent decades, rapid prototyping (RP) and solid freeform fabrication (SFF) technologies have shown great potential in tissue engineering to build biomimetic tissues and organs for replacing or improving damaged or injured tissues (Geng et al., 2005; Starly et al., 2005; Williams et al, 2005). Organ printing is the bioassembly of living 3D human organs using bioprinting technology. It is basically a biomedical application of the well established, rapid prototyping technology. Rapid prototyping is additive manufacturing or layer-by-layer material deposition (Kruth et al., 1998; Santos et al., 2006). This method allows for control of the mechanical strength of the fabricated scaffolds and easy formation of desired 3D shapes (Hollister, 2005; Hutmacher et al., 2004). The first biomedical structures made directly by SFF were reported in the early 1990s using a custom-built three dimensional printing (3DP) machine (Cima et al., 1994; Wu et al., 1996; Griffith et al., 1997). Since then, numerous already existing commercial and experimental SFF printing systems, such as fused

deposition modeling, three dimensional printing, selective laser sintering, and stereolithography have been utilized to make scaffolds for biopolymer deposition.

Each printing system is unique in its method of operation and the key operating parameters. Therefore, it follows that each system should have its advantages and limitations over the others. The following sections in this chapter will briefly present conventional 3D printing systems for tissue fabrication, the limited range of materials, optimal scaffold design, bioactivity of the scaffolds, as well as the issues of cell seeding and vascularization.

2.2 Contemporary 3D Bio-printing System

2.2.1 NovoGen MMX bioprinter

The NovoGen MMX Bioprinter shown in Figure 2.1 was designed and built by Organovo in San Diego. This bioprinter can build structures layer-by-layer using semi-solid cellular “bio-ink” with architectural support from a hydrogel, according to computer-generated templates consistent with the topology of the desired biological structure (Jakab et al., 2008; Norotte et al., 2009). The specific “bio-ink” material and the bioprinter are based on the concept of scaffold-free tissue culture. Sheets of human smooth muscle cells (SMC) and human skin fibroblasts were grown on culture plates in the presence of ascorbic acid to enhance collagen production, and then detached and wrapped around a porous, tubular mandrel to form the equivalents of media and

adventitia of blood vessels (Jakab et al., 2008). As shown in Figure 2.2, the original design of the templates and the final fused tissue structure have described the ability of the material fusing mechanism with the concept of scaffold-free tissue culture.

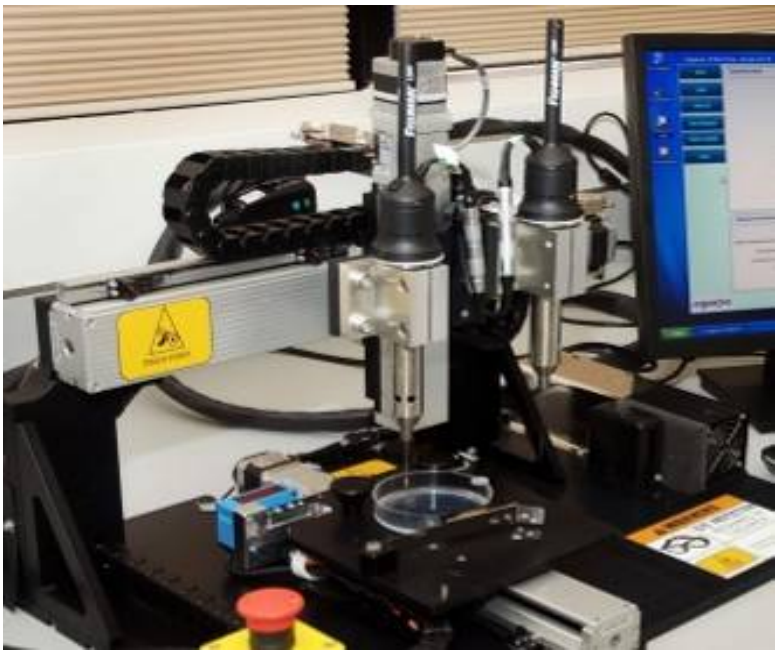

Figure 2.1: NovoGen MMX Bioprinter (Jakab et al., 2008)

The advantage of this concept technology is that the bio-ink particles represent small 3D tissue fragments. Thus, the cells within the particles are in a more physiologically relevant arrangement, with adhesive contacts with their neighbors, which may assure the transmission of vital molecular signals. However, relying on this fusing mechanism to produce tissue samples still has its weaknesses. The first disadvantage of this method is associated with the relatively high cost of the printers and materials. Second, the properties of this material are currently only suitable for

blood vessels and not for other tissue types. Third, the final tissue structure cannot match the original design because the final tissue construct becomes shorter and much narrower during fusion. Finally, it would require a few days to achieve the fusion of the building models and removal of the hydrogel in order to form a hollow structure.

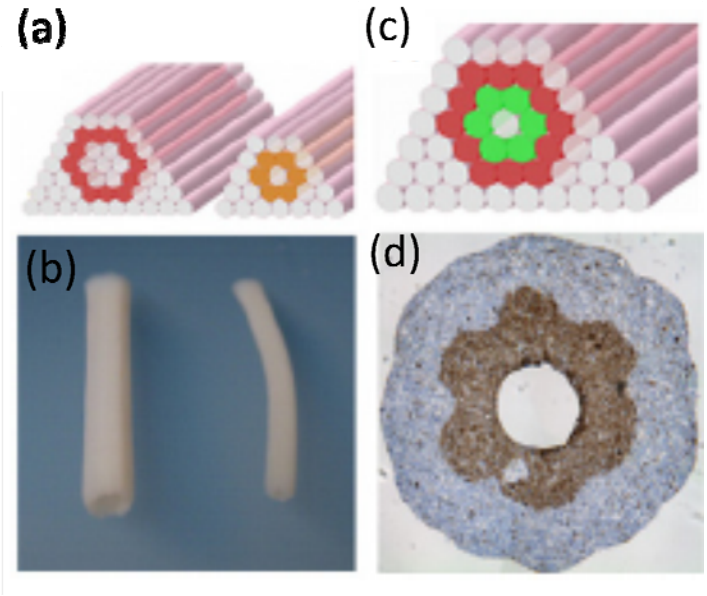

Figure 2.2: The vascular structure design and the fused constructs of different vessels diameters are fabricated by NovoGen MMX Bioprinter and the semi-solid cellular "bio-ink" material (Jakab et al., 2008). The original design of the templates is shown on the (a) and the final fused tissue structure is shown on the (b). Figure 2.2(c) is a double-layered structure design of the vascular tube. The red and green materials represent fibroblast building blocks and SMC building blocks correspondingly. Figure 2.2 (d) is the cross-sectional view of the blood vessels after fusion and the segregation of the two cell types.

2.2.2 Neatco bioprinter

The Neatco-1 and Neatco-2 printing machines (shown in Figure 2.3 and Figure 2.4, respectively) are manufactured by Neatco Inc. in Carlisle, Canada. These machines are designed for single material applications with micropipette extrusion. By restriction of the system design, the 3D models only can be formed with limited materials, such as biomaterials in liquid form. Some researchers have used “bio-ink” particles to print 2D or simple 3D structures using this printer (Jakab et al., 2008).

Figure 2.3: Neatco-1 printing system (Mironov et al., 2009)

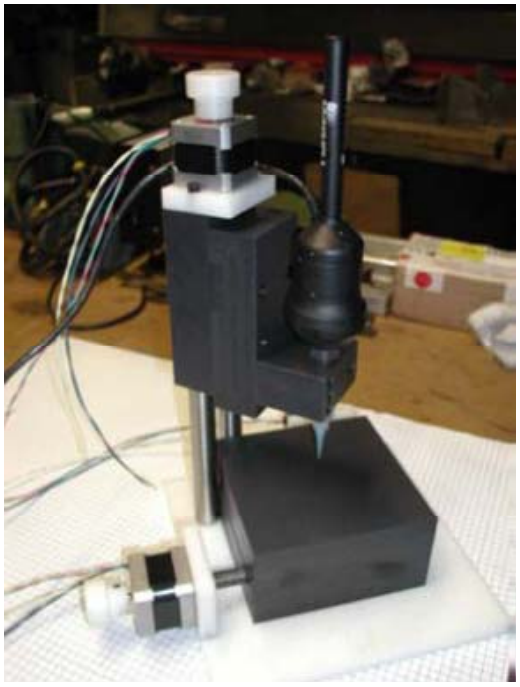

Figure 2.4: Neatco-2 printing system (Mironov et al., 2009)

2.2.3 Fab@Home Model 2

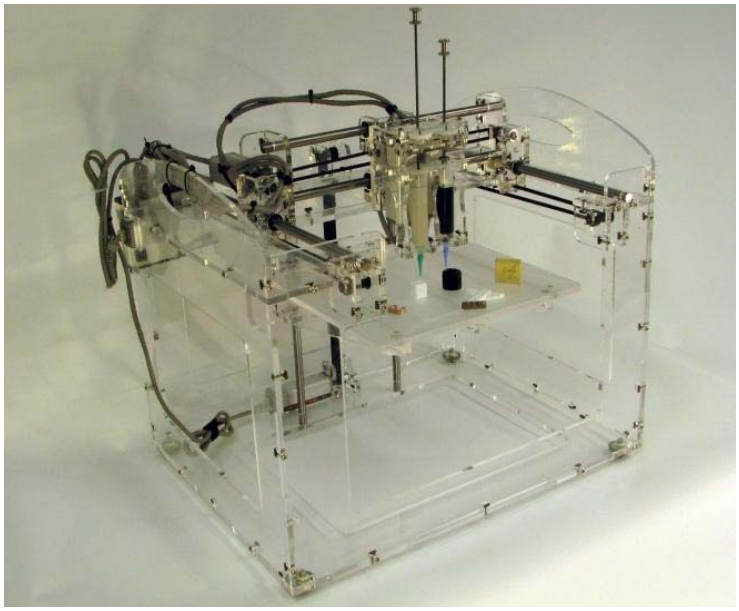

Figure 2.5: Fabbers Model2 with two nozzles connection

(http://www.fabathome.org/wiki/index.php/Fab%40Home:_Model_2_Overview)

The Fabbers model2 printer shown in Figure 2.5 is a standard gantry home-made machine, produced by Cornell University Computational Synthesis Lab in 2006 as a one year project. The main parts of this machine consist of a plastic cover, belt transmission mechanism, five DC brushed motors, and a dual syringe displacement tool. The optical feedback eliminates drift provided that the transmission is properly tightened. A single encoder count corresponded to 6μm of maximum theoretical resolution in the x direction. The printer has been successfully used with a top movement speed of 100mm/s with an acceleration of 100mm/s2. This system inherently costs less and eliminates the need to purchase an interface between the transmission and the chassis, in contrast to parts that are made entirely from acrylic. New tool heads were designed to give the printer more versatility. Aside from a traditional syringe based displacement tool, a pressure and valve based tool was developed. A pressure source forces material from the syringe reservoir at a fixed rate while the valve is open. The client program, named FabStudio, uses path planning algorithms to convert STL, tool and material information into a .fab file. The advantage of this printer is low cost (less than $2,000), easy assembling with few screws and plastic plates, theoretically high resolution for axes moving, and suitability for creating large objects. On the contrary, the disadvantage can be seen in that the printing results are still not smooth and uniform for microfabrication purposes. The design with a valve based tool at a fixed extrusion rate is also not adequate for heterogeneous printing because the valve based tool with constant back pressure can only generate continuous printing, but cannot adapt the rate for the requirement of drop on demand printing (Figure 2.6). Due to the restriction of the

design, the extrusion volume cannot be reduced to the scale of a few micro-liters. The theory of heterogeneous printing does not seem to be able to be applied by this machine.

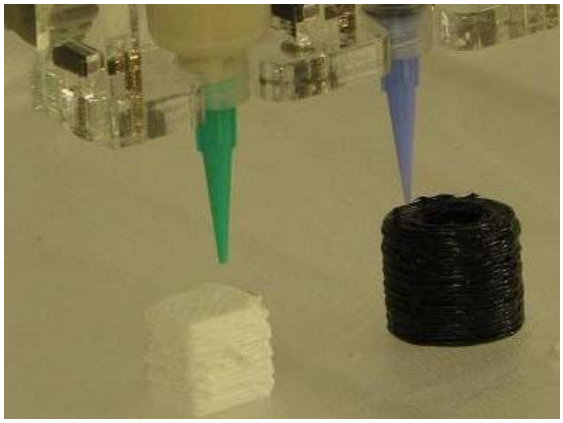

Figure 2.6: Printing results with dual syringes by using Fabbers Model2 (http://www.fabathome.org/wiki/index.php/Fab%40Home:_Model_2_Overview)

2.2.4 3D-Bioplotter

A new rapid prototyping machine for bioprinting purpose shown in Figure 2.7, 3D-Bioplotter, was created by envisionTEC, Inc. in Germany. The 3D-Bioplotter is controlled by a PC workstation which operates and monitors the system. After transferring the 3D CAD data to the PC, it is processed by the Bioplotter Software Package and then the preprocessed data is transferred to the 3D-Bioplotter for fabrication. This machine has the capability of fabricating scaffolds using the widest range of materials, from soft hydrogels over polymer melts up to hard ceramics and metals. The special dispensing head can handle high temperatures up to 250°C or low temperatures down to -2 °C as

well. The maximum axis resolution can reach up to 1 µm. Obviously, the major advantage of this machine is its capability of flexibility using a large variety of biomaterials with multi-exchangeable base plate fixtures with heating and cooling mechanism and using up to 5 different cartridges during same build job. The highly accurate deposition design and high speed for axes moving render this machine more suitable for biomedical applications. However, this machine costs at least $250,000 which would not be affordable for most researchers. This machine also does not provide any automatic solutions or methods for defining a heterogeneous structure. This drawback may cause restrictions in forming a heterogeneous tissue structure.

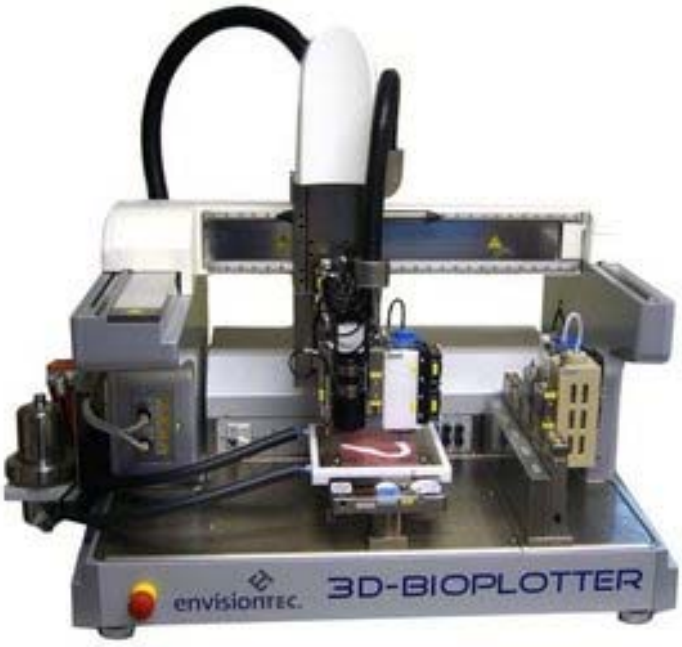

Figure 2.7: 3D-Bioplotter printing system

(http://www.envisiontec.de/index.php?id=31)

2.2.5 Rapid Prototype Robotic Dispensing System (RPBOD)

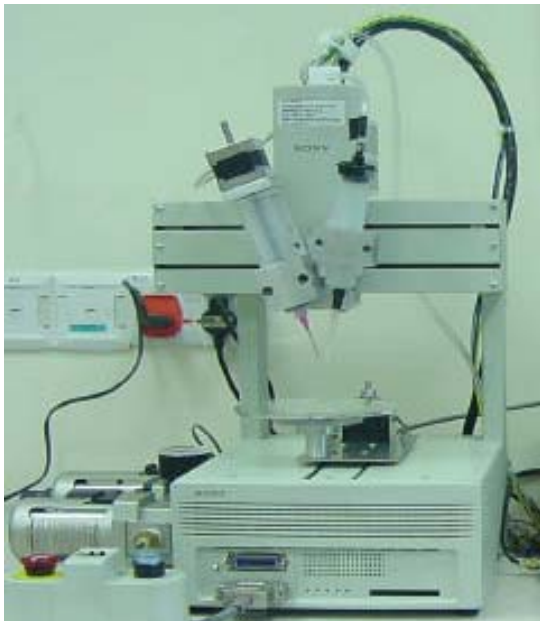

Figure 2.8: RPBOD printing machine set-ups via dual dispensing (Geng, et al., 2003)

This four-axis multiple dispenser printing system RPBOD shown in Figure 2.8 was developed by Ang et al., and features a moving stage in the Y direction and a moving holder that can travel in the XZ direction. This machine has a positioning accuracy of up to 50µm and is embedded with a computer-guided desktop robot, a mechanical pressure dispenser, and a pneumatic dispenser (Geng, et al., 2003). The mechanical dispenser is controlled by a plunger driven with a stepper motor. By controlling the displacement of the plunger, the dispensing rate can be precisely regulated, particularly at very low flow rate (such as 0.5 µl/sec). A Teflon-lined nozzle with diameter size 100-200µm tips was used to dispense material in liquid-like state (Figure 2.9). However, when the solution is of low viscosity, it flows in an uncontrollable way. Therefore the

pneumatic dispenser is not suitable for the dispensing of low-viscosity solutions in this machine. Since this machine only has one mechanical dispenser, it is impossible to achieve heterogeneous printing.

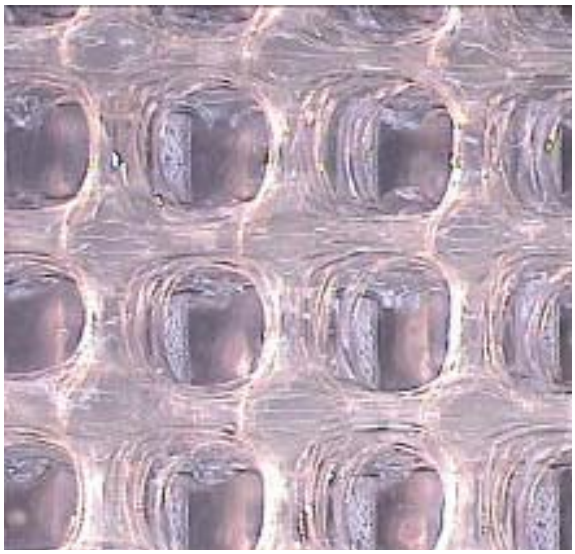

Figure 2.9: Chitosan scaffold built by RPBOD (Geng, et al., 2003)

2.2.6 Computer Aided Biological Tool

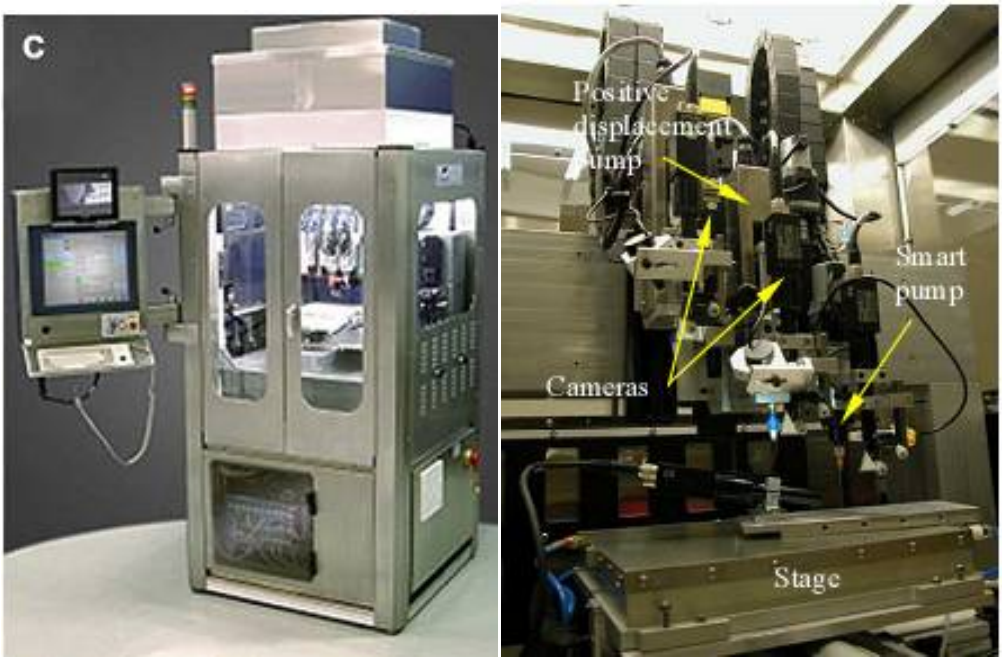

Figure 2.10: 3D robotic industrial bioprinter -- Computer Aided Biological (CAB) tool (Mironov et al., 2009)

The most sophisticated but expensive type of device shown in Figure 2.10 has been developed by “Sciperio/nScript Inc” in Orlando, FL. The Computer Aided Biological (CAB) tool utilizes a CAD/CAM approach to build 3D heterogeneous tissue structures. It has a multi-head through-nozzle deposition machine designed to print biomaterials, cells, and biologically active factors onto various supporting substrates to create substitute tissues for tissue engineering.

This system contains a moving stage in the XY direction and two printing heads which can travel in the Z direction, a fiber optic light source that is used to light up the

printing area and cure photosensitive polymers, temperature control for each print head, and an enclosed operation environment with a humidifier for controlling the humidity. The smart pump can be replaced by a piezoelectric nozzle for conformal deposition on uneven surfaces. The process of deposition is directly controlled by the motion control software. The accuracy and the reproducibility of this CAB system can reach to within a few microns. This multi functional 3D tissue printing system, CAB tool, is able to generate complex 3D porous structures with precise control. However, this system still has certain weaknesses. First, although this system is very good for 2D cell patterning, the distribution of cell printing is still not uniform for 3D tissue construction with high initial cell density (Mironov, 2007). Second, the price of this 3D printing machine is prohibitive to many researchers for commercial and experimental tissue printing purposes.

A summary of commercial 3D machines for bioprinting are given in the Table 2.1. The comparison chart includes machine price, number of nozzle, and printing resolution.

Table 2.1 Comparison of commercial 3D bioprinting systems

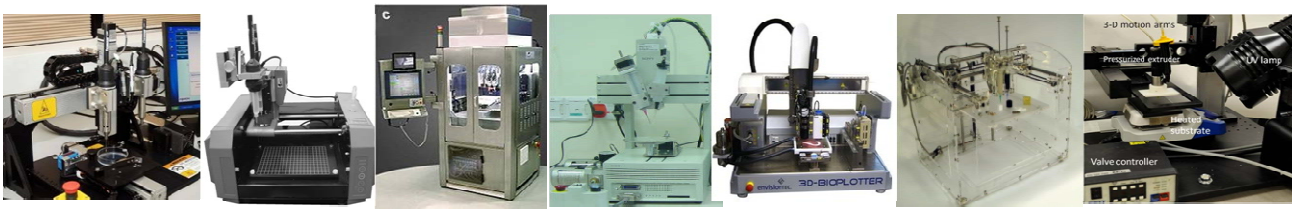

Company	Organovo (San Diego, CA, USA)	Neatco (Carlisle, Canada)	Sciperio (Orlando, FL, USA)	RPBOD (Ang et al, Singapore)	3D-Bioplotter (envisionTEC, Inc. Germany)	Fab@Home Model 2 (USA)	**OUR MACHINE**
Price	$200,000	$???	$700,000	$???	>$250,000	<$2000	**TBD**
Nozzles	2	1	2	2	5 different cartridges	2	**Max: 6**
Printing resolution	500 µm	300 µm	100 µm	100 µm	200 µm	500 µm	**100 µm**

2.3 Range of Materials

2.3.1 Material processability

SFF technologies are considered as flexible technologies in terms of material processability. Each technique requires a specific form of input material such as filament, powder, hydrogel, solid pellet or solution. Therefore, it must be ensured that the selection of materials for the scaffold is compatible with the selected SFF process

and that it can be efficiently produced in the form required. In order to melt some solid materials for fabrication, we normally use heating barrels with temperature controllers to heat up reservoirs and printing nozzles and a cooling system is utilized to solidify the structure. Other considerations during the selection of materials include accessibility issues, whether the material is toxic or non-toxic, the degradation profile and the mechanical strength of the scaffold.

2.3.2 Mechanical strength of scaffolds

Different organs or tissues in the human body have various requirements for mechanical strength. In order to mimic human organs, the scaffold must provide enough mechanical support during the reconstruction process. Mechanical integrity for the scaffold design has to be sufficient to resist operational stresses during implantation and in vivo testing. Taking bone as an example, an ideal scaffold should be biomechanically similar to the type of bone being replaced in order to function effectively as a synthetic bone replacement from the time of implantation. The compressive modulus of bone is in the range of 14 to 18 GPa for cortical bone, and 0.01 to 2.0 GPa for trabecular bone (Athanasiou et al., 2000). Therefore, the bone scaffold should be able to maintain biomechanical properties for specific human bone types until newly built extracellular matrix can well serve the restored functions, and then the scaffold can be degraded and resorbed by growing cells. To date, there has been a wealth of research investigating the relationship between scaffold degradation characteristics and the biomechanical

properties in in vivo or in vitro models (Mainil-Varlet et al., 1997; Tomihata 1997; Wang, 2003; Yuehuei et al., 2000). In particular, Yuehuei et al. found that depending upon the rate of polymer degradation, mechanical strength may decline well before adequate union of fractures or healing of tissues is achieved. The biomechanical properties of the polymer are also significant in affecting the results of the cellular response.

2.4 Scaffold Design

2.4.1 Porous structure

A structure with porous design is superior for the migration, distribution and proliferation of cells (Maquet and Jerome, 1997; Wake et al, 1994). Different native tissues require different optimal pore sizes for different cell types. Although numerous concept studies have been validated to demonstrate the existence of an optimal range of pore size for different cell types (Dalton et al., 1999; Ranucci et al., 2000; Bignon et al., 2003), little is known about specific optimal pore sizes for particular cell types. Therefore, most pore size selection is governed by general empirical guidelines.

RP-fabricated scaffolds sometimes contain visible ridges and grooves. The effect of these discontinuities in topography might affect the adhesion and migration of cells, as shown by Yin's work (Yin et al. 2004). These authors grew cardiac cells on microgrooved elastic scaffolds to investigate the topography-driven changes in cardiac

electromechanics. The grooves were 50 mm in depth and 120 mm in width. They demonstrated a direct influence of the microstructure on cardiac function and susceptibility to arrhythmias via calcium-dependent mechanisms.

2.4.2 Surface Topography

The surface roughness of the scaffold is important in cell–matrix interactions. The rough powder surface produced from powder-based RP techniques might enhance cell adhesion. However, if the surface is too rough, the cells adhering to these materials might not be able to develop separate focal adhesion plaques or connect the irregularities (Linez-Bataillon et al., 2002). In addition, the sharpness of the surface could also damage the cell. Deligianni's group studied the response of human bone marrow cells cultured on hydroxyapatite (HA) surfaces and evaluated the influence of surface roughness on cell adhesion, cell detachment strength, proliferation and differentiation, and concluded that both adhesion and proliferation of bone marrow cells are sensitive functions of surface roughness (Deligianni *et al., 2001*). In certain RP systems, such as FDM and 3D bioplotter, the smooth surface of solidified materials cannot ensure firm cell adhesion and therefore requires further surface modification or coating.

2.5 Bioactivity of the scaffold

The interaction of cells with the scaffold is governed by both physical structure and chemical signaling molecules that have a decisive role in cell adhesion and the further behavior of cells after initial contact (Bacakova et al., 2004). The extent of initial cell adhesion determines the number, size, shape and distribution of focal adhesion plaques formed on the cell membrane, which subsequently describes the size and shape of the cell-spreading area (Linez-Bataillon et al., 2002). The extent of spreading is crucial for further migration, proliferation and differentiation of isolated cells.

2.5.1 Cell seeding on 3D scaffolds

The dissemination of isolated cells within a scaffold is the first step in establishing a 3D culture, and might play a crucial role in determining the progression of tissue formation (Vunjak-Novakovic et al., 1998). In tissue engineering, one of the significant challenges in the scaffold-based approach is to distribute a high density of cells efficiently and uniformly throughout the interior of the scaffold volume (Wiedmann-Al-Ahmad et al., 2002). Seeding cells into scaffolds at high densities has been associated with enhanced tissue formation in 3D constructs, including higher rates of cartilage matrix production (Freed et al., 1997), increased bone mineralization (Holy et al., 2000), and enhanced cardiac tissue structure (Carrier et al., 1999). The only Food and Drug Administration (FDA)-approved cell seeding process involves the use of a Petri dish. Cells

are cultured to confluence inside the dish and then detached, and seeded from a suspension in medium into a pre-fabricated scaffold or hydrogel solution that then solidifies. However, this process has been shown to fail to deliver cells deep inside the scaffold with uniform distribution (Li et al., 2001; Kim et al., 1998; Xiao et al., 1999). Therefore, the cellularization of a 3D scaffold is closely related to the advances of bioreactor technologies. Bioreactors are generally defined as devices in which biological or biochemical processes develop under closely monitored and tightly controlled operating conditions (Martin et al., 2004). The role of bioreactors in processes that are key to the *in vivo* engineering of 3D tissues based on cells and scaffolds include cell seeding of porous scaffolds, nutrition of cells in the resulting constructs, and mechanical stimulation of the developing tissues (Martin et al., 2004). Types of bioreactor include the spinner flask, perfusion cartridge and rotary cell culture system (Goldstein et al., 2001). Each of these systems utilizes different physical principles and might necessitate specific design considerations in terms of scaffold shape and strength. RP systems present great flexibility in scaffold design and development. Scaffolds constructed by RP technology can be designed with interconnected flow channels to fit into the operation of the bioreactor, as shown in the work of Sakai et al. (Sakai et al., 2004). The RP fabrication method offers the flexibility and capability to couple the design and development of a bioactive scaffold with the advances of cell-seeding technologies, to enhance the success of scaffold-based tissue engineering.

2.6 Extrusion study

In general, most biopolymers could be deposited by using pneumatic nozzles. The concentration of solutions, material viscosity applied pressure, surface tension, and diameter of needle tip are the significant parameters to be adjusted to print polymer lines with the desired geometry. An Equation is shown in Equation (2.1) which can represent the flow rate exiting the needle tip (Vozzi, et al., 2002).

$$Q = ah\frac{dl}{dt} = ahv_0 \tag{2.1}$$

where *a* is the width of the extruded line to the radius of the tip and *h* is the height of the polymer pattern. *l* is the length of polymer deposited in time *t*, and hence V_0 is the velocity of the substrate with respect to the syringe. If the polymer is considered to be a Newtonian liquid, the flow in the capillary is given by Poiseulle's equation;

$$Q = \frac{\pi R^4}{8\mu}\frac{dp}{dz} \tag{2.2}$$

where *R* is the internal radius of the capillary, μ is the material viscosity, and *dp/dz* is the applied pressure gradient. Combining Equations (2.1) and (2.2) together,

$$a = \frac{\pi R^4}{8\mu v_0 h}\frac{dp}{dz} \tag{2.3}$$

A certain critical pressure *Pcrit* must be applied to the before the fluid exits the needle

tip proportional to the viscosity of the solution. Below *Pcrit* deposition cannot occur because the friction forces are greater than the driving pressure. The pressure gradient is negligible in the widest part of the syringe, and is maximum at the tapered region of the tip. In their model, *dP/dz* has been approximated to (*P+Pcrit*)/*hz*, where (*P+Pcrit*) is the applied driving pressure and *hz* is the length of the tapered region of the capillary. Therefore, Equation (2.3) can be expressed as;

$$a = \frac{\pi R^4}{8\mu v_0 h}\frac{(P+Pcrit)}{h_z} \tag{2.4}$$

Vozzi, et al. also further developed Equation (2.4) to consider the length of the tapered zone of the extruding pen *hz* as well as the applied extrusion pressure (*P+Pcrit*), where *Pcrit* is the critical pressure needed before the solution exits the pen tip.

A nozzle-based biopolymer deposition can be categorized using three extrusion modes (Figure 2.11): droplet mode, continuous mode, and contact mode. In droplet mode, the extrusion material is deposited as tiny droplets, the size of which is controllable by adjusting the applied pressure, the oscillation frequency, the diameter of printing tips, and the key parameters in nozzle system settings. This mode can generate very small droplet volume as small as picoliters to form a structure by depositing multiple droplets at desired locations on a substrate. The advantage of this mode is that it can form very fine structures by controlling the droplet size and drop position. Since this mode is highly dependent on oscillatory function to generate droplets, high viscosity

material is always a challenge to form as uniform and smooth droplets. In continuous mode, the extrusion material is forced out of the nozzle tip under an applied pressure. In general, this mode is commonly adopted in existing SFF machines to extrude lines and then form a desired structure by moving the nozzle tip for freeform fabrication. The advantage of this mode is that it can extrude a uniform line with various line widths and can handle high viscosity material by adjusting the applied pressure. However, extrusion material often swells to a dimension larger than the corresponding dimension of the nozzle tip. This is caused by changes in stress that occur in molten viscoelastic polymers as they emerge from the tip. This is also known as the Barus effect. In contact mode, the tip is very close to the substrate in order to reduce the influence of the Barus effect; nevertheless, the gap between the nozzle tip and the substrate needs to be precisely controlled for fitting different biopolymer viscosities and applied pressures.

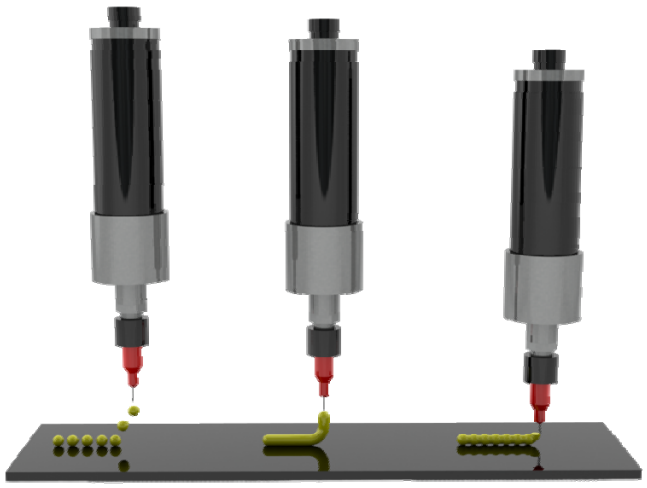

Figure 2.11: Three modes of biopolymer deposition (a) droplet mode (b) continuous mode (c) contact mode

CHAPTER 3 : A NEW FLEXIBLE AND MULTI-PURPOSE SYSTEM DESIGN FOR 3 DIMENSIONAL HETEROGENEOUS PRINTING

3.1 System configuration

The configuration of the 3D multi-nozzle printing system for freeform fabrication of tissue constructs is illustrated in Figure 3.1. The first step is to create a heterogeneous structure based on CAD software and output as separate binary STL files for each individual model component. The STL model is sliced to a set of sequential cross section APT language files with a specific thickness by using Skeinforge software. The integrated software will then be used to integrate and modify the APT language files together and send it to the control software, MACH3, directly. Once the integrated APT language file is received, MACH3 will be used to control the SFF machine to build the structure. The tool path and the printing command are sent to the motion controller to control the movement of the working arms and the valve controller. The multi-valve controller is capable of operating up to four dispense valves independently or simultaneously and features external control backpack actuators.

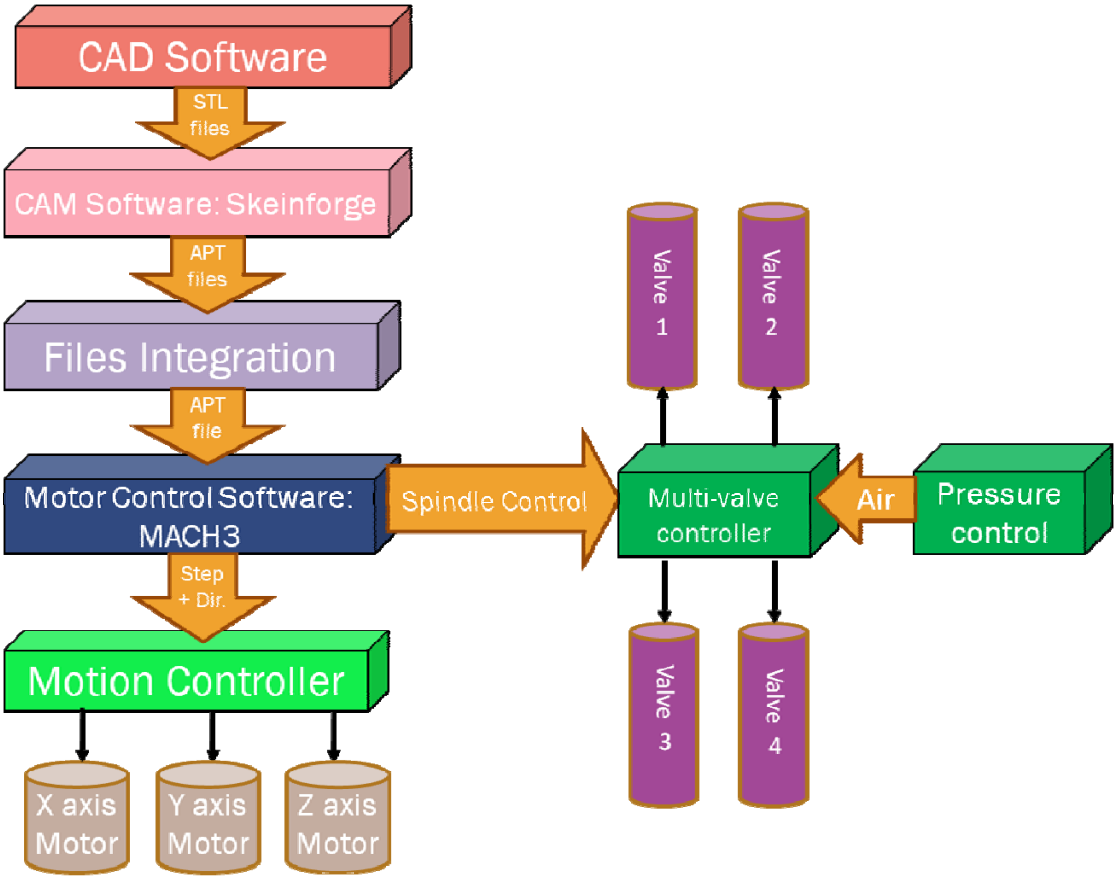

Figure 3.1: Schematic of the 3D multi-nozzle printing system for freeform fabrication of tissue constructs. First a heterogeneous structure is created by CAD software and then Skeinforge is used to slice the file into APT files. Different APT files are integrated by integrated software and a final complete APT file is generated and sent to MACH3, which controls the movement of the working arms and the multi-valve controller.

3.1.1 Motion control unit

3.1.1.1 TMS320F2812 DSP microprocessor

The mechanical moving system consists of three linear servo motors and three linear digital optical encoders with a precision of 0.5 µm used in conjunction with the Texas Instruments DSP (Digital Signal Processor) microprocessor TMS320F2812 (Figure 3.2) to measure the translational displacement and velocity of the moving arms. A specially designed H-Bridge board is employed to serve as the interface between the PWM control signal from the DSP microprocessor and each linear servo motor. A control system using a PID controller is implemented in the same DSP microprocessor chip. The program is written in C using the Texas Instrument Code Composer Studio (CCStudio) IDE. Each gain proportional, integral, and differential (P, I, and D) is tuned through mathematical calculations and experimental observations; the displacement error can hence be reduced to less than 5µm. In contrast to conventional systems, this system allows for high travelling speed of the moving arm while maintaining this low displacement error.

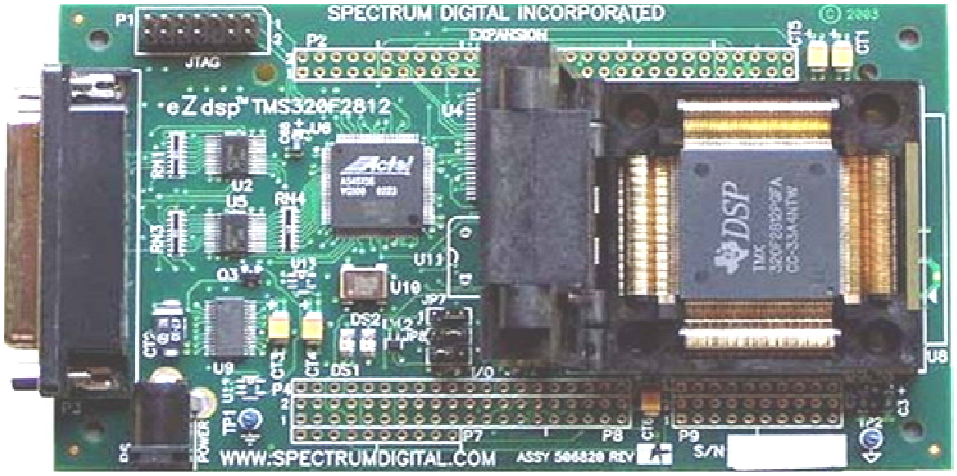

Figure 3.2: The Texas Instruments of eZDSP TMS320F2812 Microprocessor

The features of the F2812 include 150 million instructions per second (MIPS) operating speed, 128K words of on-chip memory, 64K words of off-chip memory, 30 MHz clock speed, real-time control, and expansion connectors for general purpose input output (GPIO). In particular, this board is able to provide precise control by employing two individual sets of hardware quadrature encoder pulse (QEP) for precisely reading the signal from the optical encoders.

The procedure of this printing process is shown in Figure 3.3. First, a 3D model is created using CAD system, then Modelworks slicing software is used to carve an STL 3D model into a 2D contour slice (.SLC) file [Solidscape.inc]. The developed MATLAB script is implemented to read the .SLC files and integrate the model coordinates and the printing path into CCStudio. In this control scheme, MATLAB is always the host software that reads the slice files and sends command signals to control the motion of the three arms

and to direct the nozzle controller for printing. However, two hardware QEP sets can only connect with two optical encoders for two servo motors. The usage of a second DSP board is required to provide the third hardware QEP set for three-axis motion. Synchronizing two DSP boards with the same parallel port in the same computer is a significant challenge, because the CCStudio is designed to communicate with one DSP board at a time and MATLAB running multiple CCS instances will become cumbersome and may lead to conflicts. Besides, the content of the .SLA file is written in special computer code that cannot be identified by MATLAB. Therefore, a new control method without using the eZDSP board and .SLA file is proposed for efficient and economical printing.

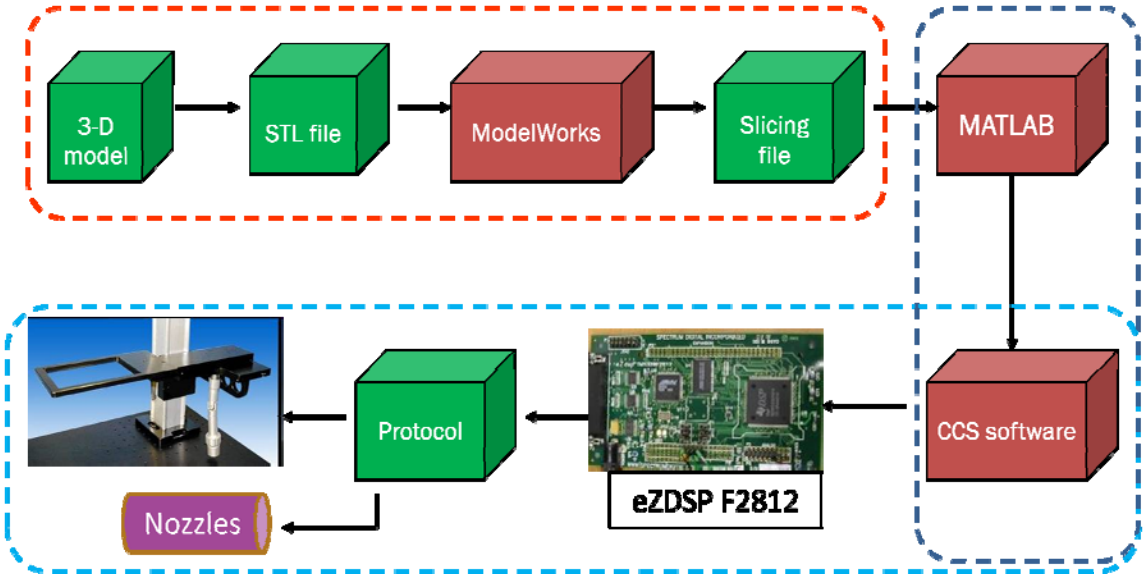

Figure 3.3: The printing process by using eZDSP F2812 Microprocessor. A 3D model is created using CAD system, then Modelworks slicing software is used to carve an STL 3D model into a 2D contour slice (.SLC) file. The developed MATLAB script is implemented to read the .SLC files and integrate the model coordinates and the printing path into CCStudio. MATLAB in this control scheme is always the host software that reads the slice files and sends command signals to control the motion of the three arms and to direct the nozzle controller for printing.

3.1.1.2 MACH3 control software

The three-axis SFF printing system consists of three linear servo motors (Pittman 8424 WDG #4) and three linear optical encoders (Heds 9100-B00) with a precision of 0.5 µm. The linear movement in the X, Y, and Z axes are 120mm, 90mm, and 35mm respectively. The motion control software “MACH3” is set up to drive not only X, Y, and Z axis motors for moving, but also the valve controller for nozzle printing. MACH3 is control software which can read APT language files and output control signals to drive up to 6-axis motor drivers. MACH3 not only can show the current position of the printing, but can also simulate the motion of the printing path. In addition, heterogeneous printing with multiple nozzles can be achieved by adding the position of nozzles into the tool table in MACH3. Once the exact position of each nozzle has been carefully measured and set up, the control software MACH3 can sequentially change the printing nozzles by enabling the tool change function. Figure 3.4 shows the initial 3D SFF system set-up with one pneumatic printing nozzle and the assembly of its parts.

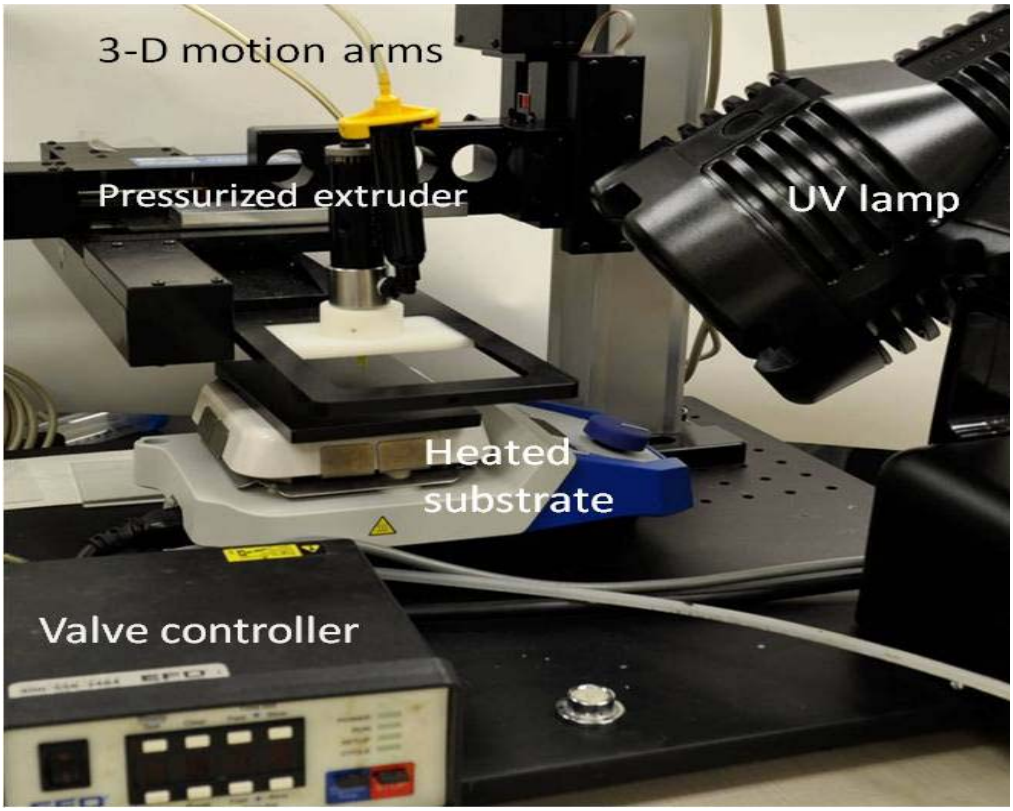

Figure 3.4: The initial system set-up with one pressurized extruder

3.1.1.2.1 Geckodrive motor controller

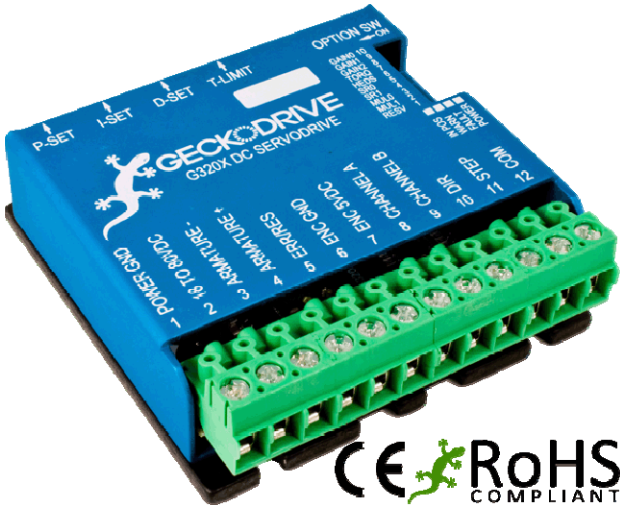

Figure 3.5: G320X DC servo drive with screw terminals and adjustable PID pots

To ensure axes moving can reach maximum resolution and stable response, the newest servo drives G320X from Geckodrive, Inc. have been used to drive the 3D printing system for linear and high speed 3-axis motion.

The G320X drive is a miniature design and all connections are on the same edge, which makes wiring easy with simple and clearly labeled screw terminals. The drive has an internal PID closed-loop control and PID pots with settable integral coefficients which make high performance moving possible. The G320X drive has a minimum fault trip of about 256 counts which is equal to 128µm when the motor and encoder are connected with it. Whenever the error is reached, the drive faults and the motor stops

immediately. Since the drive has no tuning software available for it and does not communicate at all with a computer, the drive should be tuned manually in real time by adjusting three PID pots while monitoring the response time using an oscilloscope. In general, the G320X has so far proven to be a reliable and robust drive in our applications, with demonstrated ability for high performance in motor driving. However, the maximum resolution of this drive can only reach 128µm which actually is not high enough for the fabrication of a precise 3D structure. Therefore, a new motor drive with higher moving resolution is discussed in the next section.

3.1.1.2.2 Whale3 DC servo drive

Figure 3.6: Whale3 DC servo drive with integrated connection interface

The Whale3 servo drive from CNCdrive, which is mainly designed for CNC milling machines, uses RJ45 connectors on the interface converter board and also within the drive itself so that a normal twisted pair Ethernet cable can be used between the motor and the drive. The drive can output a maximum of 80 volts and 20 amps to drive a servo motor and has a 32bit PID algorithm with 16bit PID parameters and settable sampling time to enable high moving performance. Furthermore, the drive can reach a minimum of 2 error counts which means the ideal moving error can be reduced to 1µm with no load.

The drive came with special tuning software which makes the tuning job easier, faster, and more reliable. Once the tuning work is done, the Whale3 servo drive can ensure the machine operates with maximum performance and positioning accuracy. However, the loading on our moving system is considerably heavy, especially on the z-axis, so the maximum moving error is 4µm in the x and y axes and 15µm in the z-axis. The resolution of this system is in a range suitable for use in biofabrication or other tissue engineering applications according to the pore sizes suited for different cell types (Leong et al., 2008). Therefore, the Whale3 DC servo drive has been adopted as the motor drive in our SFF printing system and is used in the printing experiments described in Chapter 6.

3.1.2 Model slicing unit

In order to obtain layered files of 3D structures, Skeinforge has been utilized to convert 3D STL models to slicing files. Skeinforge is a tool chain composed of Python scripts that convert any 3D model in STL format into APT language instructions for slicing. Due to different material properties, modifying the layer thickness, extrusion speed, and traveling velocity is necessary to acquire an optimal droplet size and extrusion volume.

3.1.3 Microvalve unit

In the market, there are numerous printing nozzles with different inside mechanisms that are available for selection. For the sake of accommodating different material properties, the printing nozzle must be able to heat up, handle high viscosity material, allow for precise extrusion, fit replaceable printing tips, and dispense pico-scale droplets. In this study, the double 741MD-SS pneumatic microvalves (EFD Inc., East Providence, RI) were selected as the printing nozzles in order to achieve heterogeneous printing. Both of these microvalves can contain different materials or biopolymers and then execute extrusion one-by-one and print layer-by-layer through automatic control software. A valve actuator called “BackPack”, a kind of solenoid, was installed with a 741MD-SS pneumatic microvalve to provide actuation speeds as short as 5 milliseconds, and cycle rates as high as 600 per minute.

A commercially available 10cc polypropylene syringe barrel, unique piston, and an adapter (EFD Inc.) were used as material container to deliver solution. The syringe barrel was connected with compressed air to provide back pressure to thrust the material into the chamber of the valve. The intensity of the pressure was totally dependent on the property of the material used. For more information, the four different printing nozzles were compared and detailed in the second section of this Chapter.

3.1.4 Electrical control unit

The multi-nozzle printing system consists of two pneumatic microvalves, two BackPack valve actuators, a multi-valve controller, and motion control software — MACH3 (Figure 3.7). Once the integrated APT language file is received, MACH3 is used to control the motion of the SFF machine and the valve controller to create the structure. The EFD VALVEMATE 8000 multi-valve controller was used to control pneumatic microvalves. Air supply was connected with two regulators to provide compressed air to both reservoirs and the BackPack valve actuators. By reading the TTL command signal from MACH3, the multi-valve controller sends a 24 Volt DC signal to drive the BackPack valve actuators to open and close. The tool path is sent to the motion controller to control the movement of the working stage and the dispenser. The control signal is sent from the host computer to move the printing nozzles in the X, Y, and Z directions based on the tool path, which are mounted on the moving stage. When one layer printing is

complete, the Z-axis moving arm will move up a defined thickness and the machine will repeat the same procedures to build the next layer until the whole model is finished.

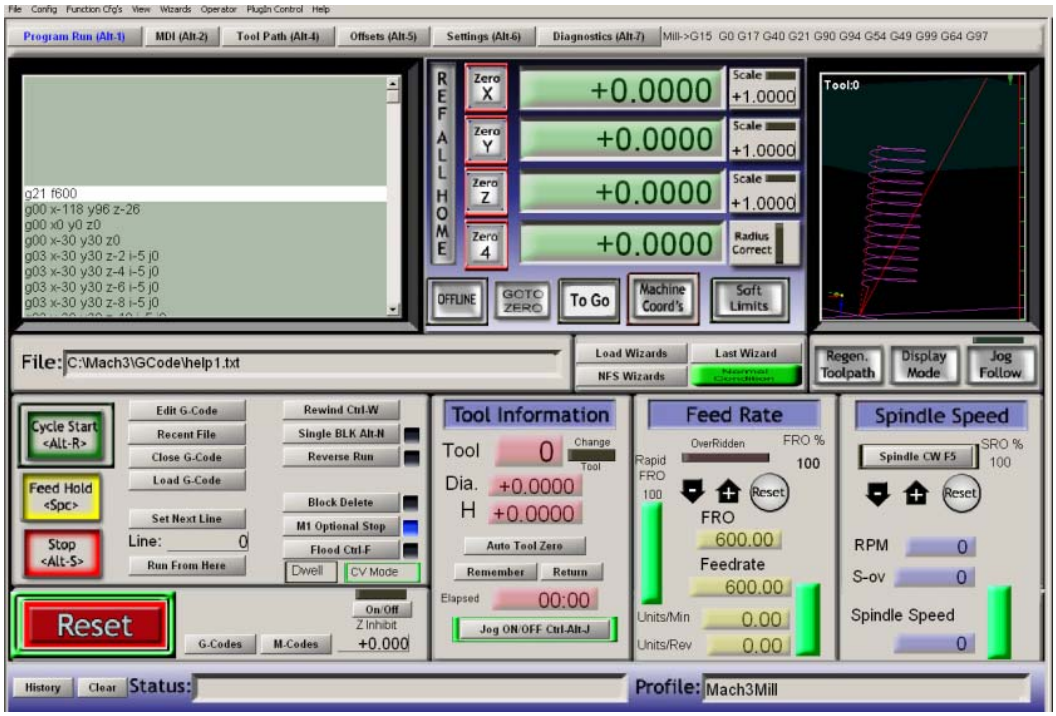

Figure 3.7: The operation interface of MACH3 control software

3.1.5 Temperature control unit

Two digital temperature controllers shown in Figure 3.8 and heating components were purchased from OMEGA Inc. (Stamford, CT) to maintain the temperature of the printing nozzles and the syringe barrels. A heating tape (FGS051-040) and a heavy duty stainless steel heating barrel utilizing a 110 Volt AC power source were connected to temperature controllers individually. These heating components were able to generate heat up to 750˚F to melt the polymer and control the phase of the polymer according to

the viscosity requirement. Two K-type thermocouples were attached to measure the surface temperature and produced voltage related to a temperature difference. Both controllers were embedded with PID control which could provide resolution up to 0.1 degree Celsius and monitor the temperature. When the temperature reaches the set point, the PID control will take over the process and keep the temperature at a steady state. The connection diagram is shown in Figure 3.9.

Figure 3.8: digital temperature controllers (CNi8DH53 and CN8501TC-R1)

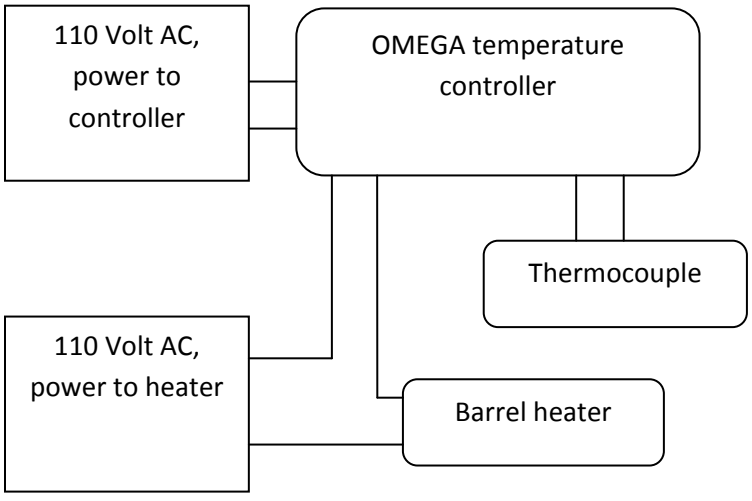

Figure 3.9: Connection diagram of the temperature controller

3.1.6 EFD multi-valve controller

The VALVEMATE 8000 multi-valve controller (EFD Inc.) was designed to control the solenoid by an electric current (Figure 3.10). This controller has some special functions, including programmable dispense time, four independent solenoid drivers and input/output communication with a host machine or software. By reading the TTL signal from the host control software, MACH3, the multi-valve controller will send out a 24-Volt square wave signal to specific solenoid and be able to control four independent solenoid drivers or BackPack acutators (shown in Figure 3.11). One end of the solenoid driver is connected to a constant compressed air supply and the other end works as a controlled air output to drive the nozzle jet. A solenoid valve has two mechanical parts: the solenoid and the valve. The solenoid converts electrical energy into mechanical energy which opens and closes the valve mechanically. In this way, the solenoid will individually control each nozzle jet to achieve the desired droplet size via controlling the compressed air, needle stroke and dispense time.

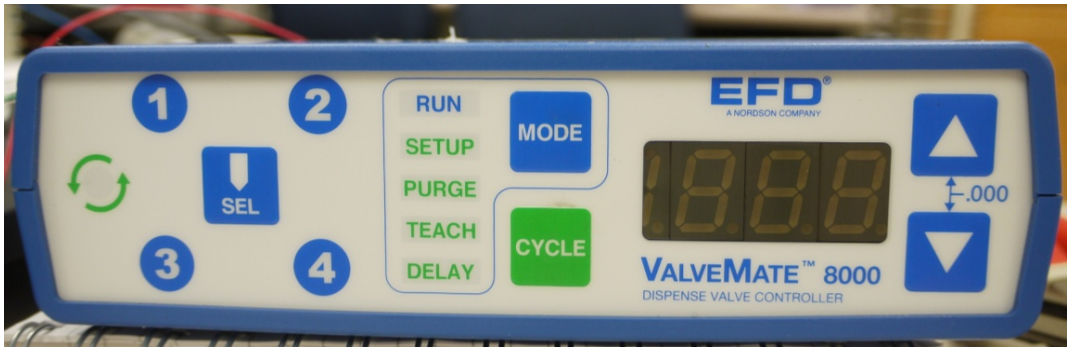

Figure 3.10: EFD VALVEMATE 8000 multi-valve controller

In this study, both the BackPack actuator and solenoid driver have been tested and compared with the printing results. The features of these two solenoids are detailed in Table 3.1.

Table 3.1 Characteristics and comparison of two solenoids

Solenoids / Features	BackPack actuator	Solenoid driver
Cycle rate with 741MD	9 Hz	6 Hz
Mounting type	Combined with nozzle	Separate from nozzle
Advantages	Integrated design Fast response	No vibration
Disadvantages	Produces high vibration	Low cycle rate

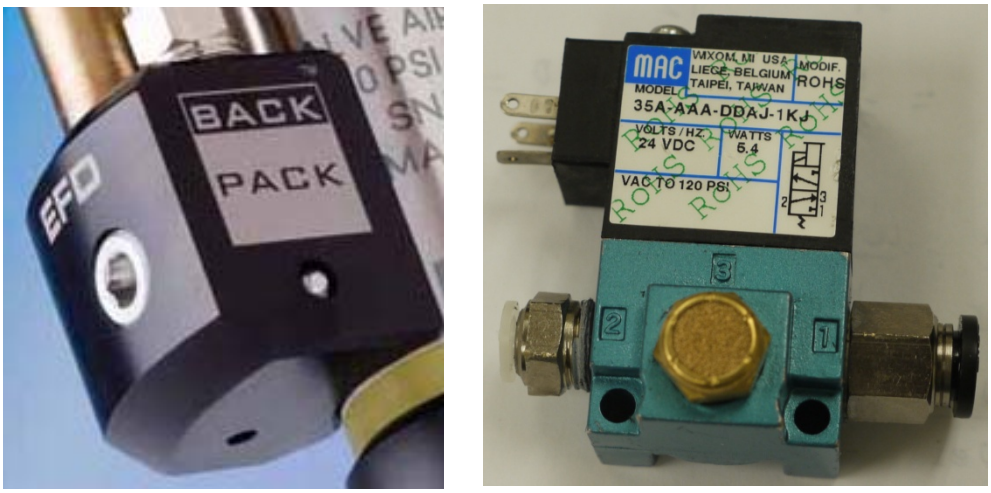

Figure 3.11: EFD BackPack actuator and solenoid driver

3.2 Printing nozzle system

In order to print 3D heterogeneous structures with different materials, the selection of the printing nozzle has shown a great impact in this study. Due to different mechanical properties of different biomaterials, various printing methods and printing nozzles are needed to be chosen very carefully to form an adequate scaffold for tissue construction. The nozzle may be able to generate pico-scale droplets with adjustable printing frequency. In addition, the reservoir as well as the printing nozzle and its accessories should be able to withstand high temperature for melting or keeping materials in liquid-based fluid state. In particular, the nozzle system must be able to be connected to and controlled by a host control system. Therefore, a printing system with flexibility to employ different nozzle systems is presented in this study. Two different types of nozzles which are commonly used for biofabrication are detailed in the following sections. One is the piezoelectric nozzle and the other is the pneumatic micro-nozzle. Each nozzle system is exceptional in its method of operation which gives each system its advantages and weaknesses over the others.

3.2.1 Piezoelectric nozzle

3.2.1.1 MJ-SF-01-50

The first piezoelectric nozzle we used in our study was the MJ-SF-01-50 (Microfab Technologies, Inc., Plano, TX), shown in Figure 3.12, was used in our study. The

dimensions of this nozzle are 50 µm inner diameter, body diameter 12mm and total length 34mm. The MJ-SF series devices from Microfab are suited for dispensing different kinds of droplets of fluids such as adhesives, inks, solder, waxes, water-based polymers and liquid-based metals with operation temperature up to 250˚C. The dispensing fluid properties significantly affect the performance of the microvalve. The MJ-SF series nozzles are limited to dispensing fluids with viscosity less than 20cP and surface tension in the range of 0.02-0.5 N/m (Microfab user manual). This device can also generate drops with volume ranging from 10-500 picoliters.

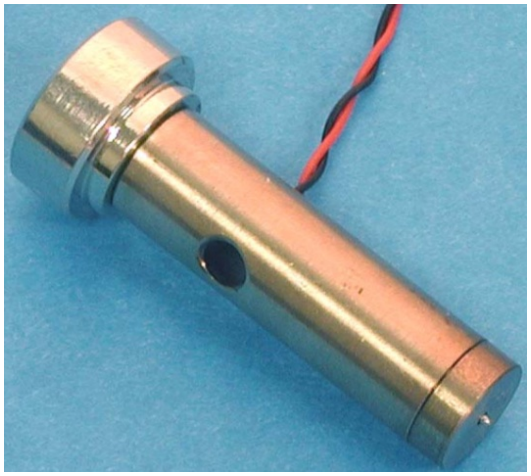

Figure 3.12: MicroFab MJ-SF-01-50 piezoelectric nozzle

To operate this device, a holding pressure is required to hold the fluid at the tip of the nozzle. Once a holding pressure is applied to the fluid, the frequency of the piezoelectric nozzle can be optimized, which allows the fluid to deposit picoliter volume drops. A periodical vibration is induced by applying a positive and a negative voltage to

drive the quartz crystals inside of the nozzle which helps the fluid stream to break into individual droplets. Both dispensing rate and droplet size can be controlled by the frequency and the voltage applied to the piezoelectric nozzle and is directly related to the viscosity and surface tension of the fluid.

The bipolar waveform is used for controlling the voltage time intervals. By modifying the following six time intervals T_{rise}, T_{dwell}, T_{fall}, T_{echo}, T_{final}, and Tlag, the expansion and contraction of the piezoelectric nozzle can generate a certain pulse width (Figure 3.13). The whole period includes the pulse width and Tlag which is the time for one cycle. The representation of the frequency is shown in Equation (3.1).

$$Frequency = \frac{1}{whole\ period} \tag{3.1}$$

Figure 3.13: Bipolar waveform is used for controlling the voltage time intervals

3.2.1.2 MJ-ATP-01-80

The second piezoelectric nozzle (MJ-ATP-01-80, Microfab Technologies, Inc., Plano, TX), shown in Figure 3.14, was then used in this research. This nozzle has 80 µm in inner diameter, 3.8mm in body diameter and 26.5mm in total length. This type of nozzle is designed for operating at low temperature and for dispensing droplets of water-based fluids up to 50˚C. The MJ-ATP series nozzles are also limited to dispensing fluids with viscosity less than 20cP and surface tension in the range of 0.02-0.07 N/m (Microfab user manual). The other operation procedures are the same as the MJ-SF series. The special reason for using this type of nozzle is that it has male threaded end fittings which can easily be attached to tubing and fittings without any leakage. The miniature dimension design enables the application of multi-nozzle printing within the limited holder area.

Figure 3.14: Microfab piezoelectric nozzle (MJ-ATP-01-80)

3.2.2 Pneumatic microvalve

3.2.2.1 HP 7x pressure-driven valve

The air pressure driven dispensing valve can successfully extrude highly viscous materials up to 100,000 cP with a maximum pressure up to 700 psi. As shown in Figure 3.15, the HP 7x dispensing valve makes it easy to apply very thick fluids such as silicones, medical-grade adhesives and epoxies through small dispenser tips. It features a unique design that increases the pressure inside a disposable syringe reservoir by a 7 to 1 ratio. Up to 700 psi (48.2 bars) of air pressure can be applied to the 3cc syringe reservoir within the HP 7x. A custom-made stainless steel barrel, a copper barrel, replaceable tips, and a nozzle heater were designed to handle the high viscosity of porogen materials. However, after extensive testing, it was found that the flow output is not uniform and cannot steadily form a continuous stream of flow with high viscosity material. Thus, the other type of pneumatic microvalve has been adopted to eliminate this problem in this study.

Figure 3.15: Microfab HP 7x Pressure-Driven Valve

3.2.2.2 741MD-SS needle microvalve

The 741MD-SS needle microvalve (shown in Figure 3.17) was then selected as the printing nozzle in this study. The dimensions of this microvalve are total length of 127.5mm, outside diameter 26.7mm, and various needle inner diameters of 100, 150, 200, 250, 330, and 410 µm. The pneumatic microvalve also has an adjustable needle stroke with a unique calibration feature that allows the user to maintain an exact deposit size of low to high viscosity fluids with exceptional control. It requires at least 70 psi (4.8 bars) air pressure to activate the "BackPack" valve actuator. This air pressure retracts the piston and needle, lifting the needle off the seat inside the dispensing tip, and permitting fluid flow through the tip. Once the cycle is complete, air pressure is

exhausted, which will cause the piston spring to return the needle back to its original position, subsequently stopping fluid flow.

The unique design of the 741MD-SS needle valve ensures very precise deposit control. The stainless steel shutoff needle is seated in the hub of the dispensing tip rather than the valve body. This design minimizes dead fluid volume by having fluid cutoff occur as close as possible to the dispensing orifice. The pneumatic microvalve can work by continuous extrusion or droplet deposition according to the printing frequency and back pressure setting. In order to obtain smooth 3D microstructures, we adopted continuous extrusion as a printing method to form a structure. The other significant factor for forming a 3D structure is related to material viscosity. Materials of relatively high viscosity have shown to be easier to build 3D structures with than lower viscosity materials. Since the material we used (42% PCL solution) has a viscosity of over 400,000 cP, it can be assumed that a 3D structure can be constructed from bottom to top without collapsing problems. However, high viscosity material might clog the stainless needle tips very easily and the applied high temperature could damage the components inside the nozzle and melt EFD plastic nozzle tips. Therefore, two custom made copper needle tips with different inner diameters, shown in Figure 3.16, were used to replace the disposable needle tips for printing high viscosity materials.

Once the heating mechanism needed to be activated in order to melt the material, a 120 cm long heating tape (OMEGA Engineering, INC, Stamford, CT) was used to maintain

the constant temperature with a temperature controller (CN8501TC-R1) by wrapping the syringe barrel. The printing nozzle was also enclosed by a heating barrel to keep the constant temperature by using another temperature controller (CNi8DH53). Two thermocouples (OMEGA) were placed between the heating tape and the syringe, and between the microvalve and the heating barrel, to monitor the temperature.

Since the disposable needle tip is a long stainless steel tip, this design is very easily clogged by high viscosity material. A custom made copper tip with inner diameter of 250µm was then designed to replace the disposable needle tip. The copper tip keeps the solution at the same temperature as the microvalve. Before dispensing, the molten solution was drawn into a 10cc syringe, and a 0.5µm syringe driven filter was used to filter particles to avoid future clogging. In order to install the microvalve onto the nozzle rack of the fabrication system, a specially made nozzle holder was designed and incorporated into the system.

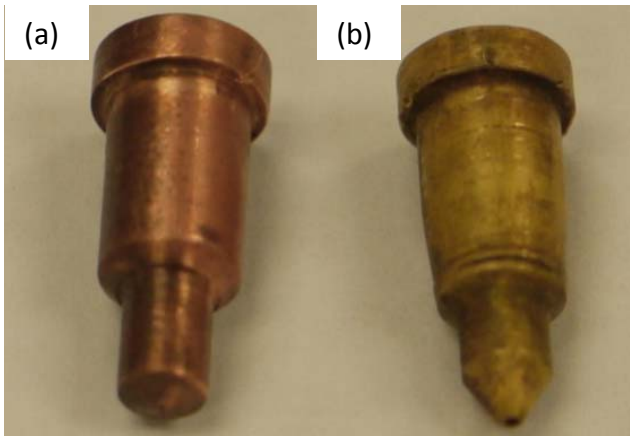

Figure 3.16: Two custom made copper needle tips with inner diameter

(a) 250 µm (b) 500 µm

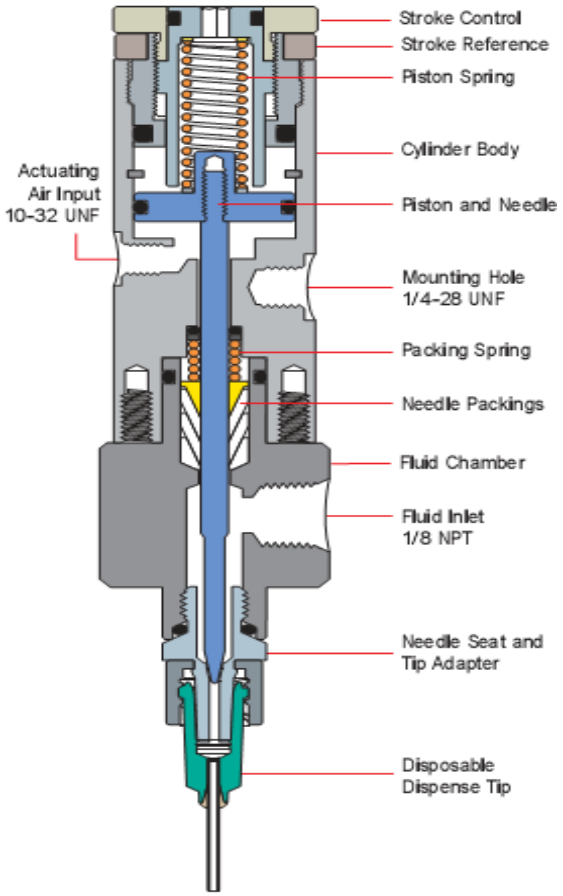

Figure 3.17: Schematic of 741MD-SS needle microvalve (http://www.nordson.com/en-us/divisions/efd/pages/default.aspx.)

Each nozzle is uniquely designed for different printing purposes, which bestows some advantages and limitations over the others. Their features and detailed comparison with advantages and disadvantages are shown in Table 3.2.

Table 3.2 Features comparison of four commercial printing nozzles

Nozzle / Features	**Piezoelectric MJ-SF-01**	**Piezoelectric MJ-ATP-01**	**Pneumatic HP 7x**	**Pneumatic 741MD-SS**
Printing Mode	Droplet	Droplet	Droplet	Droplet and continuous flow
Orifice diameters	20-80µm	20-80µm	100-500µm	100-500µm
Operation	Power: +/- 100 Volt Freq: 0-20,000Hz Pressure: >4 psi	Power: +/- 100 Volt Freq: 0-20,000Hz Pressure: >4 psi	Pressure: >100psi	Freq: 0-6 Hz Pressure:>70 psi
Material viscosity	<20 cP	<20 cP	<100,000 cP	<80,000 cP
Droplet size	picoliters	picoliters	Micro-liters	Micro-liters
Advantages	Precise drops Small dimension	Precise drops Mini dimension	Easy maintenance Extra high viscosity	Easy maintenance High viscosity
Disadvantages	Low viscosity Not continuous Complicated maintenance procedures	Low viscosity Not continuous Complicated maintenance procedures	Drop size Not continuous	Drop size Low frequency

3.3 Software Introduction

3.3.1 User friendly integrated software

Due to several types of software being necessary to be implemented for achieving the printing process, a MATLAB based GUI integration interface has been developed to minimize the operating procedures for users. As can be seen in Figure 3.18, users can easily enter the STL file names which have already been created by CAD programs, and then name the final complete APT file in the “Save as” block. Each STL file needs a tool number which corresponds to the material and the printing nozzle. To use this software, we first need to utilize a CAD program to create a heterogeneous structure which has two distinct models which are then individually saved in binary STL format files. For now, this prototype software is only designed for identifying two materials and for use with two nozzles. Since the whole printing system can add a maximum of six independent printing nozzles by changing tool settings in MACH3, the user friendly integrated software can also be modified to recognize six models as a heterogeneous structure by the proposed heterogeneous algorithm which is described in Chapter 4.

By sequentially clicking the steps on integrated software, Skeinforge is first used to slice STL files into APT language files. These two APT files are then automatically combined into a single APT file by using the proposed heterogeneous algorithm. Modification function is thereafter applied to change some commands and add a

transition code in between each layer of each APT file database. After the modification, a complete APT file has been created and is ready to import to MACH3 for simulation or printing purpose.

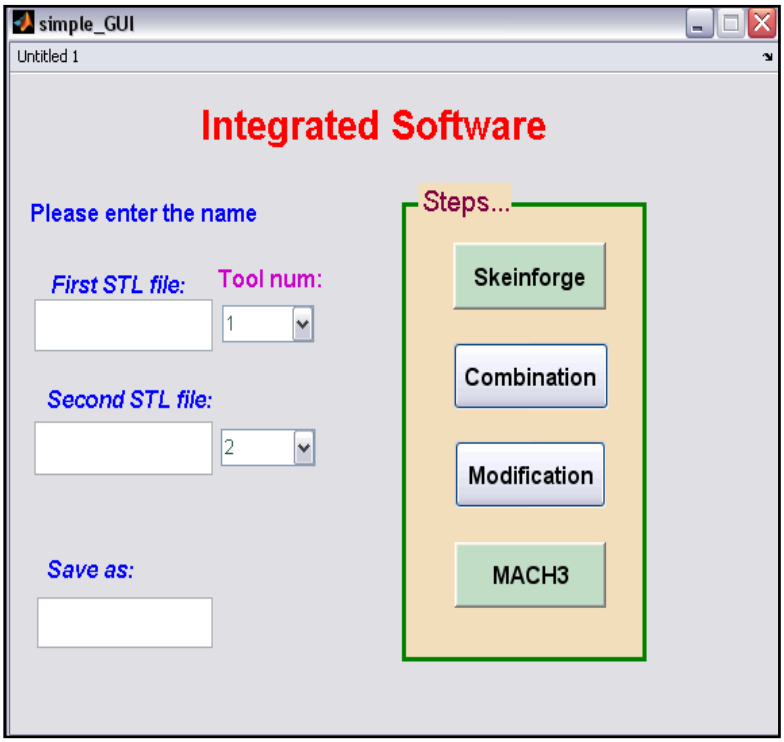

Figure 3.18: User friendly integrated software for pre-operation. When the STL files of each CAD models and the tool numbers have been selected, users can start to slice the files and modify the APT file using the integrated software.

3.3.2 Skeinforge

As shown in 3.19 Skeinforge is a GPL (***General Public License***) tool chain to forge an APT file skein for a model. The concept of this software is to carve the model into layers, which are then modified by other tools in turn such as fill, comb, tower, raft, stretch, hop, wipe, fillet, export and so on. Once all parameters in each tool dialog reach their proper settings, Skeinforge is then activated to export the APT file by importing a STL file, and to display the simulation of each layer and the whole model are shown in Figure 3.20.

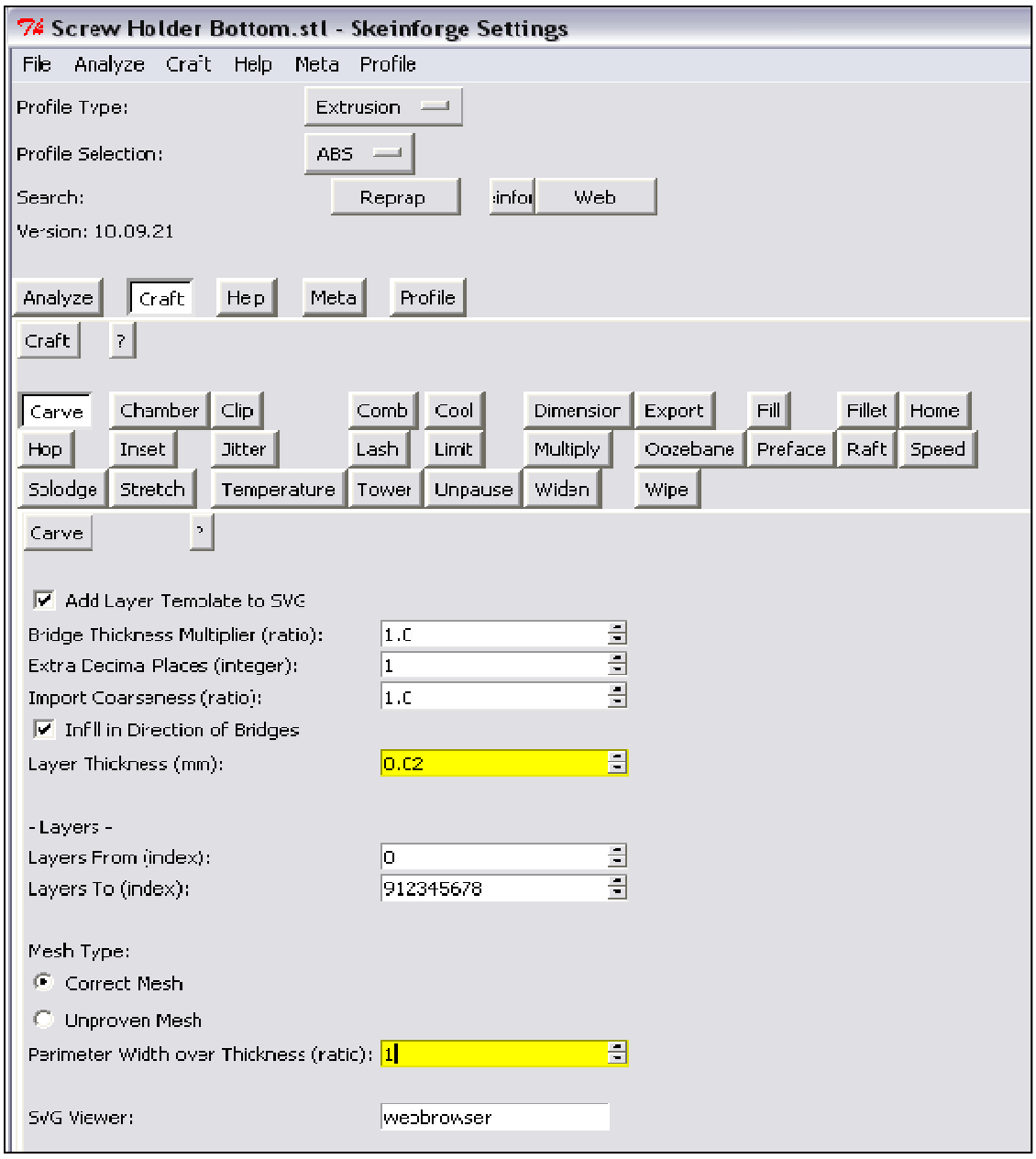

Figure 3.19: Skeinforge operation interface. Users can specify the layer thickness, printing speed, and the other printing parameters using the software.

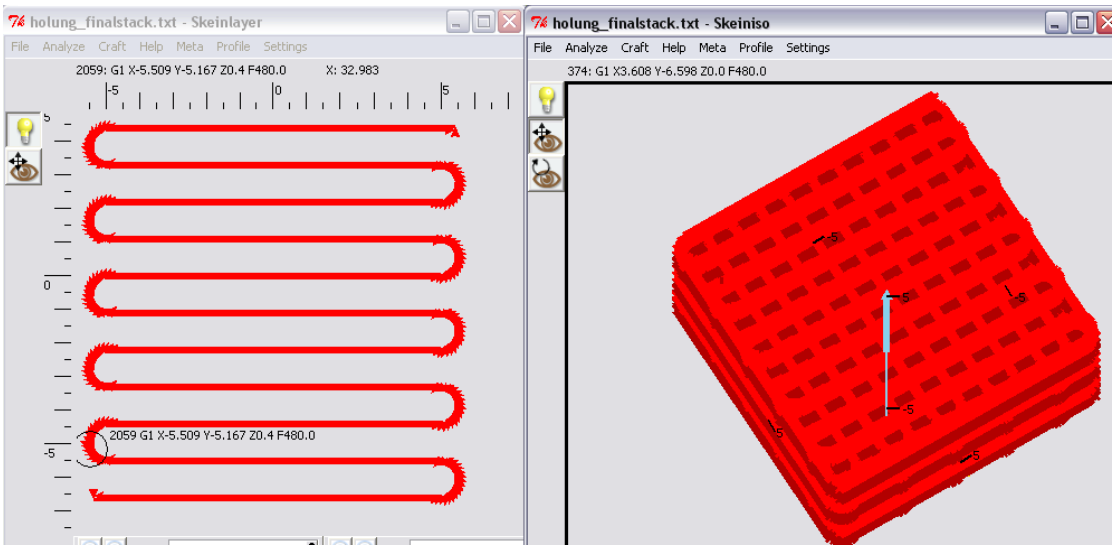

Figure 3.20: Slice simulation for one layer and for the whole structure

3.4 Scaffold and Structure Design for Our SFF Machine

In order to examine the performance of this SFF machine, the porous scaffolds and cylinder structures were designed by using Pro/Engineer and saved as STL files required by the fabrication system. The hollow cylinder structures were created with different inner diameters to test the stability and printing continuity of the SFF machine without any support material. This model serves the important purpose of obtaining the outer contour of the cylindrical surface. The porous scaffolds were also created by using Pro/Engineer and saved as STL files. Strut designs with different pore sizes and line widths were constructed to verify the accuracy and the reliability of the printing nozzles. Figure 3.21 shows a top view and a side view of a strut CAD model. By inspecting the printing results, some control parameters such as back pressure, traveling

speed, needle size, extrusion frequency, temperature setting, and material viscosity were controlled and modified in order to obtain optimal scaffolds or structures. Since a printing scaffold needs high strength and high stability to form a 3D structure, the material properties need to be carefully considered. PCL, a material commonly used to synthesize bone scaffolds, was dissolved at several different concentrations and tested in our SFF machine.

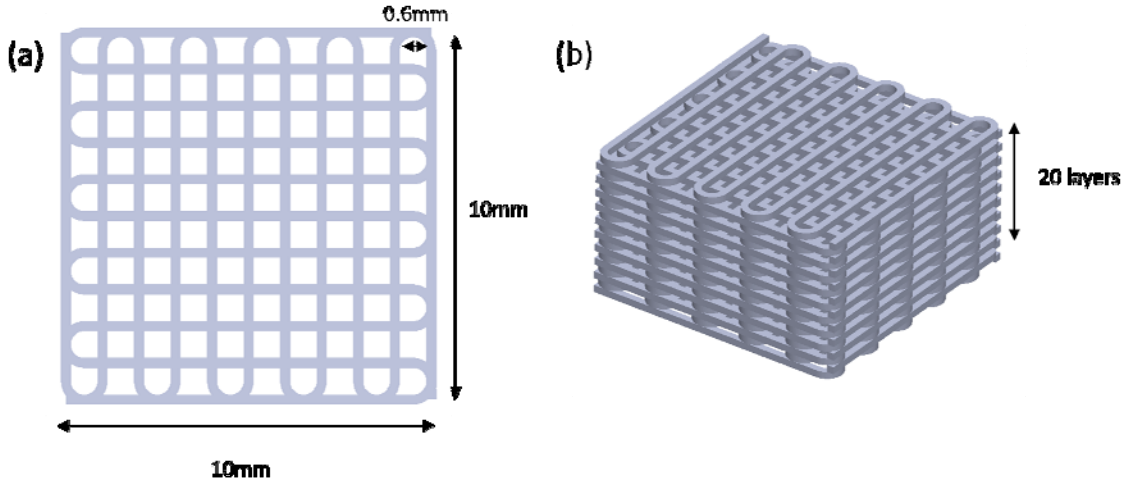

Figure 3.21 (a) Top view of the strut. (b) 3D design of a 20-layer scaffold.

CHAPTER 4 : HETEROGENEOUS ALGORITHM

4.1 Introduction

Rapid prototyping (RP) is a modern technology that can automatically fabricate 3Dimensional (3D) models embedded in a Computer Aided Design (CAD) system. Theoretically, RP can provide an easy way for researchers to build models or prototype parts with no dimensional constraints. In recent years, several manufacturing technologies have been developed and commercialized for tissue engineering applications, such as solid freeform fabrication (SFF), layered manufacturing (LM), electron beam melting, laser sintering, and electrospinning. However, these technologies are mostly designed to work with a single material, and this poses significant constraints when trying to build structure with complex detail (Liew, et al., 2001). In order to overcome this limitation, a variety of new printing processes and algorithms have been proposed and developed (Siu and Tan, 2002; Cho, et al., 2003; Liu, et al., 2004; Özbolat and Koc, 2009). Recently, heterogeneous structures have gained widespread popularity and found increasing applications in many areas including bio-manufacturing, tissue engineering, and Micro-Electro-Mechanical Systems (MEMS). Unlike with single material structures, it is possible with heterogeneous objects to define material volume regions and their interior distribution. This helps in improving material function of the overall object (Gurusamy and B.K., 2008). Due to these advantages, heterogeneous RP manufacturing has seen wide applications in tissue

engineering for building tissue scaffold structures (Leong, et al., 2003; Lin, 2008, Khalil and W.S., 2005; Koc, 2008).

The main object of this chapter is to present a novel RP processing algorithm for SFF of heterogeneous structures that is based on an Automatically Programmed Tools (APT) file to act as the input file of the model to be prototyped. A heterogeneous structure is composed of at least two digital geometric volumes where the processing algorithm is applied for gathering the entire database of each volume. Each database is constructed from Stereo-Lithography (STL) based multiple material volume regions. Next, the slicing software "Skeinforge" is used to slice models individually and output APT language files. Each of these APT files will represent an independent model and its material. All of the APT files are then integrated using a MATLAB based graphical user interface (GUI) integration interface to minimize the operating procedures for users.

This chapter is organized as follows. The next section will briefly describe the reasoning Boolean operations that will be used to illustrate heterogeneous models and the constituent assembly procedures. The key procedures of the RP processing for heterogeneous object modeling and slicing are detailed in section 3. The heterogeneous algorithm and printing procedures are described in the fourth section. Finally, an APT file based two-material heterogeneous structure will be presented as an example created by following our processing algorithm and printing method.

4.2 Description of heterogeneous structure by reasoning Boolean operations

The methodology behind heterogeneous object modeling has been widely reported (Biswas, et al., 2004; Dutta, 1998; Guptal, 2010; Yang, 2006). Kumar and Dutta (Kumar and DD., 1998) recently proposed using rm-sets to represent heterogeneous structures and defined relevant Boolean operators on rm-sets, demonstrating that the Boolean operation approach can effectively describe the composition of heterogeneous structures and explain the combination procedures thereof (Koc, 2008). Currently, most available CAD software provides some support for combining existing solid objects with Boolean operators which at least include union, intersection, and subtraction operations. Since the Boolean operators work only on solids or regions, it is essential that all solids under Boolean operations are algebraically closed.

In this section, we use the reasoning Boolean operations method to model a heterogeneous microstructure which is assembled with three different volumes of cylinders $A(M_A)$, $B(M_B)$, and $C(M_C)$ as shown in Figure 4.1. The meanings of the operation symbols are detailed in Table 4.1. The final assembly model in Figure 4.1 combines three cylinder cells, which can be represented by implementing Boolean operation $\{A\text{-}B\}(M_A) \cup \{B\text{-}C\}(M_B) \cup C(M_C)$. So based on Equation (4.1), a representation of material volume distribution H is presented by a material array M_i which defines the material volume of each object in the heterogeneous structure. The model type of each object is

represented by a model array *S* where *n* indicates the number of constituent topological compositions in *H*.

$$H = \sum_{S,i=A,B,C\ldots}^{n} S(M_i) \tag{4.1}$$

Using the final assembly in Figure 1 as an example, the first model S_A is a red cylinder (RC), the second model S_B is a yellow cylinder (YC), and the third model S_C is a blue cylinder (BC). Then the expression H can be represented as {*RC(MA), YC(MB), BC(MC*)}={60%, 30%, 10%} to indicate that the heterogeneous structure consists of three elements, where the corresponding materials: material A, B and C comprise 60%, 30%, and 10% of the total volume, respectively.

Table 4.2 reasoning Boolean operations

Function	Symbol	Expression
Union	A∪B	{ X|X∈A or X∈B }
Intersection	A∩B	{ X|X∈A and X∈B }
Subtraction	A - B	{ X|X∈A and X∉B }
Unit cell	$A(M_A)$	Material A in model A
Unit cell	$B(M_B)$	Material B in model B
Unit cell	$C(M_C)$	Material C in model C

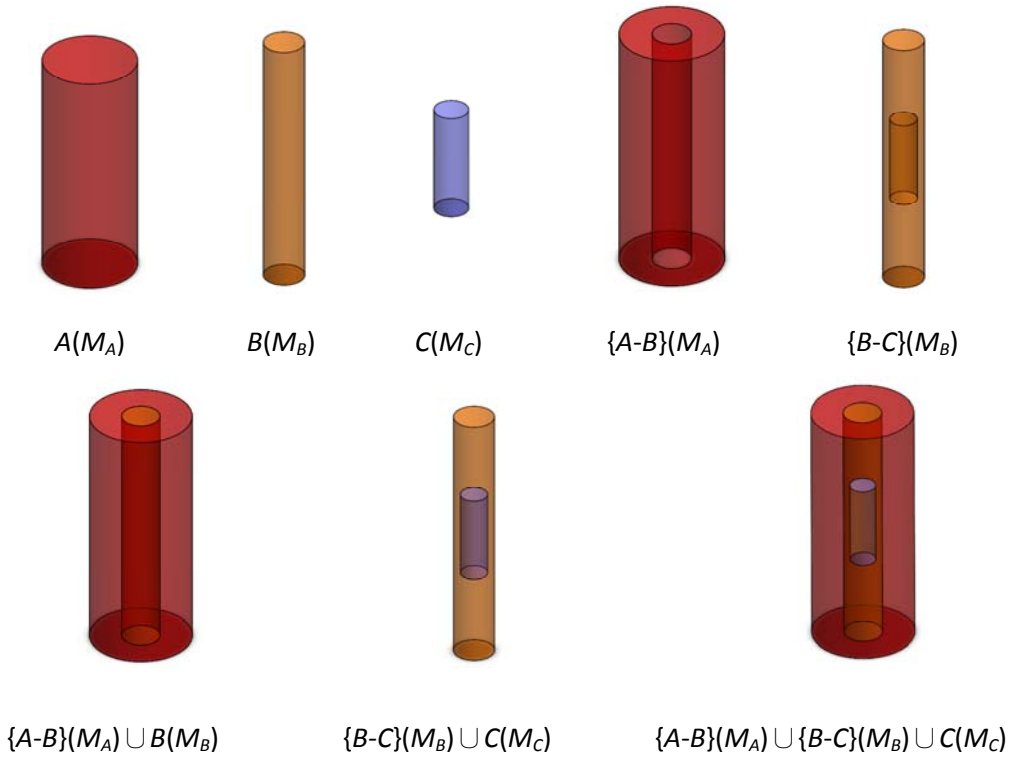

Figure 4.1: All combinations of solid objects can be represented by implementing Boolean operation. ($\cap$: intersection; $\cup$: union; -- : difference). The first three unit cells indicates material A in model A, material B in model B, and material C in model C. The last assembled model combines these three cylinder cells, which can be represented by implementing Boolean operation $\{A\text{-}B\}(M_A) \cup \{B\text{-}C\}(M_B) \cup C(M_C)$.

4.3 Algorithm for heterogeneous object modeling and slicing

It is very well known that CAD modeling can define the geometric information for even complex structures. However, modeling heterogeneous microstructures by including the material information and the variation in constituent composition along with the geometry in the solid model creates a complex situation with many variables to

account for. A model for a complete multiple-material microstructure should include not only the geometric data, but also store the material information and distributions for printing purposes (Leong, et al., 2003). However, since the standard STL format does not contain material identification and distribution, additional identification is needed to recognize different materials and the location of each volume in a multiple material structure. Some researchers have proposed incorporating material identifiers into the STL file for layered fabrication of heterogeneous structures (Sun and Lin, 2004), but that would create a data file too large and complicated for a computer to efficiently process and slice. Therefore, we developed a novel modeling method and a slicing method which can be implemented in a current CAD environment to enable convenient printing of any hybrid or heterogeneous structure with complex geometries.

The first step is to create a heterogeneous structure based on a CAD system. A brief concept of a heterogeneous model is a structure consisting of solid objects with different material distribution. In order to create a heterogeneous model with various biomaterials, CAD software should first be able to identify the position of each object within the heterogeneous structure. Since the procedure of the model slicing is based on the direction of the z axis, it is necessary for all of the objects to be created in the same coordinate system. When the position of each object has been fixed, the heterogeneous structure should be separated into independent parts and saved individually as different CAD files. Furthermore, the CAD model is converted to binary STL based models as a standard output file format used for slicing. Then, all parts can be

sliced one by one using commercially available image processing software. The slicing software uses a direct slicing method on unigraphic based models, which creates slices with equal thickness. The procedure is repeated until all of the individual parts have been sliced to a specific layer thickness and then converted into APT language files.

4.4 Heterogeneous algorithm and printing procedure

Based on the illustration shown in Figure 4.2a, the heterogeneous model can be described as a combination of Material 1, Material 2, and Material 3. According to the procedures described in the previous section, the APT files for each layer from the CAD based heterogeneous structures are generated first, followed by the slicing of the STL database into APT file format using slicing software. The structure volume geometries are constructed and sliced individually while each APT file database is associated with different materials. In order to merge several different APT file databases, the integrated software has been developed to combine all of the individual APT files and add in a “transition code” in between each layer of each APT file database. The transition code includes an extruder change command, pause command, and protection command that will serve as the junction between two APT files, which correspond to two different material models in one layer (Figure 4.2b). The functional flowchart of Combination procedure for one layer of heterogeneous models is illustrated in Figure 4.3. After combination, a complete APT file database is assembled by identifying the

height in the z-direction. In other words, each layer of a complete APT file database will be the same height, even with different material distributions.

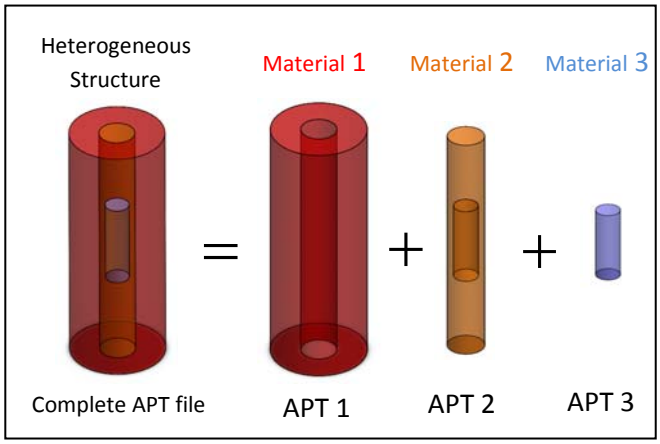

(a)

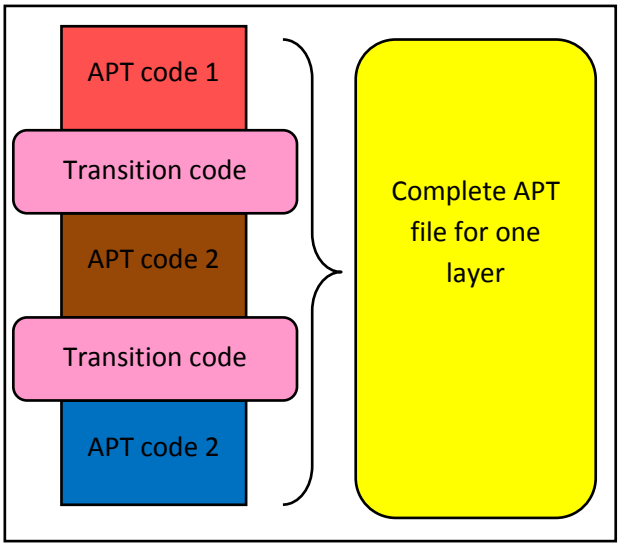

Figure 4.2: (a) Model of a heterogeneous structure consisting of three objects (b) procedure to generate the database of a heterogeneous fabrication model in one layer

A standard APT file can be briefly divided into three parts: initial section, body section, and ending section. The initial section describes the parameter settings of the machine, which includes unit selection, fan on, extruder PWM, extruder temperature, extruder speed, and the initial extruder position. The ending section includes some commands to turn off all of the extruder settings and activities and defines a final extruder position. The entire printing path of the freeform fabrication and the transition code will be stored into the body section. Once all of the parameters in these three parts have been well-defined, a complete APT file with heterogeneous printing capability is ready to be used for 3D fabrication. The data structure of the complete APT file is described as follows:

The data structure of the complete APT file

G90 // absolute distance mode

G21 // unit selection

M106 // fan on

M5 // set first extruder off

M113 PWM // set extruder PWM

M108 speed Num. // set extruder speed

Initial section

G1 coordinates F velocity // go to initial position of the first model

M3 // set first extruder on

G1 coordinates F velocity // x, y, z position and traveling speed

…

M5

G1 coordinates F velocity // go to initial position of the second model

// insert transition code

Pause command

Protection command

Extruder number M6 //Tool change

// link to second model with second extruder

Transition code

G1 coordinates F velocity // go to initial position of the second model

M7 // set second extruder on

G1 coordinates F velocity // x, y, z position and traveling speed

…

M9 //set second extruder off

G1 coordinates F velocity // go to initial position of the third model

Body section

```
// insert transition code
Pause command
Protection command
Extruder number M6    //Tool change
…
…
M5
Protection command
G1 coordinates   F velocity    // define the final extruder position
M107     // fan off
M113 0
```

Transition code

Ending section

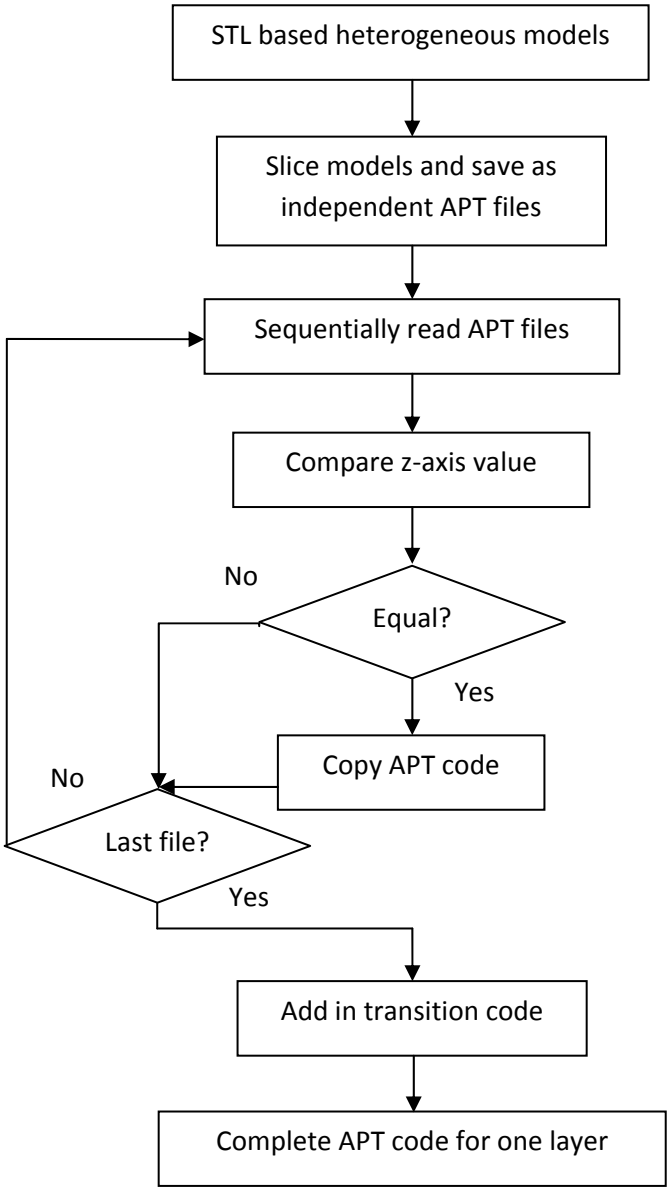

Figure 4.3: Combination procedure flow chart for one layer of heterogeneous models

Depending on the setting for the layer thickness and model volume design, the content of the output APT files will range from a few thousand lines to several hundred thousand lines. Obviously, it is almost impossible to manually and accurately combine all of these files together. To solve this problem, MATLAB based integrated software has

been created to minimize the operating procedures for users. It should be emphasized that these models should be created in the same geometric space and will be sliced with a constant layer thickness, which can be defined by end users. As shown in Figure 4.4, each colored model represents a different material and these models are combined into a single heterogeneous structure. Each layer of the models will have the same increment in thickness, and this feature will be used to determine whether or not they are in the same layer by identifying the coordinate at the z-axis. This integrated software will read all APT files from the beginning, and replicate the contents from M3 to M5 in each of the body parts. Afterwards, it will recognize the z-axis value and compare that same value file by file. If the values of the z-axis are the same, they will be considered as the same layer. If not, the software will compare the z-axis to the next file. This procedure will be repeated until all of the files have been read completely, and finally the relevant data is combined to generate a new APT file for printing.

A procedure flowchart that describes the layered fabrication of a heterogeneous structure is illustrated in Figure 4.5. The procedure starts with the creation of heterogeneous models by using CAD and then generates binary STL files. In order to make sure these models can be sliced and printed using the same coordinate, it is necessary to define structure volume geometry. After the generation of geometrical profiles for each of the structure volumes assembled in the heterogeneous fabrication structural model, the process for slicing can be defined. Slicing is uniform with a constant layer thickness, or adaptive layer thickness (Sun and Lin, 2004) according to the

exact thickness of the actual printed material for one layer, as determined during calibration for each new material.

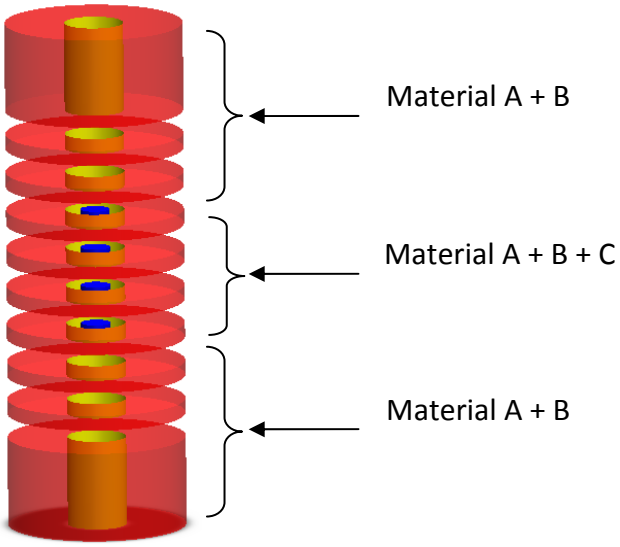

Figure 4.4: Heterogeneous model structure slicing results with same slicing thickness. The top and bottom of the structure have the same material distribution (material A and B) and the center part includes three different materials (material A, B, and C).

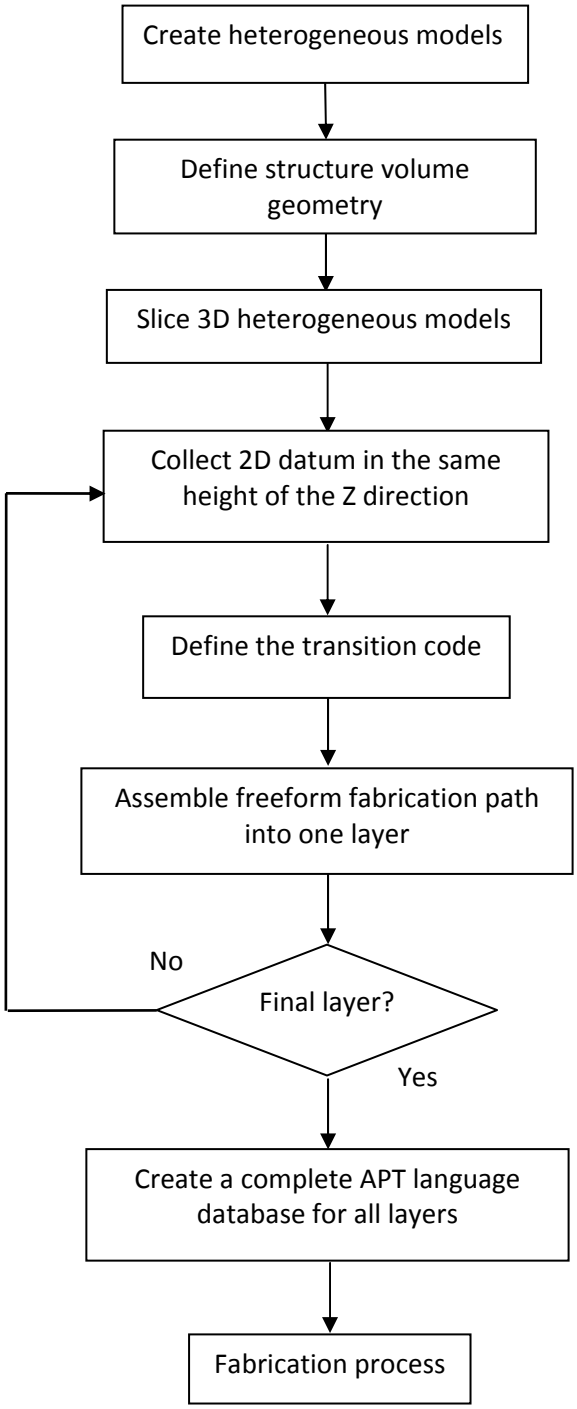

Figure 4.5: Procedure Flowchart Describing Layered Fabrication of a Heterogeneous Structure

CHAPTER 5 : MATERIAL STUDY

5.1 Poly (ε-caprolactone) (PCL)

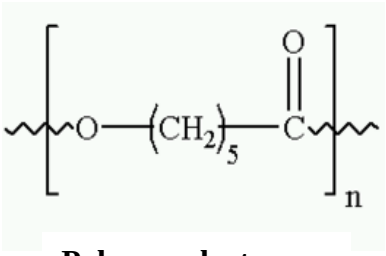

Polycaprolactone

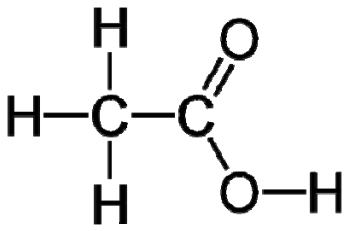

Glacial acetic acid

Figure 5.1: Chemical Structure of PCL and glacial acetic acid

Polycaprolactone (PCL) MW=80,000 was purchased from Sigma-Aldrich and used as received. Glacial acetic acid, CH_3COOH, was also purchased from Sigma-Aldrich and used as received. The viscous flow at a weight concentration of 40% (w/w) can be applied to pneumatic valve needles of diameter larger than 200µm without clogging.

PCL is a biodegradable, biocompatible, and water insoluble polyester, whose physicochemical properties are determined by its molecular weight. PCL is a semi-crystalline polymer, which has a glass transition temperature of 60 ˚C and melting point ranging between 59 and 64 ˚C (Sinha et al., 2004). It can be dissolved in glacial acetic acid, which evaporates at room temperature, allowing the PCL to remain as a solid structure in the form in which the solution was printed. Glacial acetic acid contains no

water so the solution has almost no hydrogen ions because the hydrogen molecule in –COOH has difficulty forming ions that attack the C=O bond in the PCL chain; therefore, the PCL can retain its physicochemical properties. The melting point of acetic acid is 16.5 ˚C and therefore acetic acid vaporizes quickly at room temperature. In our case, after the PCL acetic acid solution has been printed as thin lines, the acetic acid evaporates within one minute and leaves a 3D PCL solid structure.

To prepare a solution, PCL powder is blended with glacial acetic acid to make a PCL weight concentration of 42% (w/w). In order to get a fully dissolved solution, a glass rod is used to stir by hand. The bottle is placed in a sonicator for 1~2 hours and allowed to sit for one day until all bubbles are removed. The solution then can finally be used for 3D printing by pneumatic valve (EFD. Inc) with different inner diameter needles. Other concentrations of 30%, 35% and 40% - 45% are also prepared for further viscosity testing. In our case, the viscous flow at a weight concentration of 40% (w/w) can be applied to pneumatic valve needles of diameter larger than 200μm without clogging. Although the high viscosity solution makes 3D material construction and solidification easier, the 42% PCL solution is almost saturated, and its viscosity is up to 450,000 cP. In this case, high viscosity solution may easily cause printing difficulties and clog nozzles. Therefore, precise calibration for each parameter setting and needle size selection need to be carefully considered.

5.2 Alginate

Alginate was also selected as a material for tissue construction because of its high biocompatibility and biodegradability. It is a nontoxic, immunologically inert polysaccharide and has been widely used as a scaffold material for immobilization of enzymes or cells in bioreactors, and also for tissue engineering (Hara et al., 2001).

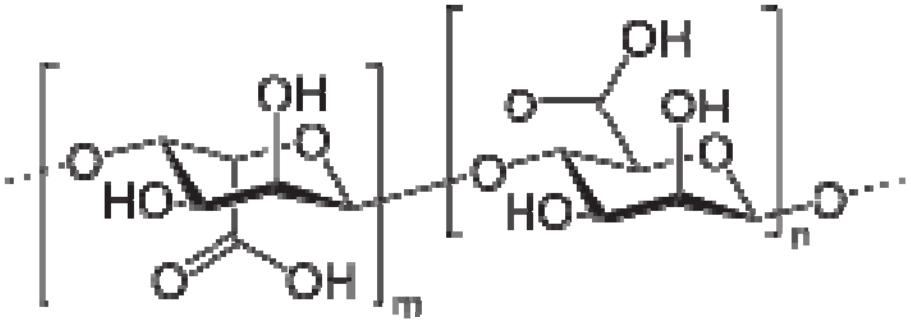

Figure 5.2: Chemical structure of alginate

Alginate is a brown-algae-derived polysaccharide composed of β-D-mannuronic acid and α-L-guluronic acid units (Grellier et al., 2009). Because of the crosslinked polymer network structure, alginate can absorb in water at a large range of concentration, and therefore the solution viscosity could be changed from very low to extremely high. By choosing proper viscosity, the solution can form different strength of structures after printing. The mechanical property of alginate is determined by the molecular weight and gelation method (De Boisseson et al., 2004). Molecular weight ranges from 10 to 1000kDa, depending on the source and process method used to

obtain alginate. The mechanical properties can be adjusted by tailoring the gelation method, including crosslinker concentration, type of crosslink material, and alginate concentration. The rate of crosslinking is also very important for final alginate structures, especially in the printing process. For example, when printing the alginate solution directly into the crosslinker container, the rate of crosslinking should be reduced in order to avoid clogging in the needle tip of the dispenser. In general, calcium ions are used to crosslink alginate from the surface and the ion can diffuse into alginate, and then solidify the structure. To conduct this printing process, alginate is printed through a thin needle tip, and the printed alginate is crosslinked in a calcium ion environment, which is usually provided using a calcium chloride solution. In this method, crosslinked alginate has been solidified and processed as micro carriers for cells (Banfi et al., 2000). Alginate can also be mixed with other biomaterials to improve its biological performance such as with chitosan (Li et al., 2005; Becheran-Maron et al., 2004). Chitosan is a polysaccharide and is prepared by N-deacetylation of chitin that is naturally derived from marine crustaceans (Welsh et al., 2002; Muzzarelli and Gooday, 1985; Kumar, 2000). It forms hydrogels by ionic or chemical cross-linking with glutaraldehyde or other crosslinkers (Mi et al., 2000). UV irradiation also has been reported to form azide-derivatized chitosan as gels (Ono et al., 2000). Many methods have been developed to modify the biological functions of chitosan, including enhancement of cellular interactions for tissue engineering approaches.

Kuo *et al*. reported the achievement of a controlled gelation rate with $CaCO_3$-GDL and $CaSO_4$- $CaCO_3$-GDL systems that form structurally uniform gels for tissue engineering applications (Kuo et al., 2001). They also demonstrated how to control the structural integrity, mechanical properties, and cell incorporation uniformity. Slower gelation systems generate more uniform and mechanically stronger gels than faster gelation systems (Kuo et al., 2001). Their results showed that the compressive modulus and strength increased with alginate concentration, total calcium content, molecular weight and guluronic acid content of the alginate.

Normally, calcium chloride solution is used as a crosslinker for alginate in 3D printing. On the other hand, if aiming to form an alginate structure in bone tissue engineering, the hydrogel should be combined with calcium phosphates (Qi, et al., 2009; Turco, et al., 2009; Yuan, et al., 2009). Yuan et al. (2009) have also reported using a freeze drying method, without the need for crosslinking, to form porous alginate scaffolds for cell encapsulation.

5.3 PEG-PLGA-PEG (triblock)

5.3.1 Thermosensitive hydrogels

Thermoreversible hydrogels are of great interest in drug delivery, cell encapsulation, and tissue engineering (Jeong and Gutowska, 2002). Early research in the field focused on synthesis of thermosensitive gel materials including poly(ethylene

glycol)/poly(propylene glycol) block copolymers (poloxamers), poly(ethylene glycol)/ poly(butylenes glycol) block copolymers, poloxamer- g-poly(acrylic acid) and copolymers of N-isopropylacrylamide that exhibited a sol-to-gel transition in aqueous solutions (Bhattarai et al., 2005). Such materials are not biodegradable which limits their use.

Aqueous solutions of new biodegradable triblock copolymers, poly (ethylene glycol-b-(DL-lactic acid-co-glycolic acid)-b-ethylene glycol) (PEG-PLGA-PEG), have been shown to have solution-to-gel (lower transition) and gel-to-solution (upper transition) transitions as temperature increases. The lower transition is important for scaffold fabrication because the solution flows freely at room temperature and becomes a gel at body temperature (Jeong et al., 1999). With increasing temperature, aqueous solutions of PEG-PLGA-PEG, molecular weights of 550-2810-55, triblock copolymer underwent solution to gel transition in the range of 30–35°C (LCST) and gel to solution transition in the range of 40–70°C (higher critical solution temperature, HCST) The transition temperatures depend on the concentration of polymers. The viscosity of PEG-PLGA-PEG triblock copolymer aqueous solution at 33 wt % concentration at room temperature was 10 cP and then abruptly increased at the sol-to-gel transition temperature (Jeong et al., 1999).

The properties of these polymer solutions prior to gelation and its mechanical strength as a gel make these thermosensitive hydrogels ideal for SFF. For PEG-PLGA-PEG hydrogel, its ability to hold its shape is not directly related to the viscosity of its initial solution (Geisler et al., 2010).

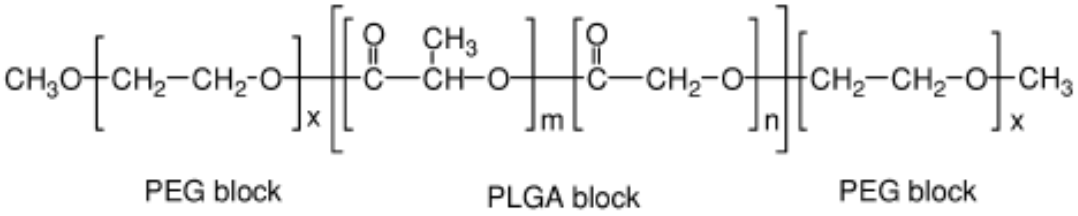

Figure 5.3: Chemical Structure of PEG-PLGA-PEG

5.3.2 Photocrosslinkable hydrogels

Photopolymerization to form hydrogels has attracted considerable interest in the field of tissue engineering and drug delivery. The reason for this interest is that gel constructs have similar water contents to the extracellular matrix and thus allow for efficient nutrient transport, which is important for maintaining cell viability, as well as contributing to biocompatibility by reducing mechanical irritation to the surrounding tissue (Amsden et al., 2007). Photopolymerization is used to convert a liquid monomer or macromer to a hydrogel by free radical polymerization in a fast and controllable manner under ambient or physiological conditions (Nguyen and West, 2002). A photon from a light source excites or dissociates the photoinitiator into a high-energy radical state. This radical then induces the polymerization of a macromer solution (Williams et al., 2005). Usually, the material before gelation is a viscous solution that is then crosslinked upon ultraviolet light (UV-) irradiation, resulting in an insoluble hydrogel. PEG with a methacrylate group can be coupled with Irgacure 2959 (I2959) as a photoinitiator (Yoshimoto et al., 2009). I2959 is reported to be biologically nontoxic.

Irgacure 2959 has a molecular formula of $C_{12}H_{16}O_4$ and its structure is shown in Figure 5.4.

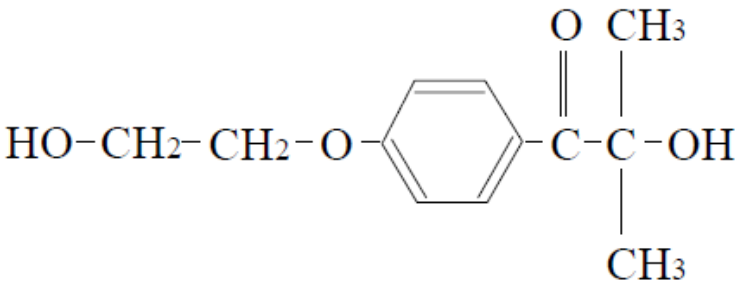

Figure 5.4: Chemical structure of Irgacure 2959

5.3.3 Thermosensitive / Photocrosslinkable hydrogel

A thermosensitive triblock copolymer that is also photopolymerizable would create a low viscous solution that can be gelled to created a mechanically strong material for three-dimensional scaffold construction. Both triblock copolymers and photopolymerizable materials have been used in tissue engineering so a blend of the two hydrogels would create a material that can be gelled either thermally, by use of UV-irradiation, or both. By varying the use of the gelling techniques, the final gel mechanical properties can be varied. With this type of hydrogel, it is possible to build a three-dimensional scaffold that is porous, biocompatible, and biodegradable with a controllable degradation, suitable for cell attachment and proliferation, able to emulate the mechanical properties of the tissues at the site of implantation.

5.4 Sucrose

Sucrose is a disaccharide derived from glucose and fructose with the molecular formula $C_{12}H_{22}O_{11}$ (Figure 5.5). In printing experiments, sucrose can be used as bioresorbable and fluidic material for printing tests. The sucrose is used as tissue engineering porogen-based fabrication system as the porogen building material (Lu et al., 2009).

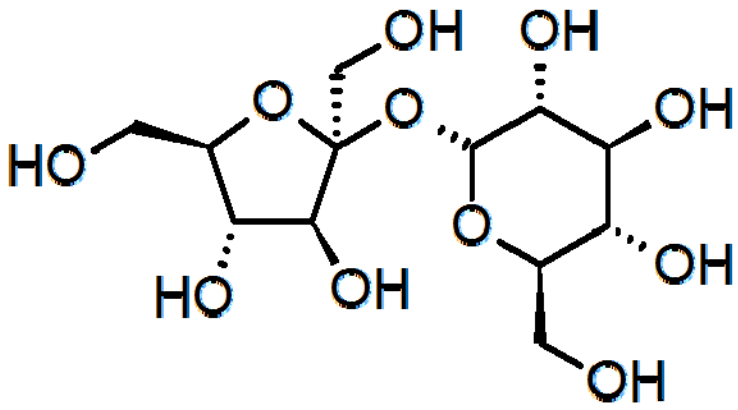

Figure 5.5: Chemical Structure of sucrose

First, use melted high viscous sucrose fluid as main material, then, add butter as lubricant, and add aluminum sulfate to reduce the mixture's melting temperature. Finally, honey can also be added to reduce melting temperature and increase the viscosity if needed.

To prepare the mixture, sucrose (Sigma) cannot be directly heated up to melting temperature; otherwise, the sucrose can easily decompose. First dissolve sucrose into

water and heat up to 100˚C until almost no water is left. Then stir the solution until the color starts to turn dark red. Furthermore, control the mixture cool down to around 85˚C, and mix butter and honey into the mixture. The significant reason for using butter as a mixture is because it can reduce the melting temperature dramatically. The sucrose solution can immediately reach the boiling temperature when the butter is added into the solution, and the change is visible to the naked eye. As the solution is well mixed, the aluminum sulfate is then added into the solution as mixture, and the melting temperature of the sucrose solution decreases to around 80˚C. If the sucrose mixture is dispensed from nozzle, the high viscous fluid will solidify within 3 seconds at room temperature.

Sucrose viscosity is highly dependent on different ratio of each component and temperature (Lin Lu, 2007). The weight of water also has a significant effect on the viscosity result. In order to reach the smooth printing and 3D construction, one possible choice is weight ratio of sucrose, honey, aluminum sulfate $(Al_2(SO_4)_3).18H_2O$, and butter using 90:0:5:3 and initial sucrose to water weight ratio is 9:5 to achieve 2,700 cp (1 cP = 1 mPa·s). The sucrose must keep a higher temperature than melting temperature, and the dispense valve needs to be heated up to keep the viscous fluid in order to have smoothly and uniformly printing results. The viscosity is defined as the ratio of the applied shear stress and the shear rate given in Equation 5.1. Poise (dynes-s/cm2) is a frequently used unit for viscosity. The various sucrose mixtures are prepared for viscosity test and the results are shown in Table 5.1 (Lin Lu, 2007).

$$\mu = \frac{Shear\ Stress}{Shear\ Rate} = \frac{\tau}{\dot{\gamma}} \qquad (5.1)$$

Table 5.1: Viscosity of various sucrose mixtures

Sucrose (g)	Alum (g)	Honey (g)	Butter (g)	Water (g)	Viscosity (cP)
25	1.25	1	0.25	5	5100
25	1.25	0	0.25	10	2200
25	2	0	0.25	50	270
25	0.25	0	0.25	75	40
90	5	0	3	50	2700

5.5 Viscosity Measurement

During material selection, material viscosity is an important factor to consider to ensure that the material can be printed into a 3D structure. In general, a material that has too low or too high viscosity cannot be built into a 3D structure smoothly and efficiently. For example, at very low viscosity, the material could leak out of the tip, and at high viscosity, the material may require high pressure that could damage the nozzle. For our experiments, a cone and plate rheometer (Brookfield Inc., MA USA, DVII+Pro, shown in Figure 5.6) was used to determine the viscosity of a variety of biocompatible materials at different concentrations. All of our material samples were placed in between the cone and the plate. A motor was connected to the cone and applied

rotational force to the testing material. As the material creates resistance to flow, the corresponding rotation of the lower plate was measured. The resistance to flow was calculated as shear stress (force divided by area) divided by shear rate (rotational speed).

Figure 5.6: Rheometer (Brookfield, DVII+Pro)

(http://www.brookfieldengineering.com/products/viscometers/laboratory-dv-ii.asp)

5.6 Flow Rate Measurement

To optimize the nozzle moving speed and estimate the manufactured part building volume, we need to know the dispensed material flow rate. Experiments were

conducted to measure the flow rate of the sucrose mixture at various parameters to understand the controllability of deposition of sucrose mixture and to improve the quality of the printed porogen. We measured the mass of the deposited solution on a balance and then divided it by the measuring time as shown in Equation 5.8. First the mass flow rate was calculated then volumetric flow rate was calculated by dividing the mass flow rate by the solution density as shown in Equation 5.9. The nozzle tips were approximately 1cm above the Petri dish surface. All the experiments used the same nozzle tip with an inner diameter (ID) of 500 μm.

$$\dot{m} = \frac{mass}{time} \quad (\text{in gram/second}) \tag{5.8}$$

$$Q = \frac{\dot{m}}{\rho} \quad (\text{in mililiter/second}) \tag{5.9}$$

Where $\dot{m}$ is mass flow rate, *Q* is the volumetric flow rate, and ρ is the density. The density of the solution is calculated by using Equation 5.10 as shown below.

$$\rho = \frac{m}{V} = \frac{mass}{volume} = g/ml \tag{5.10}$$

An adjustable air supply was connected to the reservoir, where the sucrose mixture was delivered to the microvalve for deposition. The deposited sucrose mixture was collected into a Petri dish that was placed on a balance for measuring the mass of the sucrose mixture over a specific interval of time (20 seconds in our test) to calculate the

mass flow rate as expressed by Equation 5.8. The volumetric flow rate was then determined by dividing the mass flow rate by the density of the sucrose mixture (1446 kg/m^3) as described in Equation 5.9. The density of the sucrose mixture was measured by weighing a filled 3 cc syringe. Then Equation 5.10 was used to calculate the density of sucrose mixture. Three measurements were performed and the average density was taken into the flow rate calculation.

CHAPTER 6 : SYSTEM SETUP AND EXPERIMENTAL RESULTS

6.1 System Integration

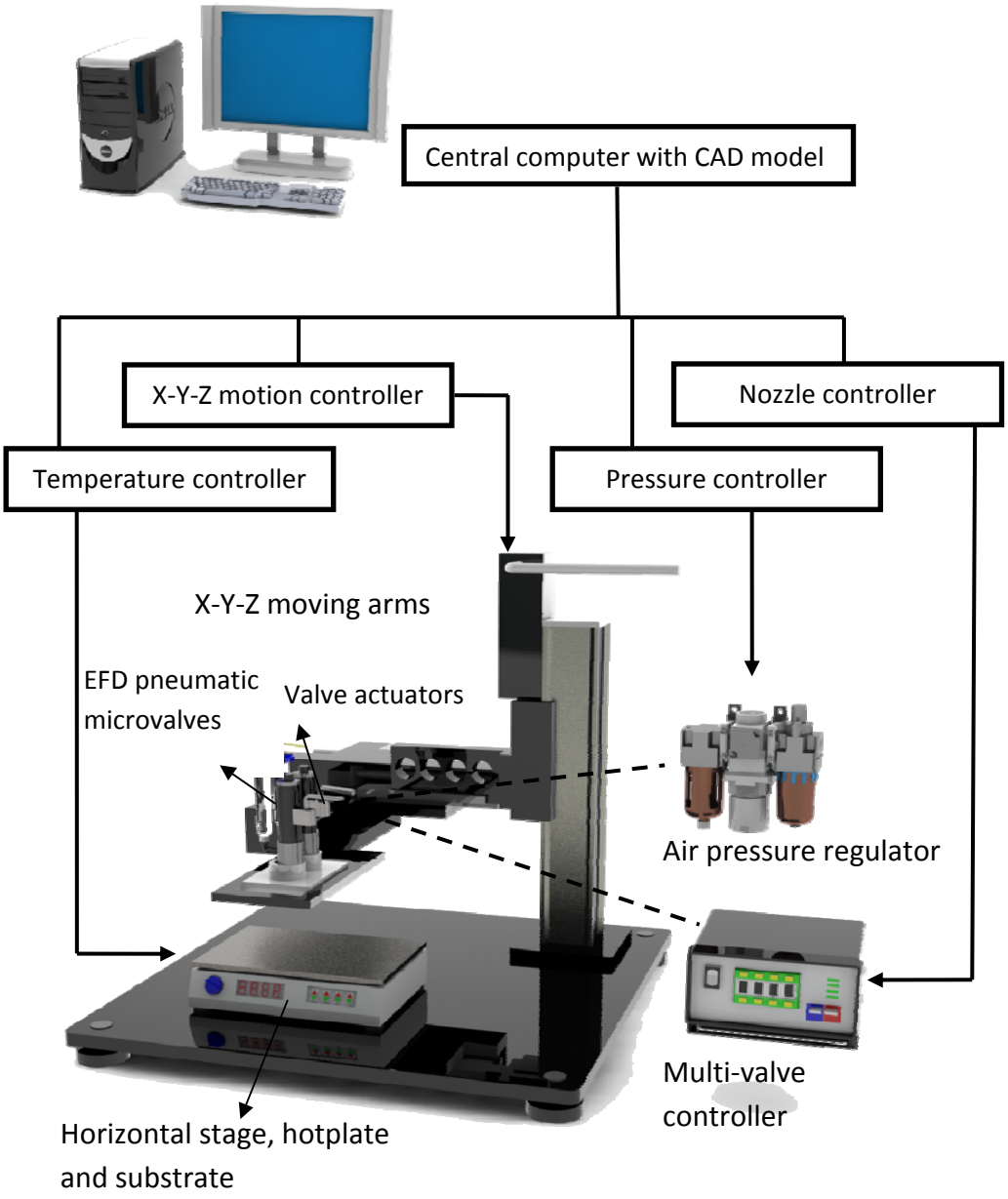

Figure 6.1: The 3D multi-nozzle heterogeneous printing system and machine integration includes a central computer, a motion controller, temperature controllers, a nozzle controller, and a pressure controller. In this experiment, we used EFD pneumatic microvalves, valve actuators, and a multi-valve controller to achieve the heterogeneous material printing.

A newly developed 3D SFF system shown in Figure 6.1 was created in this project to fabricate 3D scaffolds for tissue engineering applications. Briefly, the SFF system is a three-axis printing machine capable of moving the 3-axis arms and delivery printing nozzles in the x-, y-, and z-axes separately or simultaneously. This configuration provides the flexibility and control that enables the SFF system to create complex 3D objects. The entire system includes a multiple dispensing heads with dual-dispensing nozzles was carefully tested and installed into the printing system. Both the BackPack actuator and solenoid driver were installed and tested with a pneumatic microvalve to provide actuation speeds. A multi-valve controller was utilized to control the extrusion of two pneumatic nozzles independently or simultaneously. Two precise air pressure regulators and two digital gauges were implemented to provide precise pressure force to material reservoirs and pneumatic nozzles. Two digital temperature controllers with heating tapes and heavy duty heating barrels were utilized to maintain the temperature of the printing nozzles and the syringe barrels. A hotplate with horizontal stage was selected to provide balance and heat up the substrate for warming purpose. The motion control software “MACH3” is chosen to be installed in a central computer to drive not only X, Y, and Z axis motors for moving, but also the valve controller for printing with multiple nozzles.

6.2 The Requirements for Scaffold Fabrication

One of our objectives in scaffold printing is to maintain a high degree of accurate control over the physical and mechanical properties of the selected materials. Although a large variety of natural or synthetic biomaterials can be utilized for tissue fabrication, their ability to form 3D scaffolds is affected by different material properties and processing requirements. The four key requirements for scaffold fabrication techniques are: (1) process accuracy, (2) processing conditions, (3) consistency, and (4) repeatability (Leong et al., 2003).

1) Processing conditions: The processing procedures should not change the material properties and clinical utility of the scaffolds. In other words, the implemented technique should not change the chemical and mechanical properties and biocompatibility of the scaffold (Leong et al., 2003).

2) Process accuracy: The technique should be able to precisely produce porous 3D scaffolds in which cells can migrate and proliferate. One of the advantages of RP technology is that it confers accuracy in tailoring pore sizes and morphologies, which are determined by the user. This is difficult and in some cases impossible to achieve with conventional fabrication (Leong et al., 2003). The capability to maintain accurate pore sizes will allow for the creation of a variety of scaffolds to suit different tissue engineering applications (Leong et al., 2003).

3) Consistency: The technique should produce scaffolds with highly consistent porous structure. In addition, consistency in pore characteristics, morphologies, pore distribution, pore density and interconnectivity in all three dimensions is required in order to produce highly regular 3D structures (Leong et al., 2003).

4) Repeatability: The technique should be capable of producing scaffolds of the same specifications, pore sizes, and structural features, that exhibit minimal variations in physical forms and properties by utilizing the same set of processing parameters and conditions. The technique should consistently allow highly reproducible results to be achieved with ease (Leong et al., 2003).

6.3 Dispensing Method

The printing methodology provided by the three-axis SFF system presented in this research fulfills the requirements for scaffold construction as follows:

1) Processing conditions: The SFF system fabricates scaffolds by extruding PCL, which is prepared by adding PCL powder or pellets in acetic acid and agitating the mixture with a sonicator to dissolve. The processing procedures do not change the material properties and biocompatibility of the scaffold or cause any degradation in its mechanical properties.

2) Process accuracy: The SFF system is capable of three simultaneous translational movements along the X-, Y- and Z-axes, which have positioning accuracies of up to 4, 4, and 15µm respectively, and a minimum step resolution of 0.5µm. The SFF system is able to construct reproducible 3D scaffolds according to the precise specifications of the custom design, and has the capability to maintain accurate pore sizes of scaffolds to suit different TE applications.

3) Consistency: The SFF system is able to fabricate scaffolds with well-defined external and internal structures. As shown in Figure 6.6, the porous structures are uniform and consistent within the scaffold.

4) Repeatability: The SFF system and the printing process can provide good repeatability by applying the same sets of processing parameters and conditions. When the system has been well calibrated, it ensures the minimal variations in physical forms and features among different scaffolds.

In summary, the SFF system with the specific dispensing method showed well-defined internal and external structures, and demonstrated good repeatability by applying the same sets of processing parameters and conditions. Based on the requirements for scaffold fabrication described in the previous section, the SFF machine has shown the ability to maintain a high degree of accurate control over the physical and mechanical properties of the selected materials. The scaffold fabrication and material processing methods are potentially suitable for a variety of tissue engineering

applications. In general, the advantages of the manufacturing process demonstrated the potential of the SFF system in fabricating 3D scaffolds with precise and reproducible macro-pore architectures.

6.4 Machine Calibration Procedures

Once the 3D CAD models and the printing materials have been well defined and prepared per the requirements described in Chapters 4 and 5, the user can proceed with fabrication of the desired construct using the 3D SFF machine. Before operating the machine, some calibration procedures need to be conducted to ensure the achievement of high resolution printing.

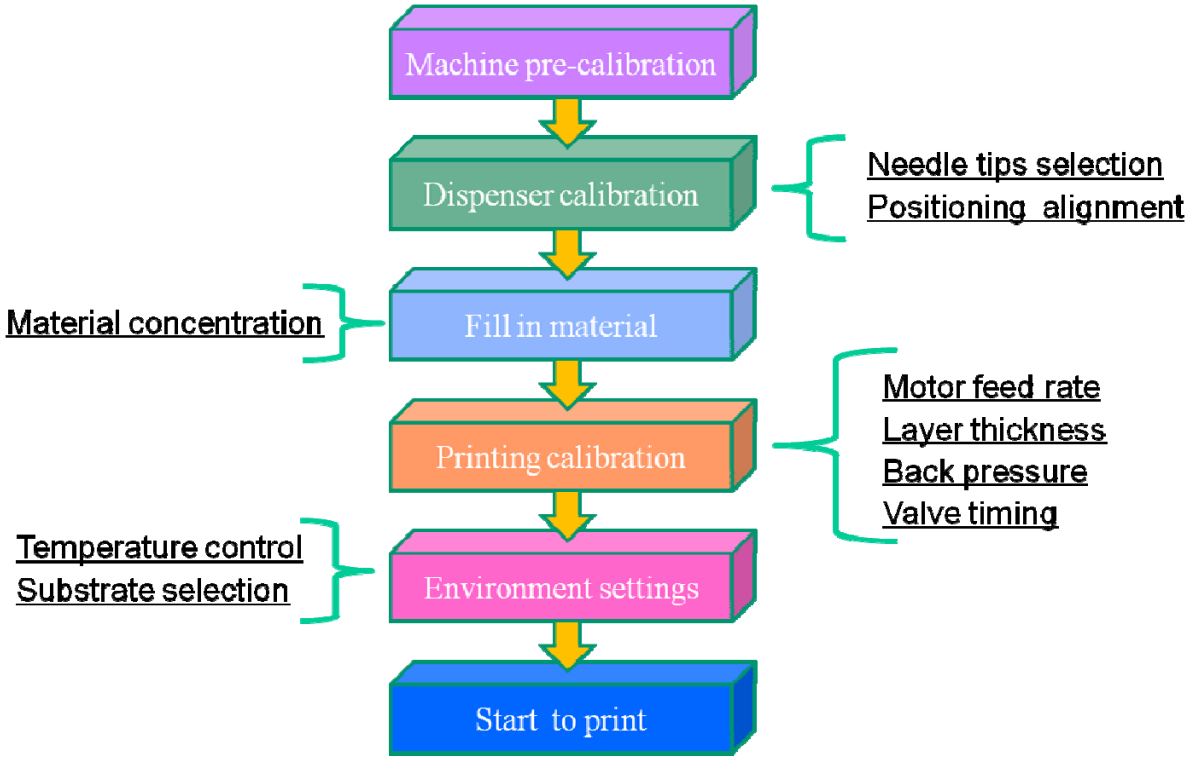

Figure 6.2: Flow chart of machine calibration procedures. The machine needs to be pre-calibration to ensure that the 3-axis moving is linear and smooth. The next step is calibration of the dispensers for needle tip selection and positioning alignment. Then the material is filled in the reservoir and necessary to be kept with a constant temperature environment around 35 ˚C and away from open space. The next step is to calibrate the printing volume by adjusting key parameters. When these key parameters have been well tuned, and the temperature control for the ambient environment has become stable, the 3D SFF machine is ready to fabricate.

As illustrated in Figure 6.2, the machine first needs to be pre-calibrated to ensure that the 3-axis moving is linear and smooth. Due to the limits of displacement of each axis, the origin should be set precisely based on the dimension of the CAD model. The next step is calibration of the dispensers, which includes needle tip selection and positioning alignment. In order to print fine filaments and avoid clogging, a proper tip size needs to be selected based on the printing material concentration and its viscosity.

The positioning alignment for multiple printing dispensers has played an important role for heterogeneous printing. In other words, the quality of the alignment method would affect the printing resolution and accuracy.

After dispenser calibration, the reservoir is filled with the printing material. As we have seen with the PCL solution as an example, we still need to consider the need for preventing the material properties from being altered in different temperature environments. It is necessary to keep the material in the reservoir and in the dispensers' chamber with a constant temperature environment around 35 ˚C and away from open space.

The next step is to set up the machine to deliver the material at a specified constant printing volume by executing the calibration of motor feed rate, layer thickness, back pressure, and the valve timing. When these key parameters have been well tuned, and the temperature control for the ambient environment as well as the material has become stable, the 3D SFF machine is ready to fabricate the specified construct on a selected substrate.

6.5 Experimental Results

6.5.1 Homogeneous Material Printing

The variable setting of the six selected key factors for cylinder and strut variable analysis was listed in Table 6.1, including motor feed rate, APF layer thickness, material concentration, inner diameter of the needle tip, back pressure of the reservoir, and the valve controller timing setup. The printed samples based on the different sets of processing parameters are shown in Figure 6.3. According to observation, the valve controller timing setup and layer thickness are the two parameters that have the greatest effect on the printing results, in particular the smoothness of the structure. A less important factor in our applications is the back pressure of the reservoir because the flow of high viscosity materials is mostly dependent on the extrusion force, in contrast to the flow of low viscosity materials which is sensitive to back pressure.

The macroscopic views of struts with different sets of processing parameters are shown in Figure 6.4, 6.5, 6.6, and 6.7. A printed strut with two different colored materials to form a heterogeneous structure is shown in Figure 6.8. These printing results illustrate the significance of the key parameters that can affect the smoothness and intactness of the printed structures. By carefully adjusting each of these processing parameters, this SFF machine should be able to produce scaffolds with well-defined and highly consistent structures.

Table 6.1: System control parameters (set up with the spindle speed in the APT file kept constant at 500 rpm and the active frequency of MACH3 nozzles kept constant at 6Hz).

Sample number	Model design	**Motor feed rate (mm/min)**	**APT layer thickness (mm)**	**Material concentration (w/w)**	**Inner diameter of the needle tip (µm)**	**Back pressure of the reservoir (psi)**	**Valve controller timing setup (sec)**
S1	Cylinder	90	0.15	40%	330	45	0.150
S2	Cylinder	90	0.15	40%	200	60	0.150
S3	Cylinder	150	0.1	40%	200	60	0.150
S4	Cylinder	150	0.1	40%	200	45	0.150
S5	Cylinder	90	0.15	42%	200	50	0.100
S6	Cylinder	90	0.20	42%	200	50	0.100
S7	Cylinder	90	0.15	42%	200	45	0.200
S8	Cylinder	90	0.15	42%	200	45	0.050
S9	Strut	90	0.2	42%	330	40	0.100
S10	Strut	90	0.05	42%	250	45	0.070
S11	Strut	90	0.1	42%	250	50	0.070
S12	Strut	90	0.2	42%	330	60	0.050
S13	Strut	90	0.08	42%	250	40	0.100
S14	Strut	90	0.1	42%	300	40	0.100
S15	Strut	90	0.05	42%	250	40	0.070
S16	Strut	90	0.08	42%	250	60	0.070
S17	Strut	90	0.08	42%	250	40	0.070
S18	Strut	90	0.08	42%	250	60	0.050
S19	Strut 3*3	90	0.08	42%	300	40	0.070
S20	Strut 3*3	120	0.08	42%	250	40	0.070

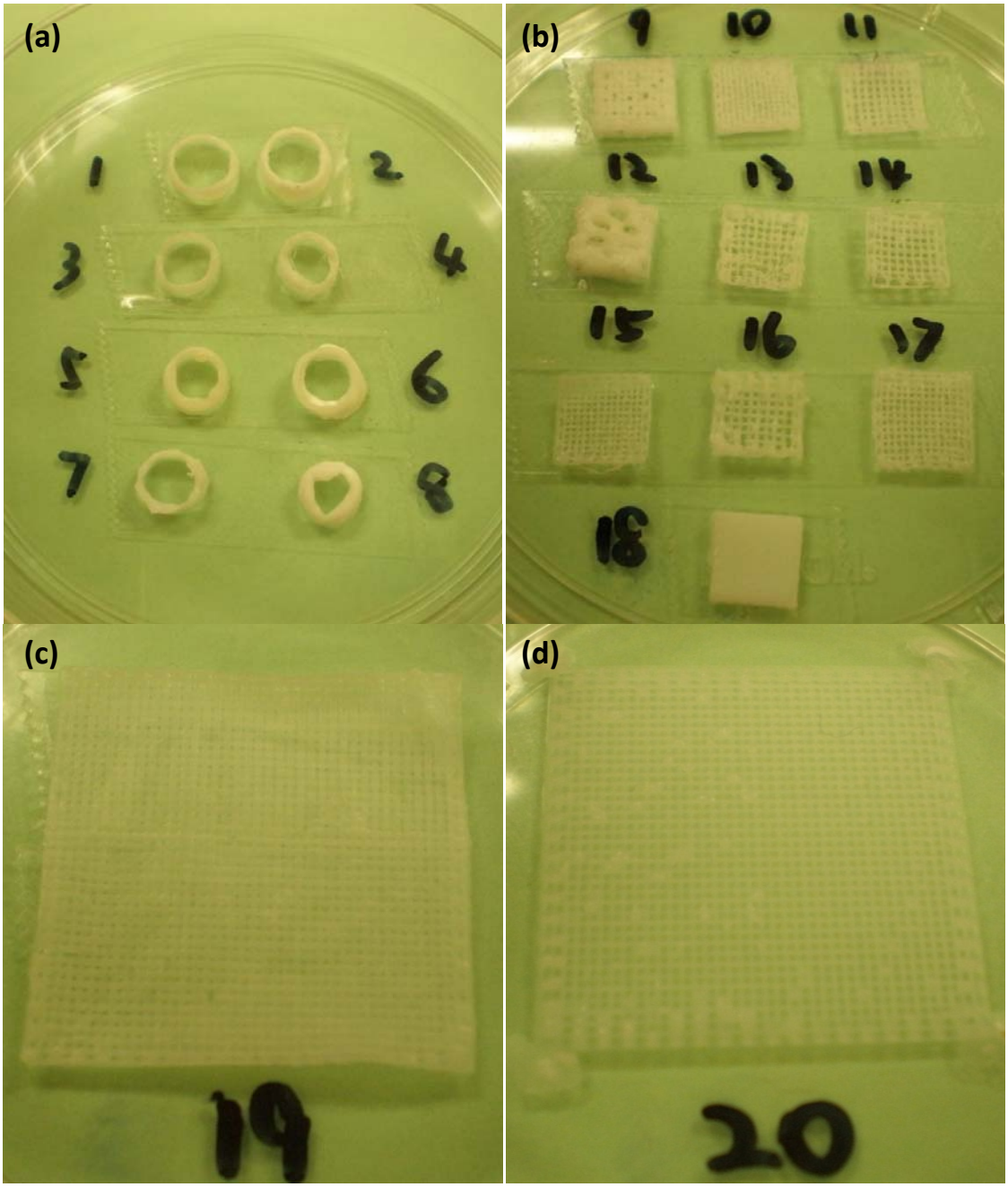

Figure 6.3: 3D constructs printed from PCL in various conformations: a) 8mm cylinders; b) 10mm x 10mm struts; c) 30mm x 30mm strut with 15 layers; d) 30mm x 30mm strut with 20 layers

Conclusions:

(1) As seen from S1 and S2, the required values for back pressure and needle tip inner diameter are interdependent, as the pressure caused by viscous flow in the needle tip is significant compared to the flow pressure supply provided by the pressure regulator; with the same layer thickness, a larger needle inner diameter allows the formation of a thinner single wall cylinder.

(2) Comparing S3 and S4 with S1 and S2, when the feed rate increases, the needle moves faster and the material extrusion at the same speed. Therefore, S3 and S4 have defects on some single points because of lacking material, and the defects can be enlarged when layer increases. In S4, the defects happened from the 4^{th} layer and the collapse situation started from 10^{th} layer.

(3) Comparing S5 and S2, the model layer thickness is also important and dependent on the material concentration and flow back pressure. PCL will dry and form solid structure on each layer, if the settings for layer thickness is not high enough, the needle will touch and scratch the printed layers, and extra material will coming and stock on some points because of the surface tension, which is shown in S5, a big PCL ball hanging on the cylinder wall.

(4) Between S5 and S6, the sample made with higher viscosity PCL formed a thicker single wall cylinder since higher viscosity material dries much faster.

(5) S7 used a larger controller setup time, and S8 used a smaller one. When the controller setup time decreases, the EFD nozzle inner extrusion stroke moves faster. Based on the theory of boundary layer of viscous flow, the Navier-Stokes equation (6.1) is:

$$\rho\left(\frac{\partial \mathbf{v}}{\partial t}+\mathbf{v}\cdot\nabla\mathbf{v}\right)=-\nabla p+\mu\nabla^2\mathbf{v}+\mathbf{f}. \quad (6.1)$$

where $\mathbf{v}$ is the flow velocity, ρ is the fluid density, p is the pressure, μ is the fluid viscosity, $\nabla\mathbf{v}$ is the stress tensor, and $\mathbf{f}$ represents body forces (per unit volume) acting on the fluid.

As long as the controller setup time and the MACH3 configuration frequency are constant, then the velocity is a constant. According to the equation, it is reasonable to assume that the density of the material is a constant during the printing procedure, and the other forces are not changing with time, so the pressure gradient ∇p is related to velocity field. In this condition, the boundary layer velocity is driven by the inner extrusion stroke in the EFD 741MD valve, so the speed of the valve movement determines the pressure gradient.

As the boundary layer velocity increases, the pressure gradient also increases because the viscosity of 40%~42% PCL is very high. So the controller setup time can

control the extrusion material significantly. Compare S8 to S1, the material is much thicker when setup time in controller changes from 0.150s to 0.050s.

(6) S9 and S12 have the same CAD model, but S12 has lower controller setup time and back pressure. The result shows that the smaller controller setup time plays most significant role in material extrusion, and the thicker PCL dries and lines stick to each other.

(7) As shown in Table 6.1 (S10, S11 and S15~17), continuous PCL lines can be formed from 42% PCL-acetic acid when the controller setup time is 0.070s.

(8) Comparing S13 and S17, where only the controller setup time is different, and also comparing S16 and S17, where only the value of back pressure is different, we can conclude that within a certain range of controller setup time, the final result does not vary detectably with back pressure between the values of 40psi and 60psi.

(9) Comparing S15 and S17, the line width and line space in each layer are the same, but S15 cannot be built up to 1mm because the strength is not high enough to hold upper layers. Nevertheless, this condition has the advantage that the thin PCL lines can stay straight on the previous lines without collapsing, because thinner PCL lines take less time to become solid polymer lines.

(10) S18 has the same CAD model as S10, but S18 PCL lines merge with each other and become a whole piece of block with a tiny mesh track on surface. The result also shows that the controller setup time is the most important factor in printing high viscous PCL-acetic acid solution.

(11) Material solidification time is very important in building 3D structure, but shorter solidification time is not always better. The difference between S19 and S20 is the feed rate, and inner diameter of the tip; the feed rate determines the total time required for printing one layer. S19 has longer printing time, so each layer is solidified by the time the next layer starts being printed. So the bottom layer of S19 did not adhere to the substrate very tightly and the PCL detached at corners. S20 has faster moving speed and the base layer adhered well to the substrate, allowing for greater stability in building a 3D structure.

To sum up, the inner diameter of the needle tip determines the line width, and higher minimum back pressure is required to extrude material from thinner tips, for which the original CAD model needs to be sliced into thinner layers. The material concentration decides solidification time; within the range of concentrations we tested, 42% PCL-acetic acid solution was optimal for printing 3D structures, and short solidification time significantly reduced the viscous liquid collapse. The EFD controller setup time is the most important factor to determine the extrusion volume, as inferred from the viscous fluid Navier-Stokes equation which states that the pressure derived

from the laminar fluid layer velocity is much higher compared to the flow back pressure, so the extrusion volume will be mainly determined by the viscous fluid pressure.

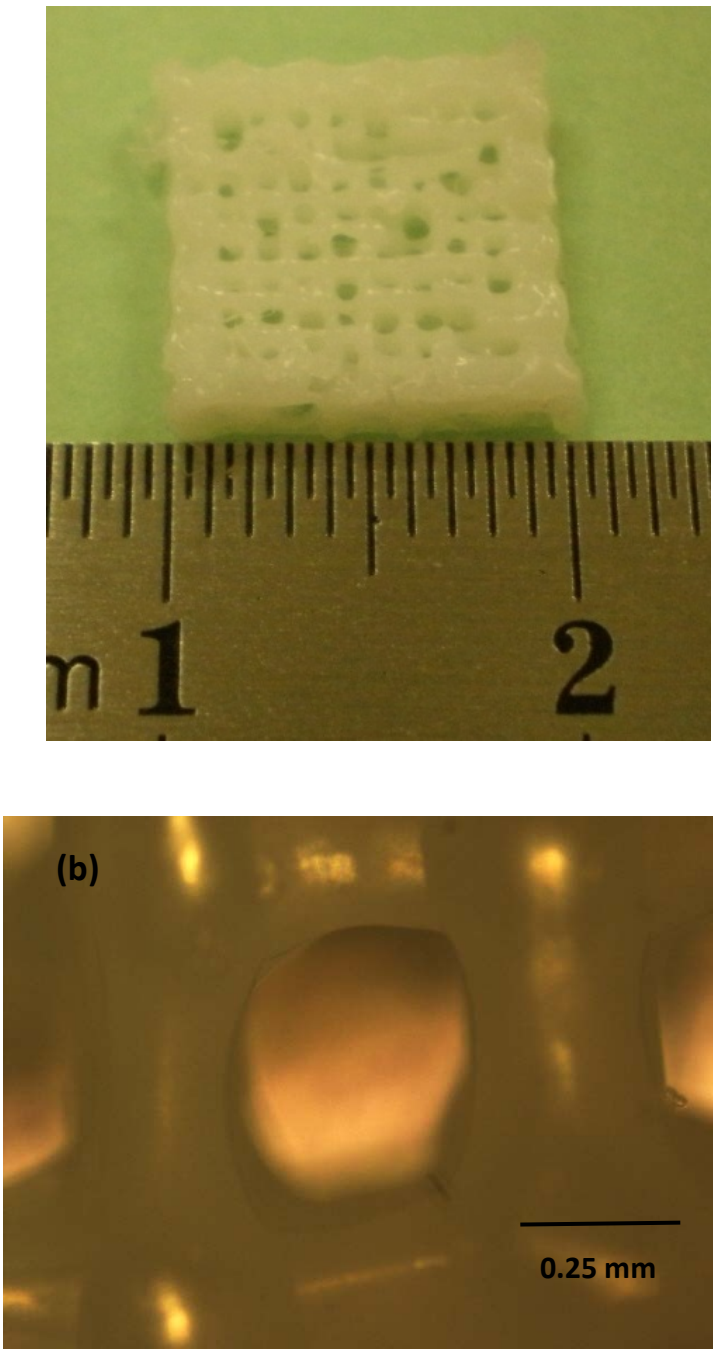

Figure 6.4: a) macroscopic view of 10mm x 10mm strut (S9); b) digital micrograph showing the detail of the line structure

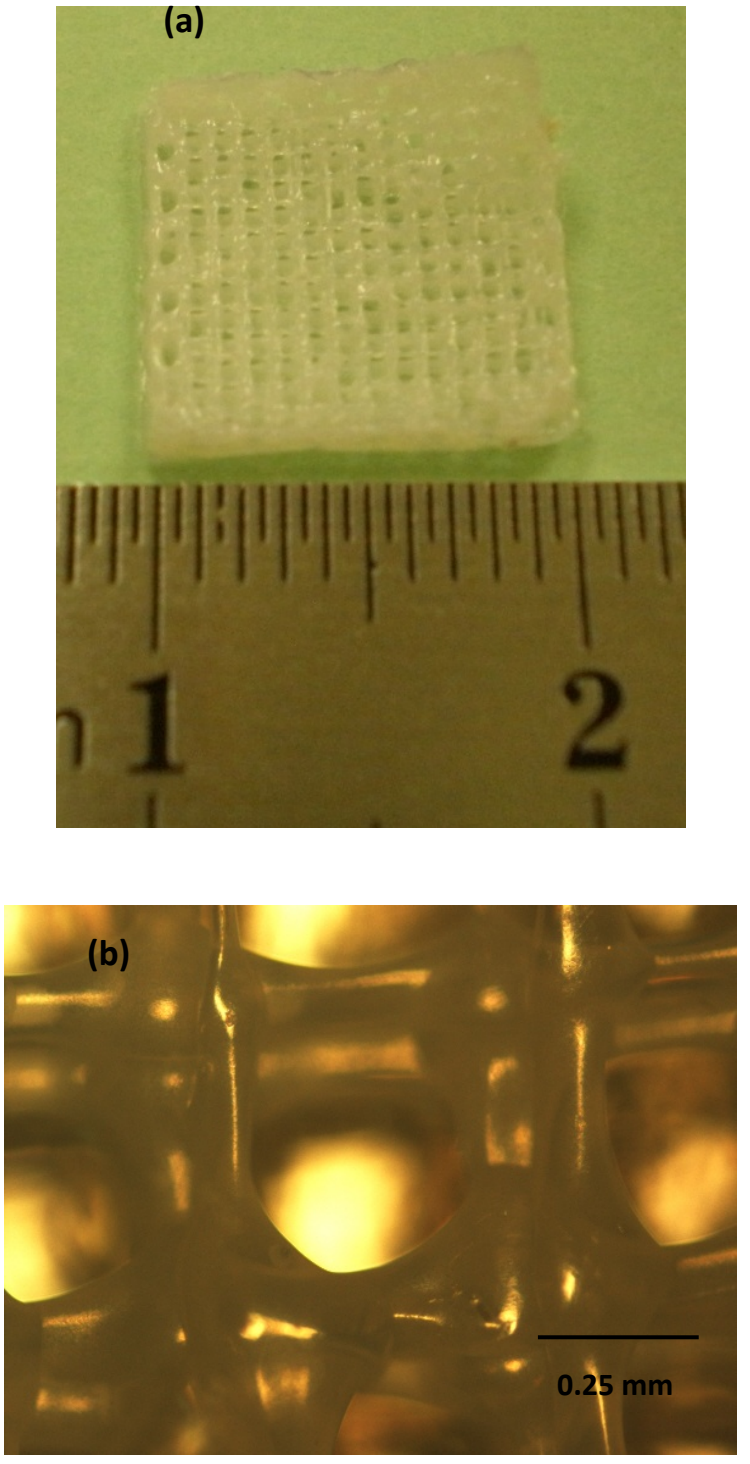

Figure 6.5: a) macroscopic view of 10mm x 10mm strut (S10); b) digital micrograph showing the detail of the line structure

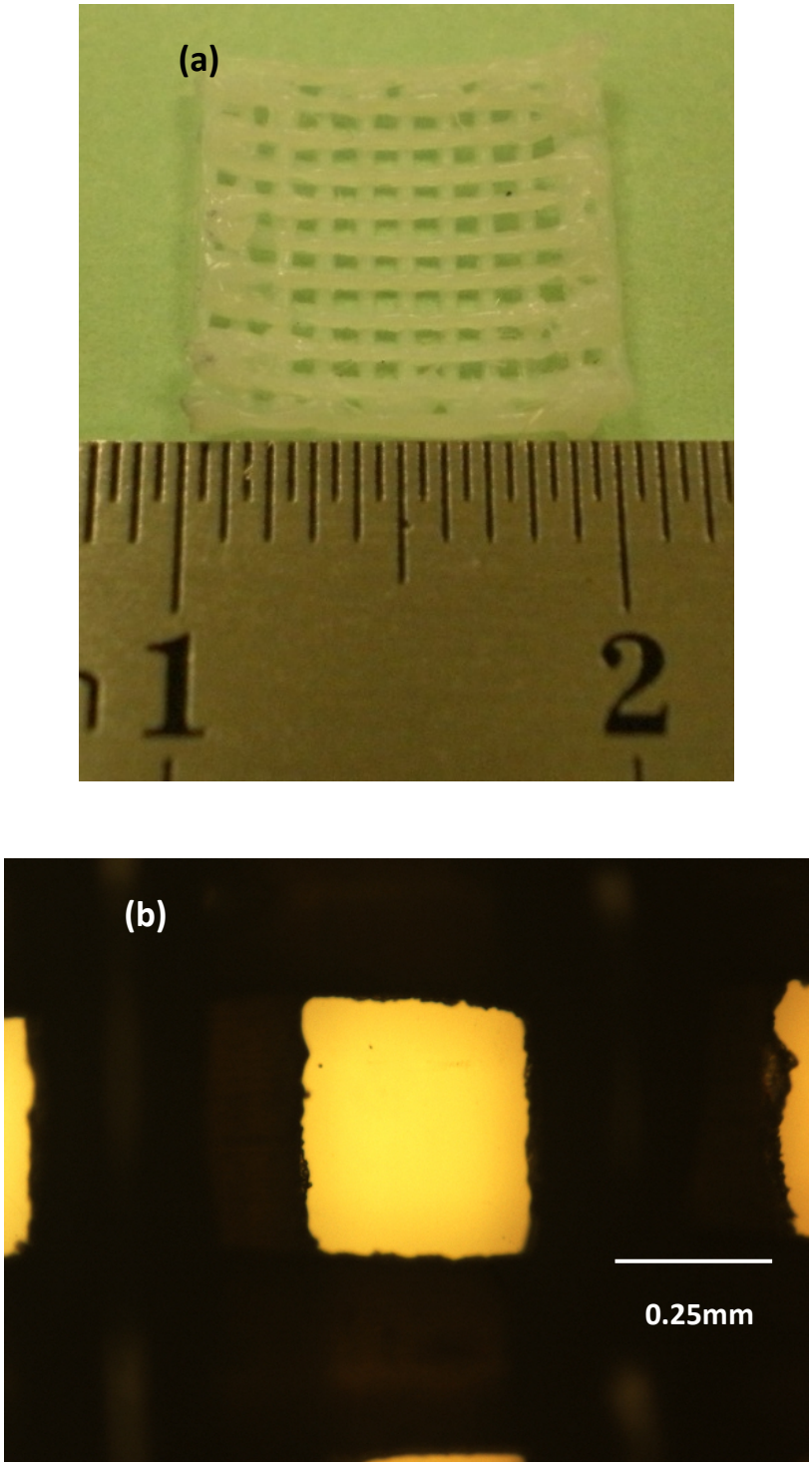

Figure 6.6: a) macroscopic view of 10mm x 10mm strut (S11); b) digital micrograph showing the detail of the line structure

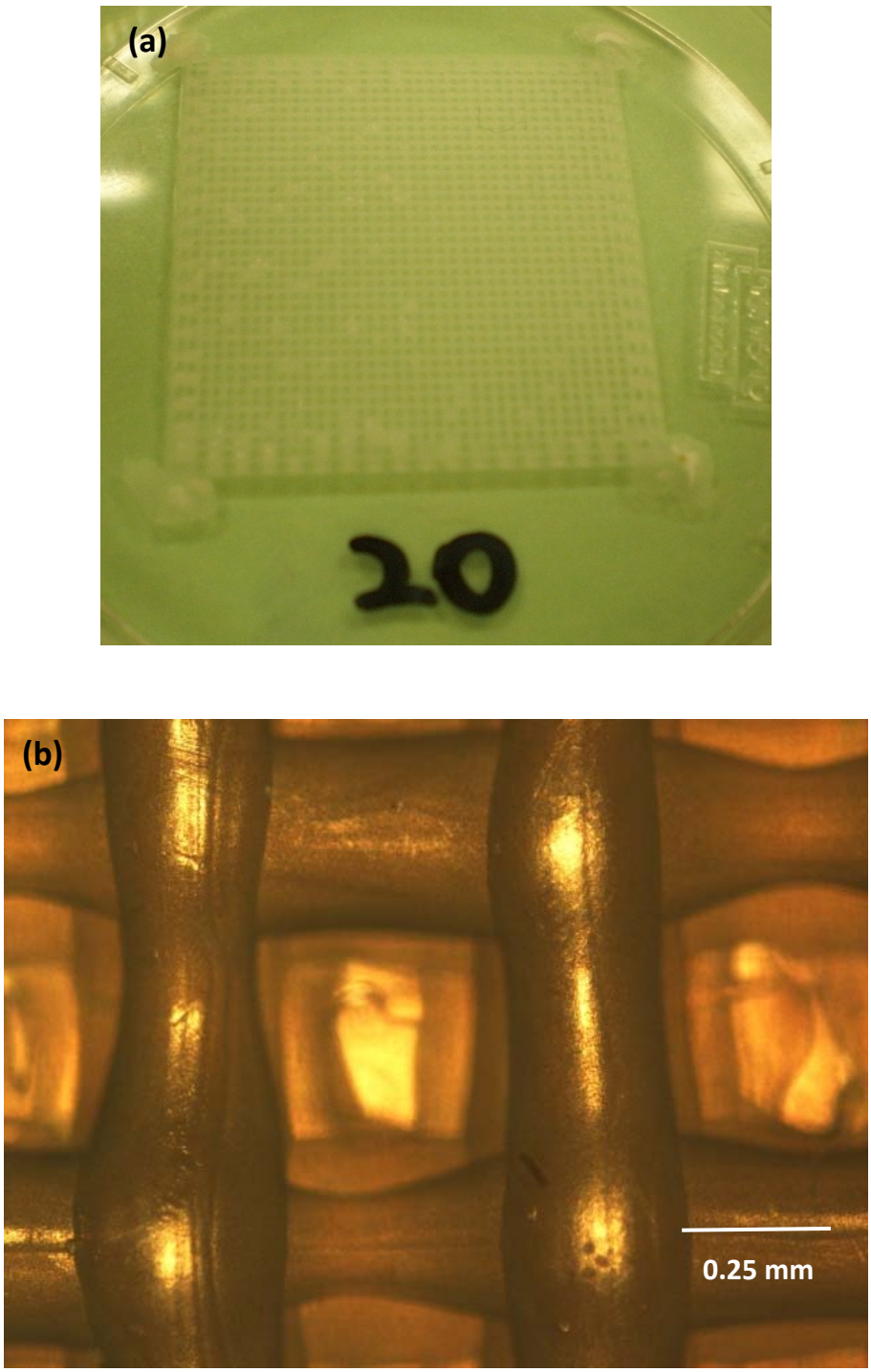

Figure 6.7: a) macroscopic view of 30mm x 30mm strut (S20); b) digital micrograph showing the detail of the line structure

6.5.2 Heterogeneous Material Printing

This section provides examples to show the capability of heterogeneous material printing with two independent printing nozzles. The first strut, shown in Figure 6.8, was printed with 10 layers. Each layer was completely printed by one nozzle with colored PCL solution. The second strut, shown in Figure 6.9, was printed with 6 layers. Each layer was sequentially printed by two nozzles with two colored PCL solutions.

The strut structure shown in Figure 6.8 has dimensions 20mm x 20mm x 1mm. The model was sliced into 10 layers and printed by two nozzles with 300 µm needle tips, using the heterogeneous printing algorithm. The gap between each adjacent filament is around 200 µm and the structure forms as uniform 0˚/ 90˚ filament orientation. One nozzle was filled with a 42% PCL solution with green food coloring and the other was filled with a 43% PCL solution with yellow food coloring. All key parameter settings for printing the heterogeneous strut with two EFD dispensers are shown in Table 6.2.

Table 6.2: The key parameter settings for two EFD dispensers

Dispenser number	Model design	Motor feed rate (mm/min)	APT layer thickness (µm)	Material concentration (w/w)	Inner diameter of the needle tip (µm)	Back pressure to reservoir (psi)	Valve controller timing setup (sec)
1 (green)	Strut 20x20x1mm	120	100	42%	300	40	0.075
2 (yellow)				43%	300	40	0.15

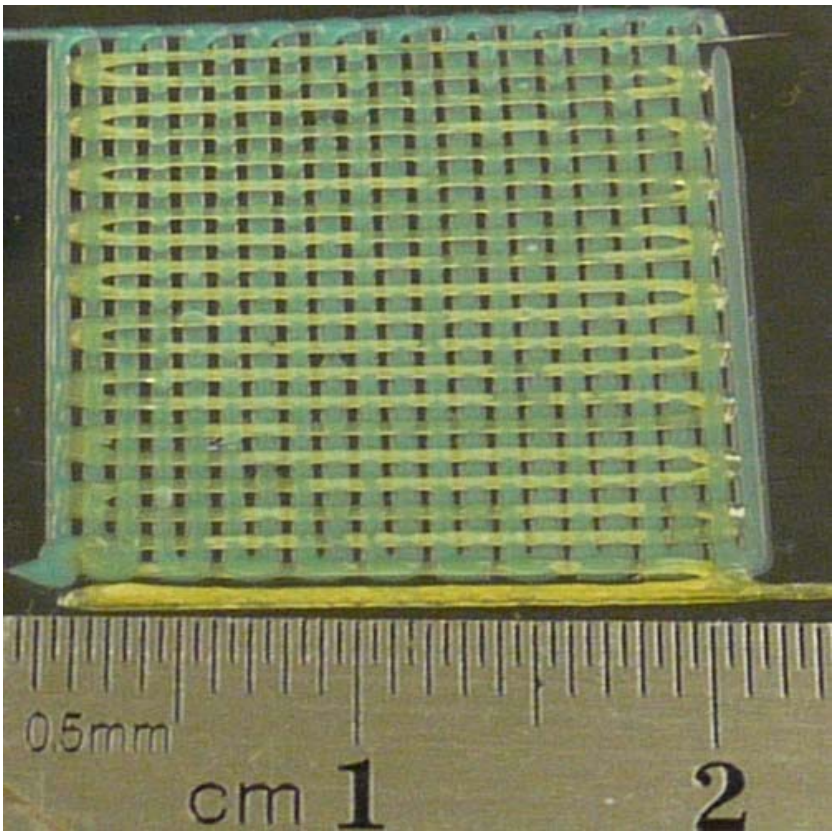

Figure 6.8: The strut was printed by two EFD dispensers using the heterogeneous printing algorithm. PCL solutions of 42% and 43% (w/w) concentrations with green and yellow food coloring were used to construct the structure. The structure has dimensions of 20 mm by 20 mm and consists of 10 layers, each layer being 100 µm in height.

The mixed strut structure shown in Figure 6.9 has dimensions 13 mm x 13 mm x 0.9 mm was printed by two nozzles with 200 µm needle tips, using the heterogeneous printing algorithm. Each layer has a thickness 150 µm and the structure is composed of 6 layers. The gap between each adjacent filament is around 200 µm. All key parameter settings for printing the mixed heterogeneous strut with two EFD dispensers are shown in Table 6.3. The first half of the strut (upper portion of the image) was printed using the first nozzle, with white PCL solution, and then the machine automatically switched to

the second nozzle to print the second half (lower portion of the image) with green PCL solution. For the second layer, the first nozzle printed the right half and then the second nozzle would arrive in position and carry on printing the left half. Likewise, the third layer reverted to the orientation of the first layer. With this method of perpendicular layering, the mixed heterogeneous strut was successfully fabricated using the 3D SFF machine with the novel heterogeneous algorithm.

Table 6.3: The key parameter settings for two EFD dispensers

Dispenser number	Model design	Motor feed rate (mm/min)	APT layer thickness (μm)	Material concentration (w/w)	Inner diameter of the needle tip (μm)	Back pressure to reservoir (psi)	Valve controller timing setup (sec)
1 (white)	Strut 13x13x0.9mm	140	150	38%	200	20	0.075
2 (green)				35%	200	20	0.15

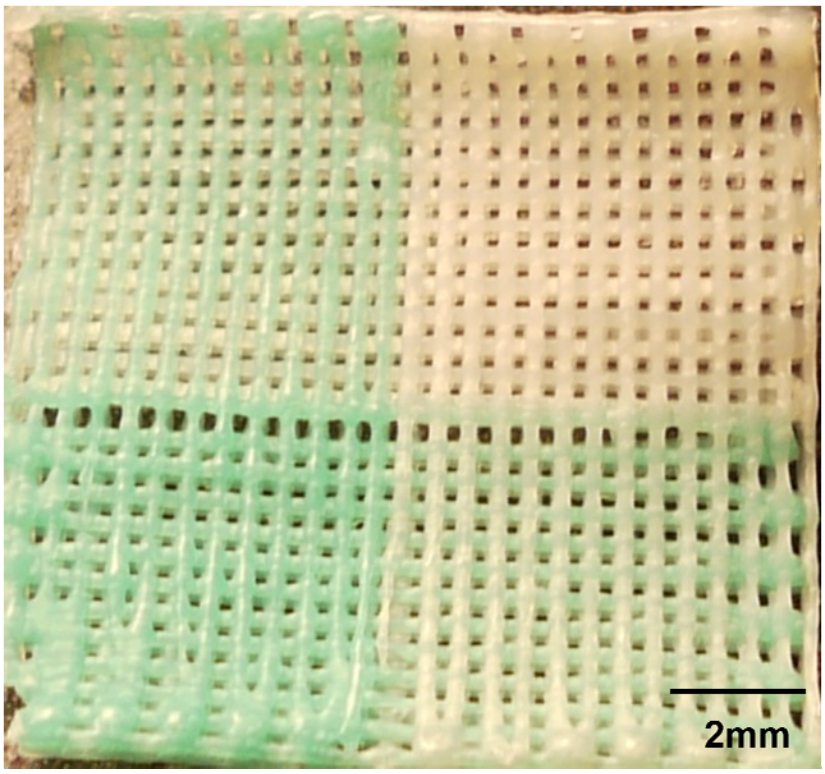

Figure 6.9: The mixed strut was printed by two EFD dispensers using the heterogeneous printing algorithm. PCL solutions of 38% and 35% (w/w) concentrations with original color (white) and green food coloring were used to construct the structure. The structure has dimensions of 13 mm by 13 mm and consists of 6 layers, each layer being 150 µm in height.

As evident from these two samples shown in Figures 6.8 and 6.9, the key parameter settings can significantly affect the printing results. As you can see, the first sample was printed under conditions of higher material concentration, larger tip size, and larger back pressure, but the resolution was not as good as that of the second sample. Compared to the second sample, the printing volume for the first sample was too high and the PCL solution could not solidify within a short time. Therefore, the structure showed a slight collapsing and liquid-like phase after 10 layers of printing.

Based on these observations, we suggest that in order to handle different materials successfully and accomplish high resolution 3D printing, the machine user should consider the guidelines below:

1. The printing material should solidify within a short time after printing. Thus, the material concentration and its viscosity must be well controlled.
2. The motor feed rate, back pressure, valve timing, and needle tip size are factors that affect the printing volume. It is important to tune these key parameters.
3. To avoid clogging of the material, the needle tip size should be carefully selected. When loading material into the nozzle chamber, the material properties should not undergo any modifications.
4. Temperature control for the ambient environment and for printing dispensers is essential.

CHAPTER 7 : CONCLUSIONS AND FUTURE WORK

7.1 Conclusions

The work in this thesis aimed to fulfill 3 specific aims as laid out in Chapter 1:

1. Develop a new multi-functional 3D printing system with high resolution for fabrication of bioactive tissue substitute structures.

2. Develop a novel RP processing algorithm for SFF of heterogeneous printing in the system.

3. Analyze and select specific parameters of this multi-functional 3D printing system for printing 3D structures using a range of model biomaterials.

Specific Aim 1 was approached by development of a new SFF-based manufacturing system for diversified biomaterial deposition. The nozzle system includes a multiple dispensing heads with dual-dispensing nozzles was carefully tested and installed into the printing system. The selected printing nozzle was then used to print different struts with various diameters and special designed 3D structures for verifying the performance of this fabrication system. The control source code module MACH3 was conducted to control the arms moving with high resolution and multiple dispenser extrusion for tissue construction. The most dominant factors and governing parameters for controlling the quality of the printed structures and scaffolds have been investigated. The operating

parameters are important in terms of depositing the proper amount of biomaterial to control the volume of the forming gel. 3D freeform scaffold fabrication was based on CAD processes, converted and extracted using slicing software. This involves obtaining the required geometric data for the scaffold in the form of a solid model from STL model. The extracted scaffold model was then sliced into consecutive 2D layers to generate appropriately formatted data to this rapid prototyping system to manufacture PCL scaffolds. This fabrication process demonstrates the ability to construct complex 3D structures from CAD design to emerging tissue engineering. The study has also developed an advanced computational algorithm for characterization of heterogeneous tissue scaffolds and composite structures.

Specific Aim 2 was fulfilled by developing a novel modeling method and a slicing method which can be employing in a current CAD processing environment to enable convenient printing of any hybrid or heterogeneous structures with complex geometries. Since the representation of heterogeneous structures has become a significant subject to describe a physical model in engineering; especially in human tissues, the composition of the human bones and organs is various in internal tissues, external surface and volumetric properties and geometries. A novel heterogeneous algorithm based on computer aided characterization approach has been developed to achieve reorganization of multiple models and printing with multiple materials in this study. The key processes of the heterogeneous modeling, characterization, and slicing

are detailed in Chapter 4. A MATLAB based, user friendly integrated software converts the theoretical heterogeneous algorithm into an executable application. This interface works as a platform to communicate with other applications and modify source files into a complete APT file for usage in MACH3.

Specific Aim 3 was achieved by conducting research in biomaterial properties and verifying the pore size and dimension of scaffolds. The designed structures with different pore sizes have significant impact related to different diameter of nozzle tips, applied pressure, and material properties. Through a series of experiments, the key dispensing parameters were identified as pressure, traveling speed, dispensing speed and a height increment of each layer. The values for these parameters, as well as material concentrations, were optimized to yield the best result. A standardized protocol for preparation of the manufacturing materials and the mechanical properties of each material were also drawn up to form proper 3D structures.

Testing and analysis of the properties of scaffolds built by our 3D SFF system were carried out. Macro-pore diameters of 300-500μm were observed which are suitable for cell growth into scaffolds. The stress-strain curves of PCL scaffolds indicated that these scaffolds should be considered for use in low load bearing applications.

In general, the SFF machine combining with heterogeneous printing capability provides much potential for the design and manufacturing of biomedical scaffolds. Rapid prototyping of scaffolds by this machine is presented using a biocompatible PCL gel. During the scaffold fabrication, high temperature is not required and with the multiple-dispenser feature, it allows fabrication with materials or material additives, which otherwise decompose under heat, as well as the incorporation of proteins and living cells. The high porosity of the resulting scaffolds can be obtained to facilitate good ventilation and cell growth.

7.2 Contributions

The proposed research and activities can help to develop knowledge and novel techniques in advanced system design for bioactive polymeric scaffolds in tissue engineering applications. My research has made the following contributions to the field of CAD based tissue engineering:

(1) A new custom designed printing machine with multi-nozzle, multi-material, and multi-function SFF system has been developed for direct microfluidic deposition to enable creation of a novel scaffold based tissue device. The deposition system is a very innovative and promising method for producing biodegradable and biocompatible scaffolds. The technique is very powerful and any desired structure can be created if the parameters are well defined.

(2) The key bio-printing process parameters were studied and identified to obtain desired 3D scaffolds or structures optimized from CAD system model design. By directly converting the CAD model information to generate the printing paths, the new direct fabrication method can enhance existing modern SFF technologies to fabricate tissue scaffolds and replacements with customized and complex architectural design.

(3) The study has also developed an advanced computational algorithm for characterization of heterogeneous tissue scaffolds and composite structures to achieve reorganization of multiple models and printing of multiple materials. The integrated software has been developed to link other application software and is able to modify and integrate source files to implement the heterogeneous algorithm in 3D fabrication.

7.3 Future Work and Recommendations

1. *In vitro* tests can be conducted to study the biocompatibility of 3D structures by evaluating the viability and proliferation of cells cultured within.

2. Modify the integrated software to utilize six printing nozzles for six-material heterogeneous printing purpose.

3. More complex structure design needs to be carried out in order to mimic the physical tissue models for the human body.

4. Incorporation of cell seeding into the 3D dispensing plotting materials.

5. The mechanical performance of the scaffolds fabricated by our SFF system should be investigated. The long term degradation test of porous scaffolds and *in vivo* degradation test should be carried out to understand the degradation behavior.

6. An FEA analysis on the scaffold to compute the effective elastic modulus would be beneficial. The failure analysis of the scaffolds should be done to validate and further understand the mechanical behavior of the porous scaffolds.

LIST OF REFERENCES

A. G. Mikos, A. J. Thorsen, L. A. Czerwonka, Y. Bao, R. Langer, D. N. Winslow, and J. P. Vacanti, "Preparation and Characterization of Poly(LLactic Acid) Foams," *Polymer*, vol. 35, pp. 1068-1077, 1994.

A. K. Elissee J, Sims D, McIntosh W, Randolph M, Langer R, "Transdermal photopolymerization for minimally invasive implantation," *Proc Natl Acad Sci USA*, vol. 6, pp. 3104-7, 1999.

A. M. Lowman, M. Morishita, M. Kajita, T. Nagai, and N. A. Peppas, "Oral delivery of insulin using pH-responsive complexation gels," *Journal of Pharmaceutical Sciences*, vol. 88, pp. 933 937, 1999.

Amsden, B.G., et al., *Methacrylated Glycol Chitosan as a Photopolymerizable Biomaterial.* Biomacromolecules, 2007. **8**(12): p. 3758-3766.

Ang, T.H. et al., Fabrication of 3D chitosan-hydroxyapatite scaffolds using a robotic dispensing system. Mater. Sci. Eng. C 2002, 20, 35–42

Arpan Biswas, V.S., Igor Tsukanov, *Heterogeneous Material Modeling with Distance Fields.* Computer Aided Geometric Design, 2004. **21**(3): p. 215-242.

Athanasiou KA, Zhu L, Wang X. 2000. *Tissue Engineering* 6: 361-81

B. D. Ratner, Hoffman, A. S., Schoen, F. J., Lemons J. E. Ed, *Biomaterials*
Bacakova, L. et al. “Cell adhesion on artificial materials for tissue engineering”, Physiol. 2004, Res. 53, S35–S45

Banfi, A., et al., *Proliferation kinetics and differentiation potential of ex vivo expanded human bone marrow stromal cells: Implications for their use in cell therapy.* Experimental Hematology, 2000. **28**(6): p. 707-715.

Bendsoe, M., and Kikuchi, N., 1988, ‘‘Generating Optimal Topologies in Structural Design Using a Homogenization Method,’’ Comput. Methods Appl. Mech. Eng., 71, pp. 197–224.

Bhattarai, N., et al., *PEG-grafted chitosan as an injectable thermosensitive hydrogel for sustained protein release.* Journal of Controlled Release, 2005. **103**(3): p. 609-624.

Bignon, A. et al., Effect of micro- and macroporosity of bone substitutes on their mechanical properties and cellular response. J. Mater. Sci. Mater. Med. 2003, 14, 1089–1097

Bock RG, Goode AJ, Novartis F. 2003. *Tissue engineering of cartilage and bone*: John Wiley and Sons. 133-47

C. J. R. Muzzarelli, G. W. Gooday, presented at Proceedings of the third international conference on chitin and chitosan, Senigallia, Italy, 1985.

C. K. Kuo and P. X. Ma, "Ionically crosslinked alginate hydrogels as scaffolds for tissue engineering: Part 1. Structure, gelation rate and mechanical properties," *Biomaterials*, vol. 22, pp. 511-521, 2001.

C. L. Liew, K.F.L., C. K. Chua and Z. Du, *Dual Material Rapid Prototyping Techniques for the Development of Biomedical Devices. Part 1: Space Creation.* Int J Adv Manuf Technol, 2001. **18**: p. 717-723.

Carrier, R.L. et al., Cardiac tissue engineering: cell seeding, cultivation parameters, and tissue construct characterization. Biotechnol. Bioeng. 1999, 64, 580–589
Cell Transplant 11(5):489–494.

Chapekar SM. 2000. *Journal of Biomedical Materials Research* 53: 617-20

Chen F.C. Spontaneous phase separation for efficient polymer solar cells, SPIE Newsroom, DOI: 10.1117/2.1200805.1149, 2008

Cherkaev, A., 1994, ‘‘Relaxation of Problems of Optimal Structural Design,’’ Int. J. Solids Struct., 31, No. 16, pp. 2251–2280.

Chu TM, Orton DG, Hollister SH, Feinberg SE, Halloran JW. 2002. *Biomaterials* 23: 1283-93

Cima MJ, Sachs E, Cima LG, Yoo J, Khanuja S, Borland SW, Wu BM, Giordano RA. Computer-derived microstructure by 3D printing: bio- and structural materials. Proceedings of the SFF symposium, 1994.

Cuckler MJ. 2004. *The Journal of Arthroplasty* 19 56-8

Cutter CS, Babak JM. 2006. *Journal of Long-Term Effects of Medical Implants* 16: 249-60

D. W. Hutmacher, M. Sittinger and M. V. Risbud, Trends Biotechnol., 2004, 22, 354.

Dalton, B.A. et al., Modulation of corneal epithelial stratification by polymer surface topography. J. Biomed. Mater. Res. 1999, 45, 384–394

Despina D. Deligiannil, Nikoleta D. Katsalal, Petros G. Koutsoukos, Yiannis F. Missirlis, “Effect of surface roughness of hydroxyapatite on human bone marrow cell adhesion, proliferation, differentiation and detachment strength” Biomaterials 2001, 22:1, 87

Dutta, V.K.a.D., *An Approach to Modeling & Representation of Heterogeneous Objects.* Journal of Mechanical Design 1998. **120**(4): p. 659-668.

E. R. Welsh, C. L. Schauer, S. B. Qadri, and R. R. Price, "Chitosan crosslinking with a water-soluble, blocked diisocyinate. 1. Solid state," *Biomacromolecules*, vol. 3, pp. 1370-1374, 2002.

Emma Cinibulk , P.O., An examination of the bioprinting process and its variations 2008.

F. L. Mi, C. Y. Kuan, S. S. Shyu, S. T. Lee, and S. F. Chang, "The study of gelation kinetics and chain-relaxation properties of glutaraldehyde-crosslinked chitosan gel and their effects on microspheres preparation and drug release," *Carbohydrate Polymers*, vol. 41, pp. 389-396, 2000.

Fambri L, Migliaresi C, Kesenci K, Piskin E. In *Integrated Biomaterials Science*, ed. R Barbucci. New York: Klumer Academic/Plenum Publishers, 2002

Fedorovich NE, Alblas J, de Wijn JR, Hennink WE, Verbout AJ, Dhert WJ. Hydrogels as extracellular matrices for skeletal tissue engineering: State-of-the-art and novel application in organ printing. Tissue Eng 2007, 13(8):1905–1925.

Freed, L.E. et al., Tissue engineering of cartilage in space. Proc. Natl. Acad. Sci.1997, 94, 13885–90

Freyman TM, Yannas IV, Gibson LJ. 2001. *Progress in Materials Science* 46: 273-82

G. Vozzi, A. Previti, D. De Rossi, and A. Ahluwalia, "Microsyringe-based deposition of two-dimensional and three-dimensional polymer scaffolds with a well-defined geometry for application to tissue engineering," *Tissue Engineering*, vol. 8, pp. 1089-1098, 2002.

G. Vozzi, C. Flaim, A. Ahluwalia, and S. Bhatia, "Fabrication of PLGA scaffolds using soft lithography and microsyringe deposition," *Biomaterials*, vol. 24, pp. 2533-2540, 2003.

Geisler, C., et al., SOFT BIOMATERIAL STUDY FOR 3D TISSUE SCAFFOLD PRINTING. Proceedings of ASME 2010 International Manufacturing Science and Engineering Conference, 2010.

Geng L, Feng W, Hutmacher DW, Wong YS, Loh HT, Fuh JYH. 2005. *Rapid Prototyping Journal* 11: 90-7

Goldstein, A.S. et al., Effect of convection on osteoblastic cell growth and function in biodegradable polymer foam scaffolds. Biomaterials 2001, 22, 1279–88

Grellier, M., et al., *The effect of the co-immobilization of human osteoprogenitors and endothelial cells within alginate microspheres on mineralization in a bone defect.* Biomaterials, 2009. **30**(19): p. 3271-3278.

Griffith LG, Naughton G. Tissue engineering – current challenges and expanding opportunities. Science 2002;295:1009–14.

Griffith LG, Wu BM, Cima MJ, Chaignaud B, Vacanti JP. In vitro organogenesis of liver tissue. Ann NY Acad Sci 1997, 831: 382–97.

H. Liu, T. Maekawa, N. M. Patrikalakis, E. M. Sachs and W. Cho, Methods for feature-based design of heterogeneous solids, Computer-Aided Design, 2004, 36:12 1141-1159

Harris L.D., Kim B.S., Mooney D.J., "open pore biodegradable matrices formed with gas forming", Journal of biomedical material research, 1998, vol. 42, pp. 396-402.

Holy, C.E. et al., Engineering three-dimensional bone tissue in vitro using biodegradable scaffolds: investigating initial cell-seeding density and culture period. J. Biomed. Mater. Res. 2000, 51, 376–382

Huang W, Carlsen B, Wulur I, Rudkin G, Ishida K, Wu B, Yamaguchi DT, Miller TA. 2004. BMP-2 exerts differential effects on differentiation of rabbit bone marrow stromal cells grown in two-dimensional and three dimensional systems and is required for in vitro bone formation in a PLGA scaffold. Exp Cell Res 299(2):325–334.

Huang.Y.X, Ren.J, Chen.C, Ren.T.B, Zhou.X.Y. Preparation and Properties of Poly(lactide-co-glycolide) (PLGA)/Nano-Hydroxyapatite (NHA) Scaffolds by Thermally Induced Phase Separation and Rabbit MSCs Culture on Scaffolds. 2008, Journal Biomaterials Applications, 22, pp 409.

Hyun Goo Kang, So Yeon Kim, Young Moo Lee, "Novel porous gelatin scaffolds by overrun/particle leaching process for tissue engineering applications," Journal of Biomedical materials, vol. 79B, pp. 388-397, 2006

J. L. Drury and D. J. Mooney, "Hydrogels for tissue engineering: scaffold design variables and applications," *Biomaterials*, 2003, vol. 24, pp. 4337-4351.

Jacobs, P.F., Rapid Prototyping and Manufacturing: Fundamentals of Sterolithograpgy. SME, Dearborn, Michigan, 1992.

Jakab K et al., Tissue engineering by self-assembly of cells printed into topologically defined structures Tissue Eng. A 2008, 14, 413–21

Jeong, B. and A. Gutowska, *Lessons from nature: stimuli-responsive polymers and their biomedical applications.* Trends in Biotechnology, 2002. **20**(7): p. 305-311.

Jeong, B., Y.H. Bae, and S.W. Kim, Thermoreversible Gelation of PEG−PLGA−PEG Triblock Copolymer Aqueous Solutions. Macromolecules, 1999. 32(21): p. 7064-7069.

Juliano, R.L. Signal transduction by cell adhesion receptors and the cytoskeleton: functions of integrins, cadherins, selectins, and immunoglobulin-superfamily members. Annu.Rev.Pharmacol.Toxicol. 42. 283-323. 2002

K. Ono, Y. Saito, H. Yura, K. Ishikawa, A. Kurita, T. Akaike, and M. Ishihara, "Photocrosslinkable chitosan as a biological adhesive," *Journal of Biomedical Materials Research*, vol. 49, pp. 289-295, 2000.

K.F. Leong*, C.M.C., C.K. Chua, *Solid freeform fabrication of three-dimensional scaffolds for engineering replacement tissues and organs.* Biomaterials, 2003. **42**(13): p. 2363-2378.

Kelly BE. 2000. *Orthopedic Technology Review* 2: 28-34

Kim, B.S. et al., Optimizing seeding and culture methods to engineer smooth muscle tissue on biodegradable polymer matrices. Biotechnol. Bioeng. 1998, 57, 46–54
Klein CPAT, Dreissen A, A., De Groot K. 1983. *Journal of Biomedical Materials Research Symposium* 17

Koc, S.P.G.a.B., *Geometric algorithms for manufacturing of freeform multi-material objects using reconfigurable tools.* Int. J. Manufacturing Technology and Management, 2008. **14**(1/2): p. 145-173.

Kruth JP, Leu MC, Nakagawa T. “Progress in additive manufacturing and rapid prototyping” CIRP Annals-Manufacturing Technology 1998, 47:2, 525

Kumar V, D.D., *Approach to modeling and representation of heterogeneous objects.* J Mech Des Trans ASME, 1998. **120**: p. 659-667.

L. Becheran-Maron, C. Peniche, and W. Arguelles-Monal, "Study of the interpolyelectrolyte reaction between chitosan and alginate: influence of alginate composition and chitosan molecular weight," *International Journal of Biological Macromolecules*, vol. 34, pp. 127-133, 2004.

L. Geng, Y.S. Wong, D.W. Hutmacher, W. Feng, H.T. Loh. and J.Y.H. Fuh, Rapid Prototyping of 3D Scaffolds for Tissue Engineering Using a Four-Axis Multiple-Dispenser Robotic System, 2003

L. Ma, C. Y. Gao, Z. W. Mao, J. Zhou, J. C. Shen, X. Q. Hu, and C. M. Han, "Collagen/chitosan porous scaffolds with improved biostability for skin tissue engineering," *Biomaterials*, vol. 24, pp. 4833-4841, 2003.

L. R. Ma P.X., "Degradation, structure and properties of porous nonwoven poly(glycolic acid) scaffolds for tissue engineering," presented at MRS, Pittsburgh, 1995.

Lam.C.X.F, Mo.X.M, Teoh.S.H, Hutmacher.D.W. Scaffold development using 3D printing with a starch-based polymer (2002) Materials Science and Engineering, C20, pp 49-86

Landers R., A. Pfister, U. Hubner,H. John,R. Schmelzeisen, R. Mulhaupt. Fabrication of Soft Rissue Engineering Scaffolds by Means of Rapid Prototyping Techniques”, Journal of Materials Science 37, pp. 3107 – 3116. 2002

Lange AE, Bhavnani M. September/October 1994. *SAMPE Journal* 30

Lee.K.W, Wang.S, Fox.B.C, Ritman.E.L, Yaszemski.M.J, Lu.L. Poly (propylene fumarate) bone tissue engineering scaffold fabrication using stereolithography: Effects of resin formulations and Laser parameters (2007) Biomacromolecules, 8 (4), pp 1077-1084.

Leong.K.F, C.C.K., Sudarmadjia.N, Yeonga.W.Y., *Engineering functionally graded tissue engineering scaffolds* Journal of the mechanical behavior of biomedical materials, 2008. **1**: p. 140-152.

Li, Y. et al., Effects of filtration seeding on cell density, spatial distribution,and proliferationinnonwovenfibrousmatrices. Biotechnol. Prog. 2001, 17, 935–944

Lickorish D, Guana L, Davies J.E. A three-phase, fully resorbable, polyester/calcium phosphate scaffold for bone tissue engineering: Evolution of scaffold design (2007) Biomaterials, 28, pp 1495–1502.

Limpanuphap S, Derby B. 2002. *Journal of Materials Science: Materials in Medicine* 13: 1163-6

Lin Lu, Biomimetic porogen freeform fabrication and biopolymer injection methods for bone tissue scaffolds, 2007. Ph.D thesis at Drexel Univ.

Lin Lu, Q.Z., David Wootton, Peter I. Lelkes, Jack Zhou, *A novel sucrose porogen-based solid freeform fabrication system for bone scaffold manufacturing.* Rapid Prototyping Journal, 2009. **16**(5): p. pp.365 - 376.

Lin, L., *Electrospun Soy Protein-based Scaffolds for Skin Tissue Engineering and Wound Healing.* Drexel University, Ph.D Thesis, 2011.

M. C. Wake, C. W. Patrick, and A. G. Mikos, "Pore Morphology Effects on the Fibrovascular Tissue-Growth in Porous Polymer Substrates," *Cell Transplantation*, vol. 3, pp. 339-343, 1994.

M. Hara, A. Yamaki, and J. Miyake, "Noninvasive detachment of cells on cells," *Materials Science & Engineering C-Biomimetic and Supramolecular Systems*, vol. 17, pp. 107-112, 2001.

M. M. Stevens, H. F. Qanadilo, R. Langer, and V. P. Shastri, "A rapid-curing alginate gel system: utility in periosteum-derived cartilage tissue engineering," *Biomaterials*, vol. 25, pp. 887-894, 2004.

M. N. V. R. Kumar, "A review of chitin and chitosan applications," *Reactive & Functional Polymers*, vol. 46, pp. 1-27, 2000.

M. R. De Boisseson, M. Leonard, P. Hubert, P. Marchal, A. Stequert, C. Castel, E. Favre, and E. Dellacherie, "Physical alginate hydrogels based on hydrophobic or dual hydrophobic/ionic interactions: Bead formation, structure, and stability," *Journal of Colloid and Interface Science*, vol. 273, pp. 131-139, 2004.

Ma Z, Gao C, Gong Y, Shen J. 2005. Cartilage tissue engineering PLLA scaffold with surface immobilized collagen and basic fibroblast growth factor. Biomaterials 26(11):1253–1259.

Marga F, Neagu A, Kosztin I, Forgacs G. Developmental biology and tissue engineering. Birth Defects Res C Embryo Today 2007; 81:320–8.

Martin, I. et al., The role of bioreactors in tissue engineering. Trends Biotechnol. 2004, 22, 80–86

McDevitt, T.C., Angello, J.C., Whitney, M.L., Reinecke, H., Hauschka, S.D., Murry, C.E., & Stayton, P.S. (2002) In vitro generation of differentiated cardiac myofibers on micropatterned laminin surfaces. J.Biomed.Mater.Res. 60. 472-479.

Mrksich, M. & Whitesides, G.M., Using self-assembled monolayers to understand the interactions of man-made surfaces with proteins and cells. Annu.Rev.Biophys.Biomol.Struct. 1996, 25. 55-78.

Mrksich, M., Chen, C.S., Xia, Y., Dike, L.E., Ingber, D.E., & Whitesides, G.M. (1996) Controlling cell attachment on contoured surfaces with self-assembled monolayers of alkanethiolates on gold. Proc.Natl.Acad.Sci.U.S.A 93. 10775-10778.

N. K. Mongia, K. S. Anseth, and N. A. Peppas, "Mucoadhesive poly(vinyl alcohol) hydrogels produced by freezing/thawing processes: Applications in the development of wound healing systems," *Journal of Biomaterials Science-Polymer Edition*, vol. 7, pp. 1055-1064, 1996.
N.L.Porter, Fabrication of porous calcium polyphosphate implants by solid freeform fabrication. A solid of processing parameters and in vitro degradation characteristics.

Nair PNR, Luder HU, Maspero FA. , Ruffieux, K., Fischer JH, Schug J., 2004. β-TCP/PLGA open porous scaffolds for the prevention of alveolar bone loss after tooth extraction: Evaluation in a mini-pig model. European Cells and Materials Vol. 7. Suppl. 2, 47

Nam S.Y., Park T.G., “porous biodegradable polymetric scaffolds prepared by thermally induced phase separation”, Journal of biomedical material research, 1999, vol. 47, pp. 8-16.

Nastaran Zahir and Valerie M Weaver**.** Death in the third dimension: apoptosis regulation and tissue architecture, Current Opinion in Genetics & Development 2004, Vol 14:1, pp.71–80

Nguyen, K.T. and J.L. West, *Photopolymerizable hydrogels for tissue engineering applications.* Biomaterials, 2002. **23**(22): p. 4307-4314.

Norotte C, Marga F S, Niklason L E and Forgacs G 2009 Scaffold-free vascular tissue engineering using bioprinting Biomaterials 30, 5910–7

O. K. Draget KI, Smidsrod O, "Homogeneous alginate gels: a technical approach," *Carbohydrate Polymer*, vol. 14, pp. 159-178, 1991.

Özbolat, İbrahim T. and Koç, Bahattin, Multi-function based modeling of 3D heterogeneous wound scaffolds for improved wound healing, Computer-Aided Design & Applications, 2009, 8 (1). pp. 43-57

P. Linez-Bataillon, F. Monchau, M. Bigerelle, H.F. Hildebrand, “In vitro MC3T3 osteoblast adhesion with respect to surface roughness of Ti6Al4V substrates” Biomolecular eng 2002, 19:2-6, 133

P. X. Ma and R. Y. Zhang, "Synthetic nano-scale fibrous extracellular matrix," *Journal of Biomedical Materials Research*, vol. 46, pp. 60-72, 1999.

Pierre Mainil-Varlet, Raymond Curtis, Sylwester Gogolewski, “Effect ofin vivo andin vitro degradation on molecular and mechanical properties of various low-molecular-weight polylactides” Journal of biomedical materials research 1997, 36:3 pp360

Pinghai Yang, X.Q., *A B-spline-based approach to heterogeneous objects design and analysis.* Computer-Aided Design, 2006. **39**: p. 95-111.

Porter N, Pilliar R, Grynpas. 2001. *Journal of Biomedical Materials Research* 56: 504-15

Qi, X., J. Ye, and Y. Wang, *Alginate/poly (lactic-co-glycolic acid)/calcium phosphate cement scaffold with oriented pore structure for bone tissue engineering.* Journal of Biomedical Materials Research Part A, 2009. **89A**(4): p. 980-987.

R. A. Jain, "The manufacturing techniques of various drug loaded biodegradable poly(lactide-co-glycolide) (PLGA) devices," *Biomaterials*, vol. 21, pp. 2475-2490, 2000.

R. A. Kandel, R. Pilliar and M. Grynpas, "Biphasic constructs for cartilage repair," European Cells and Materials, vol. 13, pp. 10, 2007.

R. Langer and J. P. Vacanti, "Tissue Engineering," Science, vol. 260, pp. 920-926, 1993.

Rajagopalan, S., Goldman, R., Shin, K. H., Kumar, V., Cutkosky, M., and Dutta, D., 2001, ‘‘Representation of Heterogeneous Objects During Design, Processing and Freeform-Fabrication,’’ Mater. Des., 22, No. 3, pp. 185–197.

Ranucci, C.S. et al., Control of hepatocyte function on collagen foams: sizing matrix pores for selective induction of 2D and 3D morphogenesis. Biomaterials 2000, 21, 783–793

S. J. Hollister, Nat. Mater., 2005. 4, 518.

S. Khalil, J.N.a.W.S., *Multi-nozzle deposition for construction of 3D biopolymer tissue scaffolds.* Rapid Prototyping Journal, 2005. **11**(1): p. 9-17.

S. Pandi Gurusamy, B.K., *Geometric algorithms for manufacturing of freeform multi-material objects using reconfigurable tools.* Int. J. Manufacturing Technology and Management, 2008. **14**: p. 145-173.

Sakai, Y. et al., A novel poly-L-lactic acid scaffold that possesses a macroporous structure and a branching/joining three-dimensional flow channel network: its fabrication and application to perfusion culture of human hepatoma Hep G2 cells. Mater. Sci. Eng. C 2004, 24, 379–386

Santos EC , Shiomi M, Oaskada K, Laoui T, "Rapid Manufacturing of metal components by laser forming" Int. Journal of Machine tools and manufacture 2006, 46:12-13 pp1459-68

Science: An Introduction to Materials In Medicine. San Diego: Academic Press, 1996.

Sinha, V.R., et al., *Poly-[epsilon]-caprolactone microspheres and nanospheres: an overview.* International Journal of Pharmaceutics, 2004. **278**(1): p. 1-23

Siu Y.K, and Tan S.T. Modeling the material grading and structures of heterogeneous objects for layered manufacturing, Computer-Aided Design, 2002, 34:10 705-716

Sodian R. 2000. *ASAIO Journal* 46: 238

Starly B, Fang Z, Sun W, Regli W., *Journal of Computer-Aided Design and Application* 2005, 2, 431-8

Steer DL, Nigam SK. Developmental approaches to kidney tissue engineering. Am J Physiol Renal Physiol 2004;286:F1–7

Sultana.N, Min Wang. Fabrication of HA/PHBV composite scaffolds through the emulsion freezing/freeze-drying process and characterization of the scaffolds 2008, Journal Material Sci., 19, pp 2555-2561

Sun W, Lal P. Recent development on computer aided tissue engineering—a review. Comput Methods Programs Biomed 2002; 67:85–103.

Taboas JM, Maddox RD, Krebsbach PH, Hollister SJ. 2003. *Biomaterials* 24: 181-94

Tomihata, K “In vitro and in vivo degradation of films of chitin and its deacetylated derivatives” Biomaterials 1997, 18:7 pp567

Tsang VL, Bhatia SN. 2004. Three-dimensional tissue fabrication. Adv Drug Deliv Rev 56(11):1635–1647.

Turco, G., et al., *Alginate/Hydroxyapatite Biocomposite For Bone Ingrowth: A Trabecular Structure With High And Isotropic Connectivity.* Biomacromolecules, 2009. **10**(6): p. 1575-1583.

Uematsu K, Hattori K, Ishimoto Y, Yamauchi J, Habata T, Takakura Y, Ohgushi H, Fukuchi T, Sato M. 2005. Cartilage regeneration using mesenchymal stem cells and a three-dimensional poly-lactic-glycolic acid (PLGA) scaffold. Biomaterials 26(20):4273–4279.

Ushida T, Furukawa K, Toita K, Tateishi T. 2002. Three-dimensional seeding of chondrocytes encapsulated in collagen gel into PLLA scaffolds.

V. Maquet and R. Jerome, "Design of macroporous biodegradable polymer scaffolds for cell transplantation," *Porous Materials for Tissue Engineering*, vol. 250, pp. 15-42, 1997.

Vikas Gupta1, K.S.K., Puneet Tandon3, *Computer Aided Design Modeling for Heterogeneous Objects.* International Journal of Computer Science, 2010. **7**(2): p. 31-38.

Vladimir Mironov, Richard P. Visconti, Vladimir Kasyanov, Gabor Forgacs, Christopher J. Drake, Roger R. Markwald, Organ printing: Tissue spheroids as building blocks, Biomaterials 2009, 30:2164-74

Vozzi G., Christopher J Flaim, Francesca Bianchi, Arti Ahluwalia, Sangeeta Bhatia. Microfabricated PLGA Scaffolds, A comparative study for applications in tissue engineering, Centro Interdipartimentale di Ricerca “E. Piaggio”, University of Pisa, Italy. 2001.

Vunjak-Novakovic, G. et al., Dynamic cell seeding of polymer scaffolds for cartilage tissue engineering. Biotechnol. Prog. 1998, 14, 193–202

Wang Y, “In vivo degradation characteristics of poly(glycerol sebacate)” Journal of biomedical materials research 2003, 66A:1 pp192

Wang.K, Thomas.C.H, Healy.K.E, Nuber.G. A novel method to fabricate bioresorbable scaffolds, 2002, pp 837-842.

Wei Sun, T.J., Feng Lin, *A processing algorithm for freeform fabrication of heterogeneous structures.* Rapid Prototyping Journal, 2004. **10**(316-326).

Whitesides, G.M., Ostuni, E., Takayama, S., Jiang, X., & Ingber, D.E. (2001) Soft lithography in biology and biochemistry. Annu.Rev.Biomed.Eng 3. 335-373.

Wiedmann-Al-Ahmad M., Gutwald R., Lauer G., Hübner U., Schmelzeisen R., How to optimize seeding and culturing of human osteoblast-like cells on various biomaterials., Biomaterials 2002 23:16, 3319-28

Williams JM, Adewunmi A, Schek RM, Flanagan CL, Krebsbach PH, Feinberg SE., *Biomaterials* 2005, 26: 4817-27

Williams, C.G., et al., *Variable cytocompatibility of six cell lines with photoinitiators used for polymerizing hydrogels and cell encapsulation.* Biomaterials, 2005. **26**(11): p. 1211-1218.

Williamsa.J.M, Adewunmib.A, Scheka.R.M, Flanagana.C.L, Krebsbacha.P.H, Feinbergd.S.E, Hollistera.S.J, Dasb.S. Bone tissue engineering using polycaprolactone scaffolds fabricated via selective laser sintering (2005) Biomaterials, 26, pp 4817–4827.

Wonjoon Cho, Emanuel M. Sachs, Nicholas M. Patrikalakis and Donald E. Troxel, A dithering algorithm for local composition control with three-dimensional printing, Computer-Aided Design, 2003, 35:9 851-867

Wu BM, Borland SW, Giordano RA, Cima LG, Sachs EM, Cima MJ. Solid free form fabrication of drugdelivery devices. J Controlled Release 1996; 40:77–87.

Xia, Y., Rogers, J.A., Paul, K.E., & Whitesides, G.M. (1999) Unconventional Methods for Fabricating and Patterning Nanostructures. Chem.Rev. 99. 1823-1848.

Xiao, Y.L. et al., Static and dynamic fibroblast seeding and cultivation in porous PEO/PBT scaffolds. J. Mater. Sci. Mater.Med. 1999, 10, 773–777

Xie.B, Parkhill.R.L, Warren.W.L, Smay.J.E. Synthesis direct writing of three dimensional polymer scaffolds using colloidal gels, 2006. Advanced Functionnal Materials, 16(13), pp 1685-1693.

Yang C, Hillas PJ, Baez JA, Nokelainen M, Bal.an J, et al., 2004. *Tissue Engineering* 18: 103-19

Yang F, Murugan R, Ramakrishna S, Wang X, Ma YX, Wang S. 2004. Fabrication of nano-structured porous PLLA scaffold intended for nerve tissue engineering. Biomaterials 25(10):1891–1900.

Yin, L. et al., "Scaffold topography alters intracellular calcium dynamics in cultured cardiomyocyte networks", Am. J. Physiol. 2004, Heart Circ. Physiol. 287, 1276–85

Yoshimoto, K., M. Ichino, and Y. Nagasaki, *Inverted pattern formation of cell microarrays on poly(ethylene glycol) (PEG) gel patterned surface and construction of hepatocyte spheroids on unmodified PEG gel microdomains.* Lab on a chip, 2009. **9**(9): p. 1286.

Yuan, N.-Y., et al., *Effects of the cooling mode on the structure and strength of porous scaffolds made of chitosan, alginate, and carboxymethyl cellulose by the freeze-gelation method.* Carbohydrate Polymers, 2009. **78**(2): p. 349-356.

Yuan, N.-Y., et al., *Effects of the cooling mode on the structure and strength of porous scaffolds made of chitosan, alginate, and carboxymethyl cellulose by the freeze-gelation method.* Carbohydrate Polymers, 2009. **78**(2): p. 349-356.

Yuehuei H. An, Shane K. Woolf and Richard J. Friedman, **"**Pre-clinical in vivo evaluation of orthopaedic bioabsorbable devices", Biomaterials 2000, 21:24, 2635-52

Z. S. Li, H. R. Ramay, K. D. Hauch, D. M. Xiao, and M. Q. Zhang, "Chitosan-alginate hybrid scaffolds for bone tissue engineering," *Biomaterials*, vol. 26, pp. 3919-3928, 2005.

Zhou, W.Y., Lee, S.H., Wang, M., Cheung, W.L. and Ip, W.Y., 2008. Selective laser sintering of porous tissue engineering scaffolds from poly(L: -lactide)/carbonated hydroxyapatite nanocomposite microspheres. Journal of Materials Science: Materials in Medicine, 19 (7), 2535_2540.

http://www.brookfieldengineering.com/products/viscometers/laboratory-dv-ii.asp

http://www.envisiontec.de/index.php?id=31

http://forgacslab.missouri.edu/bioprinter.html

http://www.zcorp.com/en/Products/3D-Printers/ZPrinter-350/spage.aspx

Nordson, Valve systems.
http://www.nordson.com/enus/divisions/efd/pages/default.aspx.

Dr. Vladimir Mironov, Director of the World's First Bioprinting Research Center 2007
http://www.musc.edu/bioprinting/html/interview.html

Solidscape.inc
http://www.solid-scape.com/pm_techdoc.html

VITA

Full name: Ho-Lung Li

Education

Ph.D., Mechanical Engineering and Mechanics, Drexel University, 2011
MS, Mechanical Engineering and Mechanics, Drexel University, 2008
BS, Energy Engineering, Tamkang University, 2003

Selected Publications:

[1] Ren, X.; **Li, H.**; Zhou, J. "Micro and nano design and fabrication of a novel artificial photosynthesis device" *ASME 2012 International Manufacturing Science and Engineering Conference MSEC2012*, June 4-8, 2012 at University of Notre Dame, Notre Dame, IN, USA

[2] **Li, H.**; Geisler, C.; Wootton, D.M.; Zhou, J. "A New Flexible and Multi-Purpose System Design for 3-Dimensional Printing". *ASME 2011 International Manufacturing Science and Engineering Conference MSEC2011*, June 13-17, 2011 at Oregon State University, Corvallis, OR, USA

[3] Geisler, C.; **Li, H.**; Wootton, D.M.; Lelkes, P.I.; Zhou, J. "Thermosensitive / Photocrosslinkable Hydrogel for Soft Tissue Scaffold Printing". *ASME 2011 International Manufacturing Science and Engineering Conference MSEC2011*, June 13-17, 2011 at Oregon State University, Corvallis, OR, USA

[4] Geisler C.; **Li, H.**; Wootton, D.M.; Lelkes, P.I.; Zhou. J. "Soft Biomaterial Study for 3-D Tissue Scaffold Printing," *ASME 2010 International Manufacturing Science and Engineering Conference*, Erie, PA, Oct. 2010.

[5] **Li, H.**; Xie, O.; Wootton, D.M.; Zhou, J. "Shape Memory Alloy and Magnetic Stirrer Activated High Pressure Optical Cell for Multiple Samples Mixing in Biophysical Study". *The International Conference on Shape Memory and Superelastic Technologies* in Pacific Grove, CA, May 16-20, 2010

[6] **Li, H.**; Jagadish, C.; Kwatny, H.; Chang, B.C. "A DSP Microprocessor Hybrid Control of an Inverted Pendulum*". IEEE International Conference on Control and Automation* in Christchurch, New Zealand, December 9-11, 2009

[7] **Li, H.**; Wootton, D.M.; Zhou, J. "A new flexible 3-D multi-nozzle printing system for fabrication of heterogeneous microstructures" in preparation to submit to *Rapid Prototyping Journal*

[8] Journal article in preparation – **Li, H.**; Wootton, D.M.; Zhou, J. "Heterogeneous algorithm for manufacturing multi-material structures using Automatically Programmed Tools"